CHEMICAL REVIEWS

Review

pubs.acs.org/CR

Methods, Mechanism, and Applications of Photodeposition in Photocatalysis: A Review

Kasper Wenderich and Guido Mul*

Photocatalytic Synthesis Group, MESA+ Institute for Nanotechnology, Faculty of Science and Technology, University of Twente, Meander 229, Post Office Box 217, 7500 AE Enschede, The Netherlands

ABSTRACT: In this review, for a variety of metals and semiconductors, an attempt is made to generalize observations in the literature on the effect of process conditions applied during photodeposition on (i) particle size distributions, (ii) oxidation states of the metals obtained, and (iii) consequences for photocatalytic activities. Process parameters include presence or absence of (organic) sacrificial agents, applied pH, presence or absence of an air/inert atmosphere, metal precursor type and concentration, and temperature. Most intensively reviewed are studies concerning (i) TiO_2; (ii) ZnO, focusing on Ag deposition; (iii) WO_3, with a strong emphasis on the photodeposition of Pt; and (iv) CdS, again with a focus on deposition of Pt. Furthermore, a detailed overview is given of achievements in structure-directed photodeposition, which could ultimately be employed to obtain highly effective photocatalytic materials. Finally, we provide suggestions for improvements in description of the photodeposition methods applied when included in scientific papers.

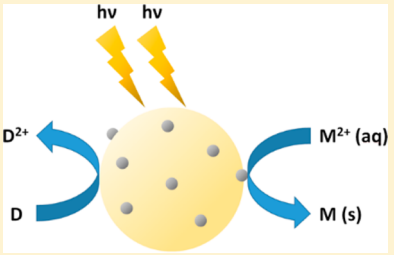

CONTENTS

Received: May 24, 2016
Published: December 5, 2016

DOI: 10.1021/acs.chemrev.6b00327
Chem. Rev. 2016, 116, 14587−14619

1. INTRODUCTION

1.1. Principles of Photodeposition of Metal (Oxide) Nanoparticles on Semiconductor Surfaces

Illumination of a slurry of semiconductor particles in an aqueous-phase solution of a metal salt often results in deposition of well-defined metal (oxide) nanoparticles on the surface of the semiconductor: this phenomenon is generally known as photodeposition. Photodeposition was already performed in 1965 by Clark and Vondjidis.[1] Using infrared studies, the authors showed that metallic silver was formed after illumination of a mixture of titanium dioxide and silver nitrate. However, the report that really sparked interest in photodeposition was published by Kraeutler and Bard in 1978.[2] In their study, platinum was loaded on titanium dioxide (TiO_2, anatase) by illuminating a slurry containing anatase powder, hexachloroplatinic acid (H_2PtCl_6), hydrochloric acid (HCl), sodium carbonate, and acetic acid, the latter being a sacrificial electron donor (see Figure 2a). During the reaction, a nitrogen purge was used to remove O_2 and CO_2, and the slurry system was heated to 55 °C. The authors showed that well-dispersed nanoparticles of Pt could be obtained. Since then, interest in photodeposition has expanded significantly (Figure 1).

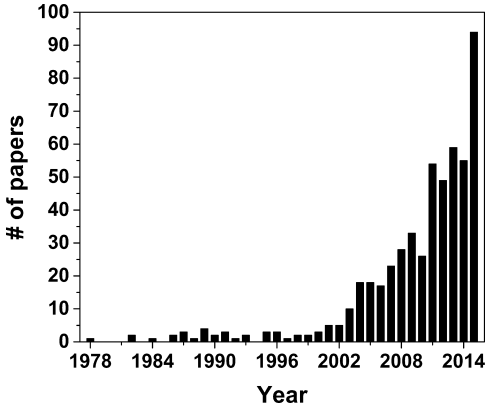

Figure 1. Overview of the number of papers published on "photodepo* AND photocat*" as a function of years, as searched in Scopus on August 29, 2016. Note: not all research related to photodeposition is included, as photodeposition is not the only name used for this phenomenon. It is also known as photoreduction or photochemical deposition.

Photodeposition is thus based on light-induced electrochemistry. A generalized equation for reductive photodeposition of a metal M is

$$M^{n+}(aq) + ne^- \rightarrow M(s) \quad (1)$$

Its counterpart, oxidative photodeposition, is the formation of metal oxide nanoparticle deposits, for example, through eq 2:

$$M^{n+}(aq) + nh^+ + nH_2O \rightarrow MO_n(s) + 2nH^+ \quad (2)$$

A schematic overview of both reductive and oxidative photodeposition is provided in Figure 2.

To allow photodeposition, the reduction/oxidation potential of the metal (oxides) to be deposited must be at favorable positions with regard to the energy-band positions of the semiconductor; that is, the conduction band (E vs NHE scale) must be more negative than the reduction potential of metals, and the valence band must be more positive (E vs NHE scale) than the oxidation potential of the species to be oxidized, being a metal (ion), water, or sacrificial agent. Examples of the band positions of several semiconductors are depicted in Figure 3;[3]

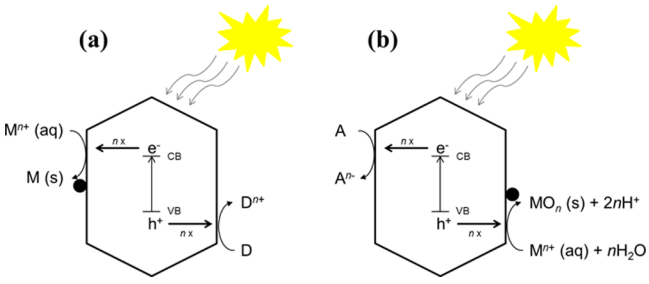

Figure 2. Schematic overview of (a) reductive photodeposition and (b) oxidative photodeposition. VB, valence band; CB, conduction band; M, metal; D, (sacrificial) electron donor; A, (sacrificial) electron acceptor; *n*, number of electrons (or holes) involved.

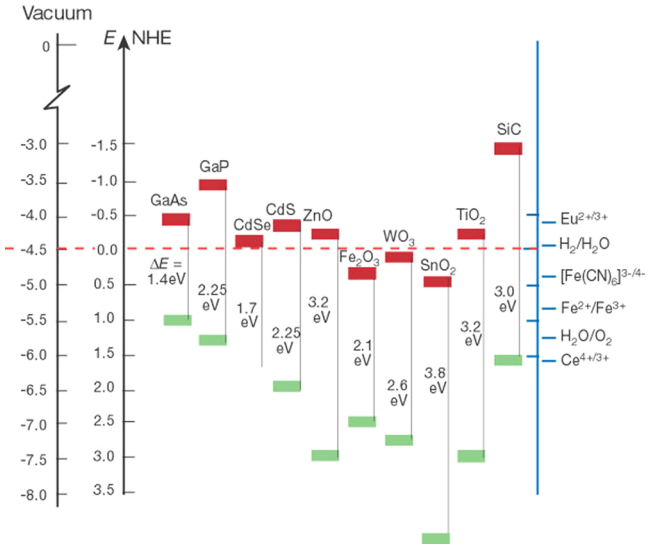

Figure 3. Schematic overview of band positions of several semiconductors on an energy scale in electronvolts with reference to the vacuum level, or in volts, with reference to the normal hydrogen electrode (NHE), as proposed by Grätzel.[3] On the right (in blue), some reduction potentials of species relevant in photoelectrocatalysis are provided. Copyright 2001 Nature publishing group.

examples of various reduction/oxidation potentials of metal precursor salts are depicted in Figure 4.[4] Second, during the photodeposition process, the photon energy of the incident light needs to exceed the band-gap energy of the semiconductor. Third, efficient charge carrier separation and migration needs to be possible. Last, the semiconductor needs to provide sufficient active surface sites for photodeposition to take place.

Variations on "classical" photodeposition also exist. For instance, some authors disperse a semiconductor in a metal precursor solution in the absence of illumination, after which the semiconductor is filtered and dried. Then, in nonaqueous gas-phase conditions, a photon-induced conversion of the surface-adsorbed precursor to the metal nanoparticles is realized.[5−8] Metal precursor species might have different compositions in aqueous and dried conditions, and therefore differences in

DOI: 10.1021/acs.chemrev.6b00327
Chem. Rev. 2016, 116, 14587−14619

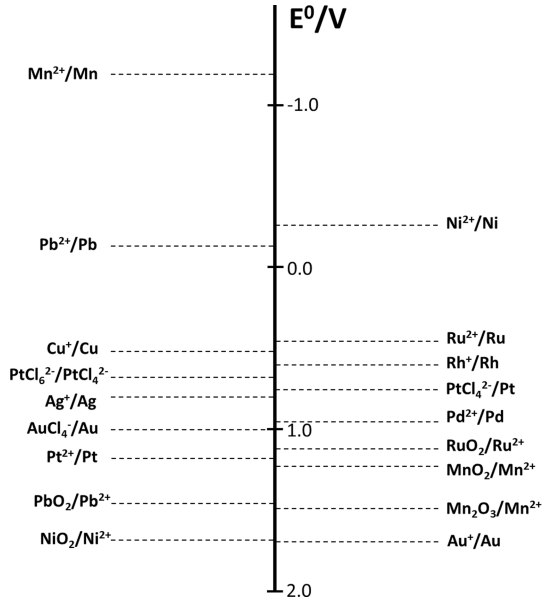

Figure 4. Schematic overview of redox potentials of several aqueous metal solutions relevant for photodeposition. Please compare to Figure 3 for values of conduction band minima and valence band maxima of TiO_2, ZnO, WO_3, and CdS. Values are taken from ref 4.

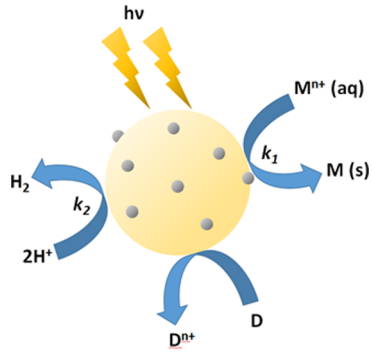

Figure 5. Scheme of reactions occurring during in situ photodeposition. A metal cation is reduced on the surface of the photocatalyst (k_1), while protons are reduced to form hydrogen (k_2). When the metal cation concentration approaches zero, the performance of a specific metal loading can be determined in the evolution of hydrogen. In this example, a sacrificial reagent D is used as hole scavenger.

reactivity, preparation time, and resulting nanoparticle morphology can be expected.

1.2. Applications of Photodeposition and Comparison to Alternative Methods

Metal (oxide) nanoparticles on semiconductor surfaces prepared by photodeposition predominantly find application in photocatalytic solar fuel synthesis,[9−11] wastewater treatment,[12,13] and air purification.[14,15] Nanoparticles, in these applications often referred to as cocatalytic nanoparticles, can significantly improve performance of semiconductors in light-stimulated reactions, including their stability.[10,13,16] With an appropriate loading, these cocatalysts have been proposed to function (i) as a charge-carrier "beacon" upon photoexcitation of the semiconductor, repressing electron/hole recombination; (ii) by providing active sites for charge-transfer reactions; and/or (iii) by providing stimulated light absorption by plasmonic field effects, particularly in the case of Au or Ag.[17]

Besides photodeposition, several methods exist to deposit cocatalytic nanoparticles on surfaces of (high surface area) semiconductors, such as impregnation,[18] chemical reduction,[19,20] electrodeposition,[19,20] atomic-layer deposition (ALD),[21] sputtering,[22] and physical mixing.[23] Compared to these alternatives, photodeposition is an attractive method: several techniques need elevated temperatures or an applied (bias) potential, while in the case of photodeposition, illumination is sufficient to create well-defined cocatalyst nanoparticles in a simple slurry reactor. Beneficial features of photodeposition include control over geometrical distribution of nanoparticles on surfaces of facet-engineered semiconductor crystals and potentially control over size and oxidation state of the deposited nanoparticles. In situ monitoring of the formation of H_2 during photodeposition is particularly interesting to determine an optimized loading of cocatalyst nanoparticles when photocatalysis is applied for water splitting.[24−27] A scheme of the reactions occurring during in situ photodeposition is depicted in Figure 5.

Comparisons in performance of semiconductors containing cocatalysts, prepared by photodeposition and other preparative techniques, are available in the literature.[23,27−33] However, a general conclusion from such comparisons cannot be drawn. Some authors claim that photodeposition is more suited than other deposition methods to obtain highly active photocatalytic systems,[23,28,32] whereas the contrary has also been reported.[29−31] Likely, the origin of these different conclusions can be found in differences in sizes of metal (oxide) particles, degree of agglomeration, or oxidation state of the as-prepared nanoparticles from different methods. Exemplary is a study by Jiang et al.,[27] in which two alternative methods of deposition were compared to prepare Pt/TiO_2 (P25, consisting of 70% anatase and 30% rutile); impregnation was achieved by use of a H_2PtCl_6 solution, followed by drying and (i) reduction in (20 vol %) H_2 at 400 °C or (ii) treatment in a 0.1 M $NaBH_4$/0.1 M NaOH solution. Photodeposition was performed with glycerol as sacrificial agent under anaerobic conditions. The authors found that Pt particle size was on the order of 2 nm and was only slightly different when the three preparation methods were compared, while the oxidation state of the Pt nanoparticles was variable. Photodeposition in the presence of glycerol (5 mL in 150 mL of solution) yielded Pt exclusively in the metallic state. Other methods resulted in combinations of Pt^0, Pt^{II}, and Pt^{IV} species, yielding a significantly lower performance in the production of hydrogen by photocatalytic glycerol reforming. This study shows that Pt^0 particles are most active in glycerol reforming and highlights an advantage of photodeposition compared to other techniques: Pt^0 can be selectively formed. The authors mention, however, that this feature can be achieved only in dilute suspension of P25 and at low glycerol concentration. When higher density suspensions were applied during photodeposition, oxidized Pt was formed, which the authors tentatively explain on the basis of a higher rate of deposition of (partially oxidized) Pt. The authors speculate that complete reduction of Pt cannot be achieved when deposition is too rapid, although this will obviously depend on the illumination time used. Further research on the effect of slurry density on the obtained Pt oxidation state is recommended.

DOI: 10.1021/acs.chemrev.6b00327
Chem. Rev. 2016, 116, 14587−14619

2. PHOTODEPOSITION OF NANOPARTICLES ON TiO_2

2.1. Introduction

Photodeposition of nanoparticles on titanium dioxide (TiO_2) has been employed by many researchers. The nanoparticles studied include noble metals such as Pt,[2,34−46] Ag,[1,47,48] Au,[33,49,50] and Pd;[51,52] metal oxides such as PbO_2[53] and RuO_2;[54] and more complex nanoparticles such as CoP_i, a water oxidation catalyst composed of cobalt and inorganic phosphate.[55] Even the photodeposition of another semiconductor, CdS, on TiO_2 has been performed.[56,57] In some cases, photodeposition has also been employed to achieve core−shell particles,[58−61] bimetallic cocatalysts,[62,63] or even trimetallic cocatalysts, sometimes involving an annealing step.[63]

Many researchers have tried to find an optimum weight loading of a cocatalyst when photodeposition was employed, to create effective photocatalytic materials.[33,44−47] However, studies on the influence of parameters, such as the role of a sacrificial reagent,[34−37] the influence of pH,[37−39,49] and the influence of metal precursor,[40,41] on chemical, structural and catalytic properties of the obtained materials after synthesis are not so abundant. In the following, we will provide more detail on studies performed on optimizing and understanding photodeposition of Pt on TiO_2.

2.2. Effect of Sacrificial Electron Donors on Properties of Pt Nanoparticles

Already in 1984, Sungbom et al.[34] demonstrated the significance of the presence of a sacrificial agent in the photodeposition process of Pt on anatase. The authors showed that the presence or absence of a combination of CH_3COOH and CH_3COONa at fixed ratio (a buffer, yielding a H_2PtCl_6 solution of pH 4.07) largely affected the obtained oxidation state of Pt, as analyzed by X-ray photoelectron spectroscopy (XPS). At low concentrations of CH_3COOH−CH_3COONa, the authors found that (at equal deposition times) Pt^{II} and Pt^{IV} had formed, rather than Pt^0. Increasing the concentration of CH_3COOH−CH_3COONa, ultimately resulted in a high concentration of Pt^0. This suggests that the extent of reduction of the Pt precursor is largely dependent on the rate of hole conversion (see Figure 5), which is typically higher in the conversion of an organic molecule as compared to oxidation of water. Interestingly, when photocatalytic methanol decomposition was performed with as-obtained Pt-loaded TiO_2, oxidized platinum was readily reduced to metallic Pt^0 in situ. Illumination in methanol-containing solutions is thus very effective in reducing platinum oxides to Pt.

The high effectiveness of methanol to obtain fully reduced Pt was confirmed by Lee and Choi,[36] who used Degussa P25 as a TiO_2 photocatalyst. They employed methanol at high and low concentrations. Complete reduction to Pt^0 particles was achieved at high concentration, whereas Pt^{II} remained dominant at relatively low methanol concentration. Methanol radicals, formed by oxidation of methanol by holes, were proposed to contribute to the reduction of Pt. A disadvantage of using a high concentration of methanol was the relatively large Pt particle size obtained.

Murcia et al.[42] studied the photodeposition kinetics of Pt on anatase in the presence of 2-propanol, under mild light intensity in N_2. In agreement with the data of Herrmann et al.,[41] the authors observed that the Pt particle size increased as a function of photodeposition time (roughly 3 nm after 15 min and 6 nm after 240 min). The precursor concentration was equivalent to a Pt loading of 0.5 wt %. At higher precursor concentrations (equivalent to 2 wt % Pt), aggregates of Pt particles were observed at both short and long photodeposition times. The growth of particles was attributed to a cocatalytic effect of Pt in reducing the $PtCl_6^{2-}$ precursor. At higher precursor concentration, the final reduction degree of the Pt particles amounted to 60%. This is somewhat contradictory to the earlier mentioned study by Lee and Choi,[36] who observed almost complete reduction. This is likely caused by the different sacrificial agent (2-propanol vs methanol), as will be discussed in the following.

A comparison of sacrificial agents in determining Pt particle size and dispersion was reported by Nakamatsu et al.[35] The Pt−Pt particle nearest-neighbor distance (determined from scanning electron microscopy), as a function of the sacrificial agent used, is illustrated in Figure 6. In agreement with Lee and Choi,[36] the

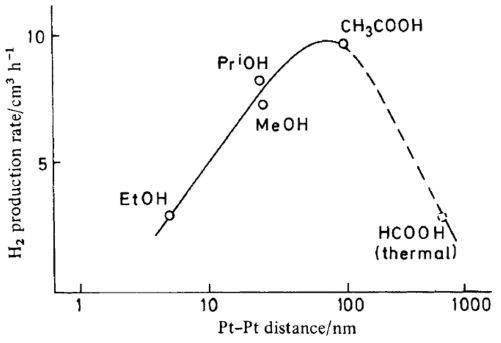

Figure 6. Effect of sacrificial agent used on Pt−Pt particle distance on P25 TiO_2, and the resulting hydrogen production rate of the photocatalysts in reforming of ethanol. Circles indicate the sacrificial agent used in the preparation of the Pt/TiO_2 samples, that is, in the photodeposition procedure, and serve as data points for this graph. The broken circle and dashed line relate to Pt/TiO_2 synthesized through thermal reduction in formic acid rather than by photodeposition. Reprinted with permission from ref 35. Copyright 1986 Royal Society of Chemistry.

authors propose a model where the radicals of the organic compounds used (methanol, ethanol, 2-propanol, and acetic acid, formed when these are oxidized by photogenerated holes), provide electrons for the reduction of adsorbed Pt species on the semiconductor surface. Nakamatsu et al.[35] observed that using radicals with a relatively high reduction potential results in a large Pt−Pt particle distance (please refer to Figure 7 for the respective redox potentials of the radicals).

We propose the trend in Figure 6 indicates that a high reduction potential of in situ formed organic radicals favors the nucleation of additional (small) Pt particles (lowering the Pt−Pt particle distance), rather than stimulating growth of existing particles. The relatively high Pt−Pt particle distance (representing a large Pt particle size) of the catalysts prepared with 2-propanol, even though the radical thereof has the highest oxidation potential, is explained by the unfortunately chosen high concentration of this sacrificial agent (50 vol %), as compared to the other sacrificial agents. This is in agreement with the data of Lee and Choi,[36] who observed significantly larger Pt particles when high concentrations of CH_3OH were used. Further investigation is recommended to substantiate the conclusions of the work of Nakamatsu et al.[35] on the effect of the sacrificial donor on Pt−Pt distance and dispersion. Interestingly, an increase in Pt−Pt particle distance induces an increase in photocatalytic hydrogen production by ethanol reforming (Figure 6), up to a distance of 100 nm, which suggests large Pt particles are more effective. Nakamatsu et al.[35] explain the

DOI: 10.1021/acs.chemrev.6b00327
Chem. Rev. 2016, 116, 14587−14619

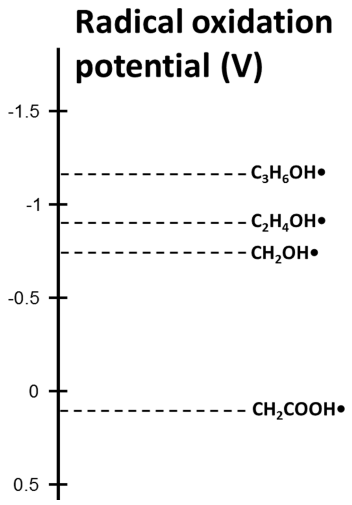

Figure 7. Radical oxidation potentials in volts vs NHE as described by Nakamatsu et al.[35]

relatively low activity in ethanol reforming of small particles with a small Pt−Pt distance to light shielding effects, limiting light-induced activation of TiO_2. Again, we recommend additional systematic study to corroborate the effect of particle size (and spatial Pt distribution) on stimulating photocatalytic reforming activity of TiO_2 (P25), including facet-preferred deposition (see section 8 of this review).

2.3. Effect of pH

pH also plays a significant role in determining morphology and composition of Pt. First we will discuss some observations reported in the absence of a sacrificial agent. Xi et al.[37] discussed that hydrolysis of $[PtCl_6]^{2-}$ (n = 0 in eq 3) occurs during the photodeposition procedure (in the absence of oxygen):

$$[Pt(OH)_nCl_{6-n}]^{2-} + OH^- \leftrightarrow [Pt(OH)_{n+1}Cl_{5-n}]^{2-} + Cl^- \quad (3)$$

where n = 0−5. This equilibrium would imply that at high pH the Pt precursor molecule contains a large fraction of OH "ligands", which likely affects the kinetics of photodeposition and the oxidation state of the obtained Pt particles. Indeed, the authors found photodeposited $Pt(OH)_2$ on anatase at low and neutral pH, while at high pH, PtO_2 was additionally present. The authors hypothesized that PtO_2 formation is possible through the following reaction, involving oxidation of the hydroxyl groups of the surface-adsorbed complex $[Pt(OH)_4Cl_2]^{2-}$:

$$[Pt(OH)_4Cl_2]^{2-} + 4h^+ \rightarrow PtO_2 + O_2 + 4H^+ + 2Cl^- \quad (4)$$

For formation of $Pt(OH)_2$, the reduction of $[Pt(OH)_2Cl_4]^{2-}$ is proposed:

$$[Pt(OH)_2Cl_4]^{2-} + 2e^- \rightarrow Pt(OH)_2 + 4Cl^- \quad (5)$$

Interestingly, the authors determined by XPS that at low pH values less Pt was deposited on the surface of TiO_2 than at high pH values, when identical photodeposition times were applied. Also, the addition of Cl^- (in the form of NaCl), turned out to be detrimental to the amount of Pt deposited. Indeed, when a large amount of Cl^- was added, Pt deposition was not detected at all at low pH. The detrimental effect of Cl^- addition in photodeposition of Pt on Evonik-Degussa P25 in acidic conditions was also confirmed for $[PtCl_n(H_2O)_{4-n}]^{2-n}$ (n = 0−4) (in the absence of sacrificial agent) by Mahlamvana and Kriek,[40] showing that photodeposition of Pt was absent when only $[PtCl_4]^{2-}$ was present in solution. Hydrolysis of $[PtCl_6]^{2-}$ in the absence of excess Cl^- thus appears to be necessary to achieve significant rates of Pt deposition on TiO_2 in the absence of a sacrificial agent.

Not surprisingly, this chemistry is largely affected by the presence of a sacrificial agent. In contrast to the previously summarized papers by Xi et al.[37] and Mahlamvana and Kriek,[40] Zhang et al.[38] demonstrate that in the presence of ethanol a high Pt photodeposition rate on (nonporous) Degussa P25 is achieved at low pH values, significantly higher than at higher pH values. Recent pH-dependent photodeposition studies by Qamar and Ganguli[39] confirmed that, in the presence of sacrificial agent, the photodeposition rate of Pt on anatase is relatively low at high pH values.

The difference in deposition rates at low or high pH in the presence of a sacrificial agent was explained by Zhang et al.[38] on the basis of electrostatic interactions. At pH values below the isoelectric point of TiO_2 (IEP = 6.25), the charges of the Pt complex in solution (negative) and the surface of TiO_2 (positive) are attractive, resulting in high deposition rates due to favorable adsorption and consequently resulting in a broad size distribution of Pt. Apparently, electrostatic interactions are particularly relevant when a sacrificial agent is present in solution. Incidentally, around the pH value of the isoelectric point of TiO_2, large agglomerates of Pt particles were found.[38] Generally, in agreement with Xi et al.,[37] even in the presence of a sacrificial agent the oxidation state is dependent on pH: metallic Pt^0 was formed at a pH lower than 5, and PtO_2 was formed at pH values higher than 9. In the pH range 5−7, both Pt and PtO were found, and in the pH range 7−9, both PtO and PtO_2 were found. Just as in Xi et al.,[37] Zhang et al.[38] attributed this phenomenon to hydrolysis of the $[PtCl_6]^{2-}$ precursor (eq 3).

These studies are very illustrative, as they demonstrate that the size and distribution, and in particular the oxidation state, of Pt particles formed on the surface of TiO_2 can be carefully controlled by adjusting the pH. Inspired by this phenomenon, Lee and Choi[36] synthesized two platinum-loaded TiO_2 (Degussa P25) samples: one containing metallic Pt at a low pH and high concentration of electron donor (methanol) and one containing oxidized Pt at a high pH in the absence of electron donor. The authors demonstrate that Pt/TiO_2 containing metallic Pt was more active in the photocatalytic degradation of several chlorinated organic compounds. Qamar and Ganguli[39] confirmed that high pH during photodeposition results in photocatalysts with low photocatalytic activity in triclopyr and methyl orange degradation, assigned to the dominant formation of oxidized Pt particles.

2.4. Effect of Pt Precursor and Temperature

Herrmann et al.[41] studied the effect of Pt precursor on photodeposition rate of Pt on TiO_2 (nonporous Degussa P25) in the absence of a sacrificial agent under anaerobic conditions. The Pt precursors used were $[PtCl_6]^{2-}$ (H_2PtCl_6), Na_2PtCl_6, $H_2Pt(OH)_6$, and $Pt(NO_2)_2(NH_3)_2$. Use of $Pt(NO_2)_2(NH_3)_2$ resulted in a significantly lower photodeposition rate than observed for the other precursors; the highest apparent quantum efficiency of deposition was on the order of 0.05. The lower photodeposition rate of $Pt(NO_2)_2(NH_3)_2$ was ascribed to a smaller adsorption coefficient, because of its nonionic character. The similarity in deposition rates from $H_2Pt(OH)_6$ and the chlorine-containing precursor solutions is somewhat remarkable. Unfortunately the pH of these precursor solutions was not

DOI: 10.1021/acs.chemrev.6b00327
Chem. Rev. 2016, 116, 14587−14619

specified, but we anticipate the lower pH and the presence of chloride in the $[PtCl_6]^{2-}$-containing solutions should induce a lower deposition rate, as demonstrated by Xi et al.[37] Further study is recommended, taking pH differences of the various precursor solutions into account.

Interestingly, Hermann et al.[41] also addressed the effect of temperature on the rate of deposition. The authors found Arrhenius-type behavior, with an apparent activation energy below 10 kJ·mol^{-1}. The authors conclude this low value suggests the rate of deposition is not limited at high temperature by adsorption of the precursor molecules or by the desorption of products (other than the deposited Pt). Unfortunately, the authors do not discuss the effect of temperature on oxidation state or size of the obtained Pt nanoparticles. They did observe that at room temperature the size is very much dependent on the deposition time, with small particles growing progressively when deposition times are extended.

2.5. Effect of Absence or Presence of Oxygen

Mahlamvana and Kriek[40] demonstrated in their photodeposition experiments that the presence of oxygen had a profound negative influence on the photodeposition rate of Pt on TiO_2 (Evonik-Degussa P25). This was attributed to O_2 acting as a competing electron scavenger. Furthermore, the authors demonstrated that the improvement achieved by purging the photodeposition reactor with oxygen-free gas was largely dependent on the type of precursor used. The order of most to least reactive precursor in the absence of oxygen was $K_2PtCl_6 > H_2PtCl_6 > [PtCl_3(H_2O)]^- > [PtCl_4]^{2-}$, with the latter showing no deposition reactivity at all (Figure 8). It is very interesting to hypothesize that $[PtCl_6]^{2-}$ is

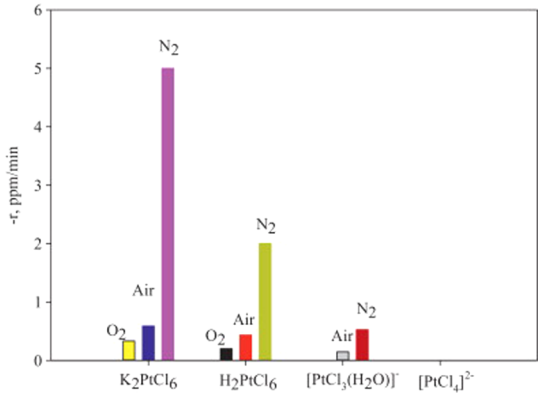

Figure 8. Initial photoreduction rates of different Pt precursors on TiO_2 in different atmospheres. Reprinted with permission from ref 40. Copyright 2014 Elsevier.

first reduced to $[PtCl_4]^{2-}$ before deposition of metallic Pt^0 occurs. However, the lack of activity in the photodeposition of $[PtCl_4]^{2-}$ observed by Mahlamvana and Kriek[40] would imply that this is not the correct mechanism. The data shown in Figure 8 are contradictory to the data previously discussed and reported by Herrmann et al.[41] Again, pH differences might be at the origin of the discrepancy in conclusions, and further study is recommended.

A summary of the effect of process parameters on photodeposition rates, oxidation state, and particle size of Pt on TiO_2 is provided in Scheme 1. This scheme should be used as a guideline, since the literature is not entirely conclusive.

Scheme 1. Overview of the Influence of Process Parameters on Morphology and Oxidation State of Pt on TiO_2

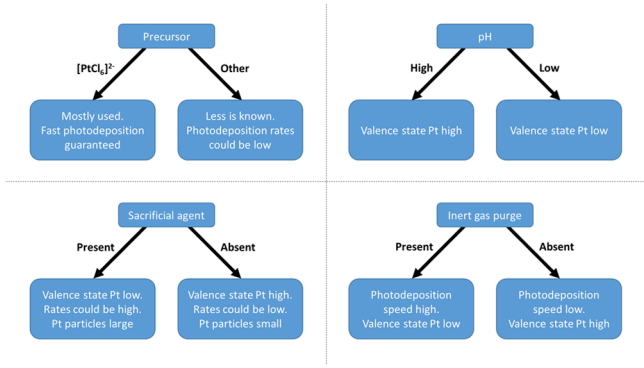

2.6. Deposition of Metals Other Than Pt

Photodeposition of Au (in the presence of methanol) on Degussa P25 has also been systematically addressed.[49] Similar to Pt, the average particle size of Au is relatively small when the pH during photodeposition is relatively high: 18 nm at pH = 3 and 4 nm at pH = 9. Therefore, the highest photocatalytic activity in oxalic acid degradation was found when Au was prepared by photodeposition at a pH above 7. Contrary to Pt, Au nanoparticles were found fully reduced after photodeposition, irrespective of the applied pH.

Differences in photodeposition behavior between Pt and Pd have been observed as well. As previously explained, Mahlamvana and Kriek[40] have shown that Cl^- is detrimental to the rate of photodeposition of $[PtCl_n(H_2O)_{4-n}]^{2-n}$ ($n = 0-4$) on Evonik-Degussa P25. For similar TiO_2 crystals, the deposition rate of $PdCl_2(H_2O)_2$ was faster than that of $[PdCl_4]^{2-}$ or $[Pd(H_2O)_4]^{2+}$, suggesting there is an optimum ratio between Cl^- and H_2O, likely affecting electrostatic interactions.[51]

Also for Degussa P25, Borgarello et al.[52] show (without explanation) that oxygen has a negative influence on the reduction degree of Rh^{III}. Likely this is due to oxygen reduction being in competition with reduction of Rh^{III}. In agreement with the previously discussed observations, Pt, Rh, and Pd reduction is complete when methanol is used as sacrificial agent.

Photodeposition on TiO_2 has also been applied for removal of metal contaminants from waste streams. Different pH dependencies in the removal rate of ionic metal compounds were found.[52,64] It was demonstrated that the presence of a sacrificial agent (citric acid) is beneficial for the rate of reduction of Cu^{II}, Ni^{II}, Zn^{II}, and Pb^{II} on TiO_2 but to different degrees.[65] Interestingly, Borgarello et al.[52] showed that it is possible to selectively remove each metal compound from a solution containing multiple metal compounds by changing photodeposition parameters. For instance, the authors demonstrated that only Au^{III} is photoreduced from an air-equilibrated solution (pH = 0) containing TiO_2 (Degussa P25), 10 vol % methanol, Au^{III}, Pt^{IV}, and Rh^{III}, whereas Pt^{IV} and Rh^{III} remained in the solution. From a perspective of the preparation of bimetallic catalysts, this suggests photodeposition will not lead to homogeneous mixtures but rather to core/shell, or single metal, spatially separated particles as a result of sequential deposition.

Finally, some researchers have tried to study photoreduction of metals on TiO_2 by in situ extended X-ray absorption fine structure (EXAFS) spectroscopy, providing significant mechanistic information on the photodeposition process. This includes

DOI: 10.1021/acs.chemrev.6b00327
Chem. Rev. 2016, 116, 14587−14619

Table 1. Properties of Samples Synthesized by Liu et al.[6]

photodeposition in	Ag loading (at. %)	Ag morphology	dispersion	RhB photodegraded[a] (%)
water	7.68	nanosheets + nanoparticles	nanosheets at top, nanoparticles at sides	82
water + ethanol	26.1	irregular polygon shape	only at top	27.3
air	1.35	nanoribbons	only at top, hardly observable	39.4

[a]Upon visible-light irradiation, over 4 h.

the deposition of Pt,[43] Au,[50] and Rh.[66,67] Interestingly, one of the studies concerning Rh/TiO_2 (where TiO_2 was present as calcined anatase) revealed that the type of sacrificial agent used affects the photodeposition rate, with the order from high to low rate being methanol > ethanol ≫ 1-propanol > 2-propanol.[66] Again, this might be related to the reduction potential of radicals formed by the hole-transfer reaction to these alcohol derivatives.

Aside from TiO_2, photodeposition has also been employed for other semiconductor metal oxides, such as ZnO,[6,68−89] $BiVO_4$,[90−92] Ga_2O_3,[24,93,94] and Ta_2O_5;[95] perovskites;[30,93,96] metal sulfides [in particular cadmium sulfide (CdS)];[25,26,97−104] and (oxy)nitrides.[8,24,93,105,106] In particular, the photodeposition of Pt on CdS[25,97−102] and Ag on ZnO[6,68−85] have been explored relatively well in the literature. We will discuss photodeposition studies on several oxides, in particular ZnO and WO_3, followed by studies on CdS and GaN:ZnO.

3. PHOTODEPOSITION OF NANOPARTICLES ON ZNO

3.1. Photodeposition of Ag on ZnO

Similar to what was discussed for TiO_2, the absence or presence of a sacrificial electron donor has a strong influence on the rate of photodeposition and morphology of Ag on ZnO.[6,68,69] Liu et al.[6] have studied photodeposition of Ag on ZnO nanorods (grown on glass substrates) in an aqueous solution, either without sacrificial agent or in the presence of ethanol. Also, they dipped a glass substrate with ZnO nanorods in an aqueous solution with $AgNO_3$, after which illumination was performed outside the $AgNO_3$ solution. The results were very different in (i) obtained Ag loading, (ii) dispersion, (iii) morphology, and (iv) consequent photocatalytic activity under visible-light irradiation. An overview of the different properties of the samples can be found in Table 1 and Figure 9. In the absence of ethanol, two different kinds of morphologies were obtained: small nanoparticles (10−20 nm in size) at the sides of the nanorods and huge nanosheets on the top when deposition was performed in the $AgNO_3$ solution. Conversion of dipped samples resulted in very little Ag, preferably at the top (indicated as "air" in Figure 9). The presence of ethanol improved the photodeposition rate greatly, and huge nanoclusters of Ag (500−800 nm in size) were exclusively formed on the top of the ZnO nanorods. We speculate that the differences induced by ethanol might be the result of a change in sorption properties of ZnO for Ag^+, related to formation of Zn−O−C_2H_5 surface species. A remarkably lower photocatalytic activity in rhodamine B (RhB) degradation under visible light was observed when ethanol was used in the photodeposition procedure. The authors attribute this to (i) Ag blocking RhB reaction sites or (ii) Ag inhibiting visible-light access to the Ag/ZnO interface, reducing the amount of surface plasmon resonance states and thus the photocatalytic activity. Although photodeposition in air of the dipped sample was an interesting experiment, the amount of Ag was quite low, and therefore a lower activity was observed as compared to the sample prepared in aqueous conditions (without ethanol).

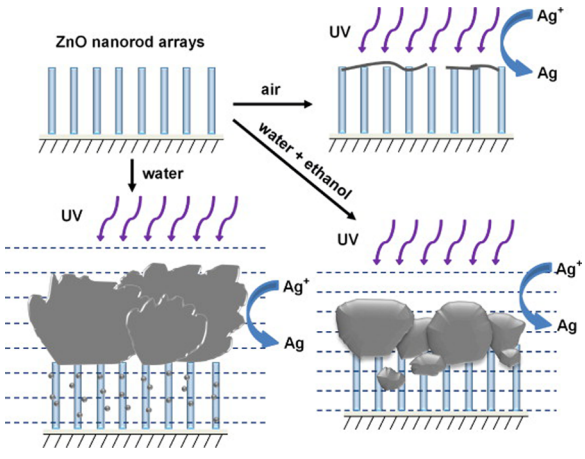

Figure 9. Schematic demonstration of the influence of reducing medium on photodeposition of Ag on ZnO nanorods. Reprinted with permission from ref 6. Copyright 2015 Elsevier.

Huang et al.[68] also discussed the effects of sacrificial agents on photodeposition rates of Ag on ZnO and the resulting morphology. These authors performed Ag photodeposition on ZnO nanoflowers with $AgNO_3$ solutions containing (i) no sacrificial agent, (ii) ethanol, and (iii) glycol. They found Ag content of 27.6, 23.6, and 35.0 wt % respectively. Although glycol enhanced the rate of Ag deposition, it is remarkable that ethanol did not, especially considering the previously discussed results of Liu et al.[6] The use of ethanol did affect the size of the Ag particles: when photodeposited in the presence of ethanol, these were considerably larger (100 nm) than in the absence of ethanol (10 nm). Ag/ZnO prepared by glycol-assisted photodeposition showed superior surface-enhanced Raman scattering (SERS) properties and performance in photocatalytic dye degradation.

In a study by Wang et al.,[69] photodeposition of Ag on tetrapodlike ZnO whiskers was performed with different concentrations of poly(ethylene glycol) (PEG) in $AgNO_3$ aqueous solution. Under the same illumination conditions, an increase in PEG concentration resulted in an increase in the amount of Ag deposited and in smaller Ag mean particle sizes. Noteworthy is the mechanism of photodeposition the authors mentioned: they attributed the reduction of Ag^+ to Ag not necessarily to electrons formed in ZnO. Instead, they mentioned that PEG captures $OH^\bullet$ radicals formed by ZnO, forming aldehyde or acid. These compounds then reduce Ag^+ to Ag.

Some authors have analyzed changes in Ag morphology as a function of illumination time.[70−75] Lin et al.[72] observed that, with increasing irradiation time, Ag quantities increased, as well as the Ag particle size, albeit moderately (13.4 nm after 5 min up to 15.9 nm after 25 min). Li et al.[73] observed similar behavior but more significantly (11 nm after 30 min up to 29 nm after 8 h). The higher Ag quantity resulted in increased performance in H_2O_2 and SERS-based rhodamine 6G (R6G) sensing, although the effect of particle size was not extensively discussed. Studies by Behnajady et al.[71] and Peng et al.[75] have shown that the performance of Ag/ZnO (in this case for methyl orange

DOI: 10.1021/acs.chemrev.6b00327
Chem. Rev. 2016, 116, 14587−14619

photodegradation) initially changes with increasing irradiation time of photodeposition but becomes constant at extended deposition times. This was logically attributed to full reduction of Ag^+ to Ag. Especially noteworthy are studies by Kawano et al.[70] and Chen and Nickel.[74] Kawano et al.[70] were mainly interested in using ZnO as a photocatalyst to remove Ag^+ from an aqueous solution. They monitored Ag deposition over time on a Zn-terminated surface (0001) and an O-terminated surface ($000\bar{1}$). After 10 s of illumination, a considerably higher amount of Ag particles was found at the Zn-terminated surface than at the O-terminated surface (ratio 20:1), indicating that the Zn-terminated surface was far more active. Increased irradiation times showed a considerable growth in the Ag particle size deposited on the O-terminated surface, which was not observed for the Zn-terminated surface. The authors state that the latter might have been the result of (i) insufficient Ag ions being present in solution or (ii) as-deposited Ag changing the absorption efficiency of the material. Chen and Nickel[74] studied the photodeposition kinetics of Ag on ultrafine ZnO in the presence of Zn^{2+} and excess OH^- ions in deaerated ethanol. They found that, in the presence of excess Zn^{2+} ions, mainly large metallic Ag particles were formed, whereas in the presence of excess OH^-, initially Ag_2O was formed, which was transformed to metallic Ag in the course of time.

A major advantage of performing photodeposition of Ag on ZnO is that Ag will stabilize ZnO.[76,77] Xie et al.[76] performed photodegradation of crystal violet (CV) using a UV lamp over eight cycles in the absence or presence of Ag on ZnO, as demonstrated in Figure 10. A drastic decrease in activity was

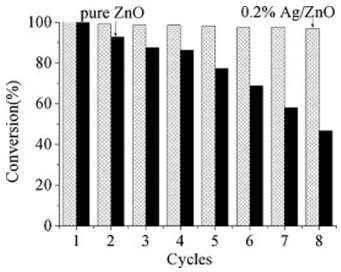

Figure 10. Photocatalytic conversion of crystal violet by use of pure ZnO and Ag/ZnO over multiple cycles. The activity of ZnO decreased, whereas the activity of Ag/ZnO did not. Adapted with permission from ref 76. Copyright 2010 Elsevier.

observed for unloaded ZnO, whereas for ZnO loaded with 0.2 wt % Ag hardly any deactivation was observed. The authors discussed that, according to Kislov et al.,[78] photocorrosion of ZnO ($ZnO + 2h^+ \rightarrow Zn^{2+} + 0.5O_2$) mainly happens at surface defect sites. Xie et al.[76] demonstrated through photoluminescence studies that, during photodeposition, Ag is deposited preferably at these defect sites. Therefore, photocorrosion of ZnO is prevented, and thus the photocatalyst is far more stable.

One aspect we will address is the use of X-ray photoelectron spectroscopy (XPS) to analyze the surface oxidation state of the formed Ag particles. Theoretically, according to the Handbook of X-ray Photoelectron Spectroscopy,[107] metallic Ag can be recognized by, among others, binding energies of 368.2 and 374.2 eV, corresponding to Ag $3d_{5/2}$ and Ag $3d_{3/2}$, respectively. After photodeposition, many authors reported a shift in the binding energy of Ag $3d_{5/2}$ and Ag $3d_{3/2}$ to lower energy.[68,69,77,79−83] Those authors attributed this to spontaneous electron transfer from Ag to ZnO at the interface, due to Fermi level alignment. Binding energies of Ag $3d_{5/2}$ reported by the authors are in the range 366.5−367.7 eV. It should be noted that distinguishing between metallic Ag, Ag_2O, and AgO by XPS is difficult, because their Ag $3d_{5/2}$ binding energies are very similar, with some reports even claiming that the binding energies for Ag_2O and AgO are at lower positions than that of metallic Ag.[108,109] This implies that the reported values could also be attributed to the formation of surface Ag_2O or AgO. Some authors discussed the possible formation of Ag_2O by photodeposition.[68,69] Still they concluded metallic Ag should be present, since in X-ray diffraction (XRD) data they exclusively observed metallic Ag and did not detect any peaks corresponding to Ag_2O. Wang et al.[69] investigated whether an O 1s peak could be assigned to Ag_2O and reported the contrary. Interestingly, all the authors mentioned performed their photodeposition experiments without any inert purge gas. Thus, photodeposition of Ag on ZnO was most likely performed in oxygen-rich conditions, which might contribute to Ag_2O or AgO formation. Zhang et al.[84] reported that when the solution was purged with N_2 during the experiment, peaks were observed at 368.3 and 374.2 eV. These peaks do correspond to metallic Ag $3d_{5/2}$ and Ag $3d_{3/2}$, respectively, and are clearly different from the earlier reported values. On the other hand, Chen et al.[85] also performed photodeposition with a N_2 purge, and they did report a shift in XPS binding energy. Although we do not exclude the possibility that the shift in binding energy is the result of interaction between Ag and ZnO, we urge researchers to perform photodeposition of Ag on ZnO in deaerated conditions. In this way, it is less likely that Ag_2O or AgO will be formed, and assignment of the XPS spectra is more straightforward. In addition, as-synthesized samples can be analyzed by, for instance, X-ray Auger spectroscopy, which might be more conclusive than XPS regarding the oxidation state of the obtained Ag.

A brief summary of the properties of Ag particles on ZnO as a function of process conditions during photodeposition is presented in Scheme 2. As previously discussed, systematic

Scheme 2. Overview of the Influence of Process Parameters during Photodeposition on Morphology and Oxidation State of Ag on ZnO

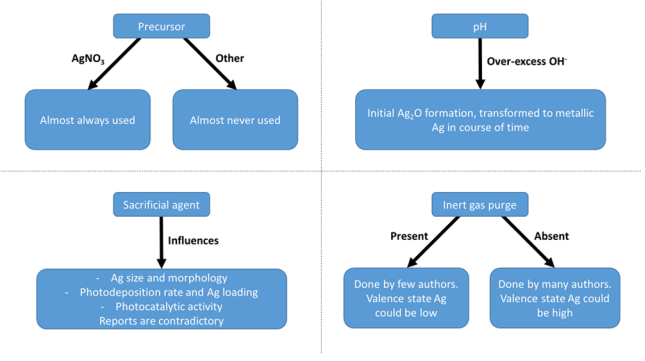

study of the effect of these parameters is needed to arrive at more conclusive preparation criteria to obtain a certain Ag particle size and/or oxidation state on the surface of well-structured ZnO.

3.2. Photodeposition of Au, Pd, and Other Catalysts on ZnO

Although most studies have focused on photodeposition of silver on zinc oxide, other studies describe the photodeposition of gold[86,110−114] and also of palladium,[115−118] cadmium sulfide (CdS),[119,120] copper,[87,121,122] platinum,[123,124] nickel,[125] and

DOI: 10.1021/acs.chemrev.6b00327
Chem. Rev. 2016, 116, 14587−14619

mercury.[126] In several of these studies, the concept of photodeposition was used only to remove metal ions from solution. However, controlled deposition of mainly Au and Pd on ZnO was also studied, to prepare effective photocatalysts. Au/ZnO catalysts have been predominantly used in CO oxidation,[110−112] dye photodegradation,[86,114] and removal of bacteria.[114] Pd has been used for gas sensing[115,116] and generally enhancing photocatalytic activity.[117,118] An increase in photocatalytic activity of ZnO after deposition of Au or Pd is attributed to enhanced charge-carrier separation and enhanced rates of electron-transfer reactions.[86,114,117,118] Wu et al.[113] have discovered furthermore that Au/ZnO displays surface plasmon resonance (SPR) properties. Liqiang et al.[118] demonstrate, through XPS analysis, that O_2 adsorption is favored when ZnO is loaded with Pd. Enhanced O_2 adsorption after deposition of Pd on ZnO was also observed by Chang et al.[116]

Similar to photodeposition of Pt on TiO_2, the rates of photodeposition of Au or Pd on ZnO, and the accompanied obtained morphology, is quite dependent on (i) the absence or presence of a sacrificial agent, (ii) pH, (iii) properties of the applied light source, and (iv) irradiation time. For preparation of Au nanoparticles, typically $[AuCl_4]^-$ is used, although deposition from potassium gold cyanide is also feasible.[127] Methanol[127] and ethanol[86,128] have been used as sacrificial agents. Park et al.[127] have demonstrated that methanol enhances the rate of Au deposition. Some authors have used an inert gas purge, although little is known about the effect of oxygen on the deposition rate and obtained oxidation state of Au nanoparticles.[128]

Carabineiro et al.[110] have investigated the influence of pH, irradiation time, and morphology of ZnO on the structure and activity of 1 wt % Au nanoparticles in catalytic CO oxidation. The authors compared photodeposition to other preparation methods (impregnation). Au particles prepared by photodeposition were less effective than those prepared by impregnation, likely induced by the relatively large particle sizes obtained after photodeposition. The most active particles were prepared by photodeposition at pH ≈ 5.5.

Wu and Tseng[86] demonstrated that the size of Au nanoparticles on ZnO nanorods can be controlled through varying the precursor ($HAuCl_4$) concentration and irradiation time. Low irradiation times and low $HAuCl_4$ concentration led to the smallest particles, which remains unexplained. The authors confirmed small particles favor catalytic activity: when the Au particles exceed sizes of 30 nm, even a detrimental effect on the photocatalytic activity was observed. The authors tentatively explain this observation by unfavorable light scattering by the larger Au particles, reducing the probability of light absorption by the ZnO nanorods.

Naknam et al.[112] studied the influence of lamp intensity on morphology of Au nanoparticles when deposited on ZnO. When the lamp intensity was increased, the illumination time was decreased, so that the amount of photons used to illuminate ZnO remained constant. The pH was altered to 8 by use of Na_2CO_3. The loading and mean particle size of Au particles remained similar, but the degree of agglomeration increased significantly with increasing lamp intensity. In a different study from the same research group,[111] it was demonstrated that the morphology of ZnO plays an important role in determining the size of Au particles photodeposited. When photodeposition of Au took place on nanorodlike microflowers or large nanorod structures of ZnO, the Au particles were considerably larger than when the photodeposition took place on smaller ZnO nanorod structures. It thus appears the surface area of ZnO should also be taken into consideration when optimizing the photodeposition procedure for Au particles. Wu et al.[113] discussed that the content and deposition site of Au nanoparticles photodeposited on ZnO nanorods can be controlled with $HAuCl_4$ concentration and illumination time. In other studies, the amount of Au loading on ZnO was varied by He et al.[114] and by Su and Qin.[129] He et al.[114] observed that increasing the Au loading up to 10 mol % results in increasing methylene blue and salicylic acid photodegradation rates. Interestingly, the authors demonstrated through electron spin resonance (ESR) spectroscopic measurements that photodeposition of Au on ZnO leads to an enhancement in light-induced generation of hydroxyl radicals and superoxide and singlet oxygen.

In summary, data in the literature seem to suggest (i) low $HAuCl_4$ concentration, (ii) high surface area of ZnO, and (iii) long illumination time (at low light concentration) are beneficial to obtain small, individual Au nanoparticles, whereas the oxidation state usually is Au^0, irrespective of the presence or absence of a sacrificial agent.

Precursors for the photodeposition of Pd on ZnO include $PdCl_2$[115,116,118] and H_2PdCl_4.[117] Methanol,[115] ethanol,[116] and acetic acid[118] have been used as sacrificial agents for the photodeposition of Pd on ZnO. Chang et al.,[116] who used ethanol in their photodeposition procedure but did not purge with an inert gas, observed a Pd $3d_{5/2}$ binding energy peak corresponding to PdO, in addition to a peak corresponding to metallic Pd, when the sample was analyzed by XPS. The authors claimed that they did not observe PdO through XRD and transmission electron microscopic (TEM) studies, and therefore they assigned the observed PdO signal to ion-sorbed oxygen coordinating with the Pd surface. However, surface oxidation of nanoparticulate by prolonged extensive exposure to atmospheric conditions is quite common, and therefore we anticipate this ion-sorbed oxygen should be interpreted as surface PdO. Remarkably, Jin et al.,[117] who did not use any sacrificial agent or gas purging (but did use a different precursor), did not observe a binding energy peak corresponding with PdO, suggesting that in their procedure metallic Pd was formed selectively and was not prone to surface oxidation. Liqiang et al.,[118] who used both a sacrificial agent and nitrogen purging, also observed metallic Pd formation. Remarkable is that Jin et al. report a Pd $3d_{5/2}$ peak at 334.5 eV, whereas Liqiang et al. report a Pd $3d_{5/2}$ peak at 335.5 eV. Bulk Pd has a $3d_{5/2}$ peak at 335.1 eV, so the lower energy of 334.5 eV is in less agreement with literature.[107] Both Jin and Liqiang and their co-workers have looked into optimal Pd loadings. Jin et al. found an optimal loading of 0.05 mol % (corresponding with 0.065 wt %) Pd on ZnO nanorods for rhodamine B degradation, whereas Liqiang et al. found an optimum of 0.5 wt % Pd on ZnO nanoparticles in photocatalytic degradation of n-C_7H_{16}. In summary, photodeposition conditions appear to be not very determinative for the obtained oxidation state of Pd on ZnO, although a nitrogen purge and sacrificial agent seem to favor reduced Pd particles. Very little is known on the effect of photodeposition conditions on the obtained Pd particle size, and a systematic study is recommended.

Gomathisankar et al.[88] focused on the deposition of Cu particles on ZnO. Copper was photodeposited on ZnO with methanol as a sacrificial agent, while hydrogen evolution was measured in situ. The authors applied illumination from a 500 W xenon lamp and measured a light intensity of 1.0 mW/cm^2 in the 320−410 nm range. The authors found that a maximum in H_2 formation yield (from methanol reforming) was reached when 6

DOI: 10.1021/acs.chemrev.6b00327
Chem. Rev. 2016, 116, 14587−14619

wt % of Cu was deposited on ZnO. Through photoluminescence studies, the authors show that photodeposition of Cu suppressed electron/hole recombination, indicating that Cu acts as an electron trapping site. The stability of Cu was not discussed in detail, while oxidation of as-deposited Cu by in ZnO-generated holes is feasible. Additional H_2 generation can be assigned to proton reduction, with Cu acting as a sacrificial agent. This is illustrated by the overview of redox potentials in Figure 11.

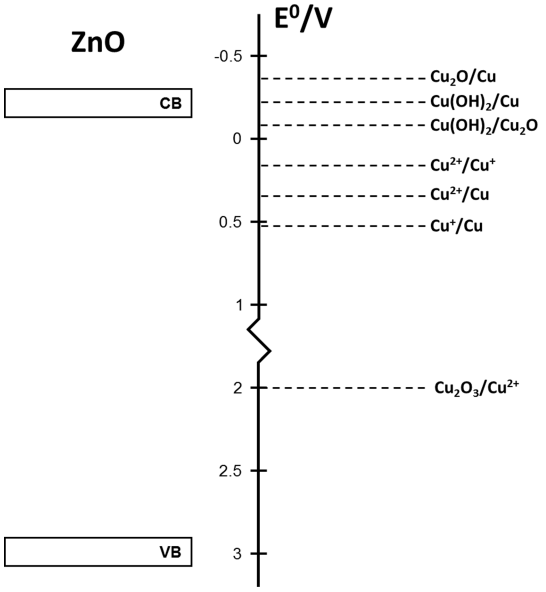

Figure 11. Band positions of ZnO (left) and redox potentials of several Cu species (right) vs NHE. Values are taken from ref 4. Clearly, Cu salts can be reduced on the surface of ZnO, but as-deposited Cu can also be oxidized.

4. PHOTODEPOSITION OF PARTICLES ON WO_3

Tungsten oxide (WO_3) is another semiconductor that is of significant interest to the community studying photocatalysis. Although its conduction band energy level is not at a favorable position for the reduction of protons (see Figure 3), it is nontoxic, stable under acidic conditions, and has a relative narrow band gap.[130−133] The latter makes the material very suitable for solar-driven photocatalysis, for example, in purification of water[134,135] or air.[136,137] Also of interest is the implementation of WO_3 in a Z-scheme for full water splitting.[31,138,139] Recent studies have demonstrated that WO_3 can be loaded through photodeposition with Pt,[31,32,133,135,136,140−154] Pd,[155,156] Ag,[7,157] and Au.[154,158−160] In many cases, an increase in photocatalytic activity has been observed. Finally, Reiche et al.[161] have demonstrated that Cu^{2+} removal from aqueous solutions is possible by performing photodeposition of Cu on WO_3. Copper removal is usually carried out by electrolysis, ion exchange, adsorption on activated carbon, chemical precipitation, reverse osmosis, or solvent extraction, but these methods are not effective at low concentrations. Photocatalytic deposition of copper onto semiconductor surfaces (mainly TiO_2) has been proposed as a low-cost and efficient technique.[162] In section 4.1, we will extensively evaluate the deposition of Pt on WO_3.

4.1. Photodeposition of Pt on WO_3

In recent years, photodeposition of Pt on WO_3 has gained widespread attention. Multiple studies have shown that loading tungsten oxide with Pt nanoparticles by photodeposition can enhance the photocatalytic activity in oxidation of pollutants in wastewater or air, for example, 4-chlorophenol, methyl orange, isopropyl alcohol, or ethylene.[133,135,136,140,145] For example, in a study by Abe et al.,[140] photocatalytic decomposition of acetic acid, acetaldehyde, and isopropyl alcohol (IPA) was studied by use of (Pt/)WO_3 under visible-light irradiation ($400 < \lambda < 500$ nm). Unloaded WO_3 showed some activity in the decomposition of acetaldehyde, but for acetic acid and isopropyl alcohol this was hardly present. When photodeposition of Pt on WO_3 was performed, activities were enhanced drastically: 30- and 100-fold increases in rates of acetic acid and IPA decomposition, respectively, were observed. For acetaldehyde, an increase also took place, but it was not as dramatic as for the other two compounds. It should be noted that different optimal loadings were found for the respective reactions (1 wt % Pt for acetic acid decomposition, 0.1 wt % for acetaldehyde, and 0.5 wt % for IPA); the origin of these different optimal loadings is unknown and requires further study. For example, photocatalytic decomposition of acetic acid is depicted in Figure 12. Upon visible-light

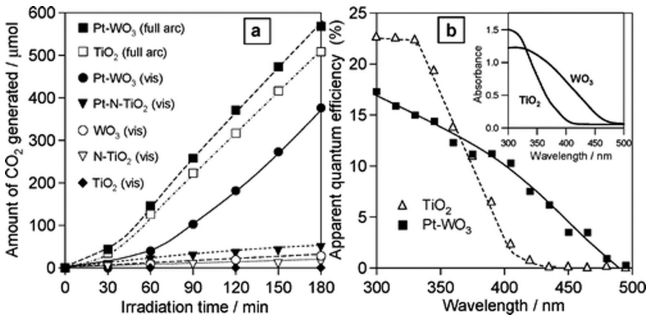

Figure 12. (a) Photocatalytic CO_2 production from acetic acid degradation with different photocatalysts at either full-arc ($300 < \lambda < 500$ nm) or visible-light ($400 < \lambda < 500$ nm) illumination. (b) Action spectra of photocatalytic degradation of acetic acid with TiO_2 or Pt/WO_3. Reprinted with permission from ref 140. Copyright 2008 American Chemical Society.

activation (Figure 12a), the activity of WO_3 is significantly improved by Pt deposition (Pt/WO_3), even being significantly higher as compared to TiO_2. This is related to the improved light-absorption properties of WO_3 (Figure 12b).

An explanation for the positive effect of Pt has been provided by the authors as well. For oxidation of the mentioned compounds, the corresponding reduction reaction has to be the reduction of oxygen:

$$O_2 + e^- \rightarrow O_2^- \qquad -0.284 \text{ V vs NHE} \tag{6}$$

$$O_2 + H^+ + e^- \rightarrow HO_2 \qquad -0.046 \text{ V vs NHE} \tag{7}$$

The conduction band of WO_3 is not at a favorable position for these reduction reactions, meaning that single-electron reduction of oxygen cannot be performed with WO_3. However, theoretically, the photocatalyst should be able to perform simultaneous multielectron reactions in O_2 reduction:

$$O_2 + 2H^+ + 2e^- \rightarrow H_2O_2 \qquad +0.682 \text{ V vs NHE} \tag{8}$$

$$O_2 + 4H^+ + 4e^- \rightarrow 2H_2O \qquad +1.23 \text{ V vs NHE} \tag{9}$$

Abe et al.[140] discussed that Pt nanoparticles might act as traps for electrons, making the as-mentioned multielectron reactions feasible. Indeed, the authors have shown convincingly with

DOI: 10.1021/acs.chemrev.6b00327
Chem. Rev. 2016, 116, 14587−14619

photoacoustic spectroscopic measurements that photoexcited electrons can react with O_2 when Pt is loaded on the WO_3 surface. Some researchers have discussed as well that the lack of single electron transfer, producing $O_2^{-\bullet}$ or $HO_2^{\bullet}$, has significant (positive) consequences for the selectivity of Pt/WO_3 in photocatalysis.[141,143,144]

The formation of H_2O_2 in aqueous-phase photocatalytic experiments with Pt/WO_3 (eq 8) has been confirmed by several studies.[133,141−143] Kim et al.[133] used photodeposition to prepare Pt/WO_3 (typically 0.5 wt % Pt), which was used to photodegrade multiple organic components under visible-light illumination (λ > 420 nm). The authors demonstrated that $OH^{\bullet}$ radicals are produced through the photoreductive decomposition of H_2O_2. Pt was found to positively affect the rate of H_2O_2 production in the initial phase of the photocatalytic experiments (see Figure 13). The latter could only have formed through the earlier

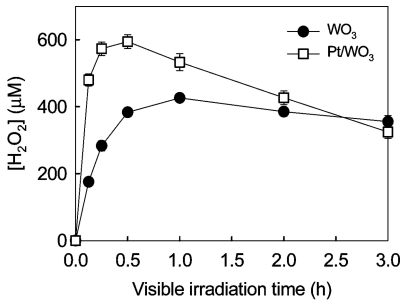

Figure 13. H_2O_2 production as a function of irradiation time as measured by Kim et al.[133] Suspensions of WO_3 and Pt/WO_3 (0.5 g/L, initial pH = 3.0) were illuminated with visible light (λ > 420 nm); methanol (0.8 M) acted as an electron donor. Reprinted with permission from ref 133. Copyright 2010 American Chemical Society.

mentioned two-electron reduction of oxygen. Tomita et al.[141] confirmed convincingly that photocatalytic phenol production from benzene took place through $OH^{\bullet}$ radical attacks, although they propose that formation of $OH^{\bullet}$ radicals is also feasible by the oxidation of water.

As evident from the information provided above, studies have mainly focused on the performance of Pt/WO_3 in photocatalysis, while optimization of the photodeposition procedure used to prepare Pt nanoparticles has received significantly less attention. In most cases methanol has been used as a sacrificial agent,[133,136,141,143,145−148] although ethanol[148,154] and oxalic acid[160] have been used as well. In some cases, photodeposition was initiated without a sacrificial agent, and methanol was added in a later stage.[135,140,149] To the best of our knowledge, it is not clear why this was done. H_2PtCl_6 has always been used as a precursor. Other process parameters applied in the literature are less consistent. For instance, some authors made use of a purge of inert gas,[136,143,148] whereas others do not specifically mention this.[135,141,149,150] Also, different illumination sources and times were used in photodeposition. For instance, Kim et al.[133] used 30 min of illumination with a 200 W Hg lamp, whereas Abe et al.[140] used 4 h of illumination (of which 2 h were with MeOH) with a 300 W Xe lamp in combination with a cutoff filter at 400 nm. Qamar et al.[148] even demonstrated that photodeposition could be achieved with a 355 nm laser beam rather than with conventional illumination. In this study, higher photocatalytic activity in R6G degradation was observed when Pt/WO_3 was prepared through 1 h of laser irradiation rather than by 1 h of conventional illumination.

The morphology of WO_3 was also different between photodeposition studies. Some authors used commercial WO_3,[133,143,145] whereas others synthesized their own WO_3 particles.[148,150−152] Some researchers tried to photodeposit Pt on different WO_3 samples, either by using different commercial WO_3 brands or by synthesizing the WO_3 themselves.[135,136,141,144,147,153] In some cases the Pt loading served only to activate WO_3 and consequently only the Pt/WO_3 samples were compared.[135,141,144] In other cases the activities of different WO_3 samples were compared before and after loading of platinum.[136,147,153] For these studies, quite different results have been obtained. Both Xu et al.[147] and Aminian and Ye[153] did not observe any change in the order of photocatalytic activity in acetic acid or isopropyl alcohol (IPA) degradation between different self-synthesized WO_3 samples before and after loading with Pt. However, in the latter case a comparison was also made with commercial WO_3, which became relatively more active than the self-synthesized samples after Pt deposition. Also, it is noteworthy that the Pt/WO_3 samples already showed some activity in the dark in IPA decomposition.

In an interesting study by Wicaksana et al.,[136] not only the influence of morphology on the photodeposition process but also the influence of the type of illumination was investigated. The authors synthesized WO_3 particles with different morphologies and different crystal structures, and they performed photodeposition of Pt particles on these crystals with either 3 h of visible-light illumination or 1 h of UV illumination. From TEM studies, the authors concluded that use of different WO_3 samples (hexagonal nanorod bundles, monoclinic nanocubes with some orthorhombic $WO_3 \cdot {}^1/_3H_2O$, and monoclinic, commercial WO_3 nanoparticles) will result in different kinds of Pt deposits (Figure 14). Also the applied wavelengths of illumination have a significant effect on the obtained Pt morphology. It should be noted that XPS studies on as-synthesized, platinized nanocubes demonstrated that Pt was not purely metallic (Pt^0), but slightly oxidic (Pt^{II}). When visible-light illumination was employed, the relative Pt^{II} amount was considerably larger than when UV illumination was used. The authors suggest that the total amount of absorbed visible photons was not sufficient to fully reduce the Pt precursor. For all samples, the authors observed a higher photocatalytic activity in (gas-phase) ethylene conversion when UV light was employed rather than visible light. Remarkably, loading the monoclinic WO_3 samples with Pt resulted in a larger increase in photocatalytic activity than when hexagonal WO_3 nanobundles were used. Hence, the order of activity of WO_3 samples was different before and after Pt loading.

A parameter that has been studied in some detail is the percentage of weight loading on the photocatalytic activity of Pt/WO_3.[145,154] For instance, Sclafani et al.[145] have prepared Pt/WO_3 with different loadings of Pt (ranging from 0.5 to 3 wt %). In their photodeposition procedure, methanol was used as a sacrificial agent, a nitrogen purge was applied to remove O_2 from solution, and illumination times of 24−48 h were used, depending on the amount of Pt to be reduced. Illumination was stopped when the MeOH concentration remained constant. The as-prepared Pt/WO_3 samples were analyzed by several techniques, including XPS. The XPS spectra showed that Pt/WO_3 with Pt loading of 0.5 or 1 wt % was oxidic in nature (Pt^{II}), whereas the other samples contained metallic Pt^0. This difference in oxidation state of the Pt is surprising, as we would expect that this state would be dependent on photodeposition parameters such as the presence of a sacrificial reagent and/or purging with

DOI: 10.1021/acs.chemrev.6b00327
Chem. Rev. 2016, 116, 14587−14619

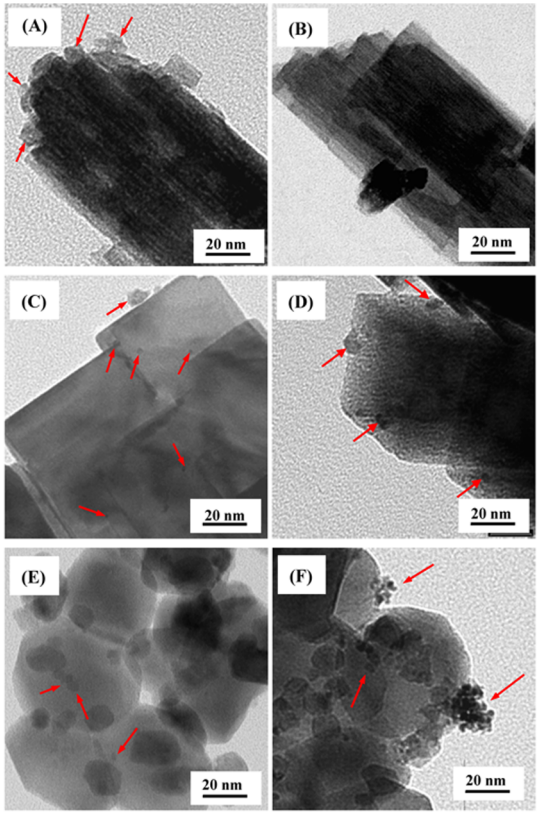

Figure 14. TEM images of Pt/WO_3 obtained by photodeposition of Pt on (a, b) WO_3 nanorod bundles, (c, d) WO_3 nanocubes, and (e, f) commercial WO_3. Photodeposition was performed with (a, c, e) UV-A light or (b, d, f) visible light. Pt deposits are indicated with arrows. Reprinted with permission from ref 136. Copyright 2014 Multidisciplinary Digital Publishing Institute.

an inert gas, not on the weight loading. The authors also found that an increase in platinum concentration in the precursor solution resulted in larger Pt particles. Sclafani et al.[145] demonstrated in phenol photo-oxidation that samples with higher Pt weight loading (2−3 wt % compared to 0.5−1 wt %) showed higher photoactivity. In their discussion, they attributed this to differences in Pt oxidation state: metallic Pt is typically significantly more effective in catalyzing reduction reactions.

Qamar et al.[154] optimized the loading of Pt in Pt/WO_3 in the photo-oxidation reaction of methyl orange. They showed that 1 wt % was the optimal loading, obtained after 6 h of illumination in their (conventional) photodeposition setup. At lower illumination times, lower activities were observed, likely the result of incomplete Pt photodeposition. Other studies have looked at the optimal loading of Pt in photocatalytic degradation of acetic acid (1 wt %[140,147] or 1.5 wt %[146]), acetaldehyde (0.1 wt %),[140] isopropyl alcohol (0.5 wt %),[140] and amaranth (1 wt %).[149] A loading of 0.2 wt % turned out to be optimal for the partial photo-oxidation of cyclohexane,[143] and 0.1 wt % was optimal for production of phenol from benzene.[141]

Despite the many different parameters used in photodeposition studies, the particle size of Pt is often remarkably similar. In most cases this is, on average, in the range 2−10 nm,[133,140,141] with the exception of one study where Pt clusters of 30 nm were reported.[146] Indeed, Shiraishi et al.[143] found that Pt particle size was more or less independent of Pt loading (with methanol as a sacrificial reagent in the photodeposition). They found that at 0.2 wt %, the average Pt particle size was 4.7 nm, and at 1.3 wt %, the average Pt particle size was 4.8 nm. Still, these results are somewhat surprising. Clustered growth of Pt particles has been shown for Pt on TiO_2[42] or Ag on ZnO,[72,73] and we do not exclude this phenomenon for WO_3. Also, Sclafani et al.[145] advocated an increase in Pt particle size as a function of increased Pt loading on WO_3.

From these results, it becomes clear that metallic Pt is necessary for effective photocatalysis, but optimization of process parameters is needed during photodeposition to obtain small Pt^0 particles and high catalytic performance. A summary of the current standing and procedures used is provided in Scheme 3.

Scheme 3. Overview of Process Parameters Used in Photodeposition of Pt on WO_3[a]

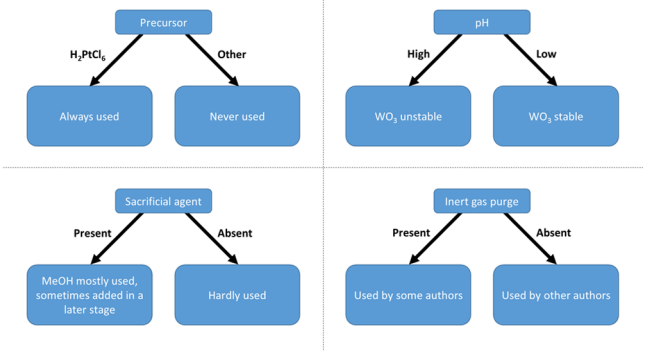

[a]Generally, a sacrificial agent and inert purge will benefit the formation of Pt^0 particles, although the effect of these parameters on the obtained size of the particles is unclear. Photodeposition needs to be performed at acidic pH to prevent dissolution of WO_3.

4.2. Photodeposition of Other Metals on WO_3

Besides Pt, other noble metals have been photodeposited on WO_3 as well, such as Au,[154,158−160] Ag,[7,157] and Pd.[155,156] Qamar et al.[154] demonstrated that photodeposition of Au on WO_3 might be less interesting than Pt. The photocatalytic activity of WO_3 in methyl orange and 2,4-dichlorophenoxyacetic acid decomposition was drastically enhanced when Pt was photodeposited on the sample, whereas Au turned out to be detrimental for this activity. The authors attributed this difference to the size of the Pt particles (2−4 nm at 1 wt % loading) and the Au particles (10−15 nm at 1 wt % loading). They claimed that shadowing of the WO_3 took place due to the relatively large size of the Au particles. In contrast, Karácsonyi et al.[160] and Iliev et al.[159] observed higher activities in oxalic acid degradation for Au/WO_3 over, respectively, Pt/WO_3 and bare WO_3.

In photodeposition of Ag and of Pd on WO_3, enhancements in photocatalytic activity have been observed: for Ag/WO_3, in the decolorization of Acid Red 88[157] and in acetaldehyde degradation,[7] and for Pd/WO_3, in methylene blue,[156] oleic acid,[155] and acetaldehyde degradation.[155,156] It should be noted that in the studies concerning decolorization of Acid Red 88, an even further improvement in activity was observed when CuO was additionally impregnated on Ag/WO_3. Generally, as with Pt, the increased activity was attributed to Ag or Pd acting as electron-transfer catalysts, thus promoting charge separation. As shown for Pt/WO_3 by Kim et al.,[133] Katsumata et al.[157] demonstrated that, for Ag/WO_3, $OH^\bullet$ radicals are formed due to photoreduction of oxygen under visible light. The authors observed initially H_2O_2 production as well, and they attributed the $OH^\bullet$ formation to H_2O_2 decomposition. Strangely, the

DOI: 10.1021/acs.chemrev.6b00327
Chem. Rev. 2016, 116, 14587−14619

concentration of H_2O_2 decreased after 15 min in the experiment, likely due to reaction with additional electrons. H_2O_2 formed by Pd/WO_3 was also discussed by Sakai et al.[156] However, these authors attributed the formation of H_2O_2 to superoxide formation. As the conduction band of WO_3 is not at a favorable position for this formation, we think it is more likely that H_2O_2 was formed due to the multielectron reduction reaction of oxygen (eq 8).

It should be noted that in some applications Ag photodeposition was merely performed, since $AgNO_3$ was used as a sacrificial electron acceptor in water oxidation with WO_3[163−165] or even Pt/WO_3.[141,166] When formation of $OH^•$ takes place (due to H_2O_2 decomposition), it should be kept in mind that the highly reactive nature of the radicals can also oxidize metallic nanoparticles such as Ag to Ag^+. This has not been extensively addressed.

In the photodeposition of Pd on WO_3, Sakai et al.[156] have demonstrated that reduction of $PdCl_2$ to predominantly metallic Pd can take place with black-light illumination (i.e., UV illumination) in deaerated conditions (under Ar), surprisingly without the addition of a sacrificial agent. The authors have investigated the optimum loading of Pd on WO_3 thoroughly, comparing activity in the degradation of aqueous methylene blue (MB) and gaseous acetaldehyde. Like Abe et al.[140] for Pt/WO_3, they found that the optimum loading differed for different photocatalytic reactions: 0.5 wt % Pd was optimal for enhanced MB degradation, whereas 0.1 wt % Pd was optimal for acetaldehyde decomposition. In the studies of Abe et al.,[140] the rate of acetaldehyde decomposition at optimal Pt loading (0.1 wt %) was significantly lower than for Pd/WO_3 in the study of Sakai et al.[156] This would imply that Pd/WO_3 not only would be cheaper to use than Pt/WO_3 for acetaldehyde decomposition ($22.70/g of Pd as opposed to $35.59/g of Pt as of August 22, 2016)[167] but also might also be more effective. However, to corroborate this conclusion, acetaldehyde decomposition should be performed with WO_3, Pt/WO_3, and Pd/WO_3 under identical reaction conditions.

Shibuya and Miyauchi[155] studied the photodeposition of Pd on films of hexagonal WO_3 nanotrees in the presence of ethanol at different irradiation wavelengths (λ = 330, 400, 500, or 600 nm). The location where Pd was deposited was dependent on the wavelength. At 400 nm, the Pd particle density at a lower position from the top of the nanotrees was significantly higher than when 330 nm was used. The authors attribute this to visible light penetrating deeper into the WO_3 nanotrees than UV light. Also, the nanotrees were more crystalline at the bottom than at the top, explaining the absence of Pd particles on top of the nanotrees when visible light was used. Shibuya and Miyauchi[155] also observed positioning of Pd particles at the bottom of the nanotrees at λ = 500 and 600 nm. However, hexagonal WO_3 should not be able to reduce Pd at these wavelengths due to a too-large band gap.[168,169] The authors studied the photocatalytic activity of their Pd/WO_3 systems for decomposition of oleic acid and acetaldehyde, and they found that when the Pd particles were deposited on the bottom rather than on the top, this had a beneficial influence on photocatalytic activity. The authors attributed this, among others, to Pd particles deposited at the top shadowing the WO_3 nanotrees.

4.3. Photodeposition of Ag/AgX (X = Cl or Br) Particles on WO_3

In recent years, loading WO_3 species with Ag/AgX (X = Cl or Br) has also attracted attention.[170−172] These core/shell particles are plasmonic photocatalysts, where the core is made of a AgX semiconductor and the shell is made of Ag.[170] Although the synthetic procedure of these cocatalysts is not through conventional photodeposition (where a metal ion in solution is reduced or oxidized on the surface of the photocatalyst), it is worth mentioning that an easy photochemical reduction route is used to create these particles. Typically, AgX crystals are deposited on (a form of) WO_3 particles, for example, by ion exchange.[172] Then illumination takes place and the outer AgX is reduced to Ag, creating a Ag/AgX particle. As-synthesized Ag/AgX/WO_3 species have been used for several photocatalytic applications: $Ag/AgBr/WO_3·H_2O$ for destruction of *Escherichia coli* (and degradation of methyl orange),[172] Ag/AgCl/WO_3 nanoplates for decomposition of RhB,[171] and Ag/AgCl/$W_{18}O_{49}$ for degradation of methyl orange.[170]

4.4. Photodeposition on Composite Photocatalysts Containing WO_3

Photodeposition does not necessarily have to be performed on a single semiconductor. Studies are known where the concept of photodeposition was applied to prepare metal-loaded composite photocatalysts. WO_3 has been part of various composites in photocatalysis, including WO_3/TiO_2,[159,160,173,174] WO_3/C_3N_4,[175] $CaFe_2O_4/WO_3$,[176] and $CoFe_2O_4/WO_3$.[177] In such a case, either (i) the photodeposition has been performed on one of the two photocatalysts first, after which the other photocatalyst was added,[160,175,176] or (ii) the composite photocatalyst was synthesized first, after which the photodeposition took place.[159,173,174,177] For example, Karácsonyi et al.[160] performed photodeposition of Au and Pt on WO_3/TiO_2 composites. In this case, Au or Pt was photodeposited on either TiO_2 or WO_3 first. Afterward, the other metal oxide was added to the system. Reference samples (Pt/WO_3, Au/WO_3, Pt/TiO_2, and Au/TiO_2) were made as well. The production of H_2 was studied when oxalic acid was degraded in O_2-deficient conditions under UV illumination. The performance of the catalysts, from most to least active, was $Pt/TiO_2 > Au/TiO_2 > Au/WO_3 > Pt/WO_3$. The poor performance of Pt/WO_3 is not surprising: after all, there is no O_2 to be reduced and the CB of WO_3 is at an unfavorable position for the production of H_2. The authors found that, for their hybrid systems, 3.5−10 wt % WO_3, relative to TiO_2, and 1 wt % of the cocatalyst (Pt or Au) was in most cases optimal for the oxalic acid degradation rate. However, the best results were obtained when the noble metal was first photodeposited on TiO_2, rather than on WO_3.

5. PHOTODEPOSITION OF NANOPARTICLES ON OTHER OXIDES

Although preparation of metal nanoparticles by photodeposition has most frequently been reported for TiO_2, ZnO, and WO_3, in this section, we briefly describe other metal oxides functionalized by photodeposition.

5.1. Gallium Oxide (Ga_2O_3)

Despite the wide band gap of 4.5 eV,[93] photodeposition on Ga_2O_3 has been studied by Maeda et al.[93] and Busser et al.,[24,94] as the related compound $(Ga_{1-x}Zn_x)(N_{1-x}O_x)$ is a very promising photocatalyst (which will be discussed in section 7). Maeda et al.[93] studied, among others, the photodeposition of $Rh_{2-y}Cr_yO_3$ on β-Ga_2O_3 by irradiating a solution containing the photocatalyst, $(NH_4)RhCl_6$, and K_2CrO_4 for 4 h (λ > 200 nm, 0.5 wt % Rh, 0.75 wt % Cr). No sacrificial agent was used, but the solution was purged with inert gas. The authors demonstrated that $Rh_{2-y}Cr_yO_3/\beta$-Ga_2O_3 was roughly 10-fold more active in

DOI: 10.1021/acs.chemrev.6b00327
Chem. Rev. 2016, 116, 14587−14619

photocatalytic splitting of water than bare β-Ga_2O_3 (illumination at $\lambda > 200$ nm). Busser et al.[24] studied the two-step photodeposition of Rh/Cr_2O_3 core/shell particles on Zn-loaded Ga_2O_3 (and also on Ga_2O_3). An aqueous solution was prepared with Zn−Ga_2O_3 and methanol as a sacrificial agent. Degassing took place with N_2. While stirring, the authors added a small amount of $Na_3RhCl_6{\cdot}3H_2O$ corresponding to 0.025 wt % Rh. After 5 min, illumination was started with a Hg lamp at 350 W, resulting in the photocatalytic reduction of Rh^{3+} to Rh^0:

$$Rh^{3+}(aq) + 3e^- \rightarrow Rh^0(s) \quad (10)$$

The authors measured the production rate of H_2 in situ, evolving as a result of methanol reforming. After a plateau was reached (with a slight decreasing slope), the light was switched off and an additional amount of $Na_3RhCl_6{\cdot}3H_2O$ corresponding to 0.025 wt % was again added (Figure 15). The light was switched on

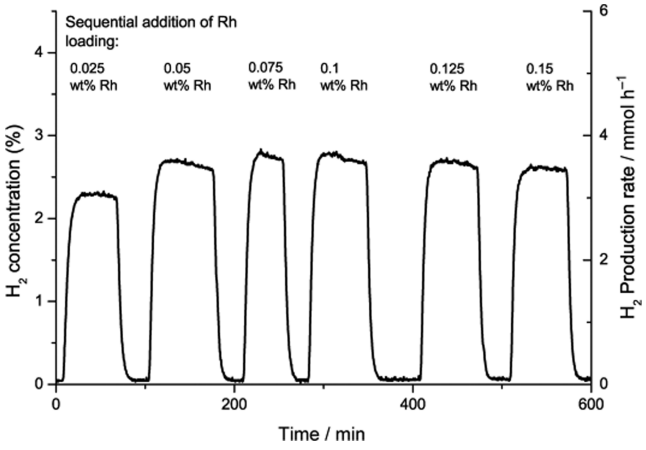

Figure 15. H_2 production measured in situ during photodeposition of Rh on Zn−Ga_2O_3. The photodeposition has been performed stepwise. Reprinted with permission from ref 24. Copyright 2012 Wiley.

once more,and again the production rate of H_2 was measured. The authors repeated these steps multiple times to find the optimal loading of Rh, which was 0.1 wt %. A similar stepwise photodeposition process was performed to obtain Rh/Cr_2O_3 particles on Zn−Ga_2O_3. In this case, (0.15 wt %) Rh/Zn−Ga_2O_3 was exposed to a solution containing K_2CrO_4, allowing the following reaction:

$$2CrO_4^{2-}(aq) + 10H^+ + 6e^- \rightarrow Cr_2O_3(s) + 5H_2O(l) \quad (11)$$

An optimum of 0.09 wt % of Cr_2O_3 was found. With the found optimal loadings, the authors demonstrated that there was a difference in H_2 production rate behavior either when stepwise photodeposition of Rh/Cr_2O_3 particles took place on Ga_2O_3 or when photodeposition took place simultaneously. Higher H_2 production rates were observed with the former. Whether Rh/Cr_2O_3 is present as core/shell particles will be discussed in section 7.

In a similar study with the same reactor, Busser et al.[94] performed two-step photodeposition of CuO_x and Cr_2O_3 on β-Ga_2O_3, with $Cu(NO_3)_2$ as precursor for the former. The authors found that photodeposition of CuO_x resulted in particles deposited on the Ga_2O_3 surface in the size range 1−10 nm (average 2 nm). The small particles corresponded to Cu_2O, whereas the larger particles corresponded to metallic Cu. XPS confirmed that Cr was present as Cr_2O_3. The authors found that small amounts of Cr were sufficient to obtain overall photocatalytic water splitting (which was not observed without Cr). With a Cr loading of 0.09 wt %, the authors found an optimal Cu loading of 0.66−1 wt % for overall water splitting. Busser et al.[94] studied the influence of the order of Cr_2O_3 and Cu photodeposition: Cr_2O_3 before, after, or simultaneously with Cu photodeposition. Sequential deposition of Cu after Cr_2O_3 resulted in the highest performance, which makes a core/shell model of CuO_x/Cr_2O_3 unlikely. The authors propose that CuO_x and Cr_2O_3 particles need to be photodeposited in close proximity to obtain excellent activity. When the two articles by Busser et al.[24,94] are compared, it seems that Rh/Cr_2O_3/Zn−Ga_2O_3 results in higher activities in photocatalytic water splitting than CuO_x + Cr_2O_3/Ga_2O_3.

5.2. Bismuth Vanadate ($BiVO_4$)

Bismuth vanadate has a narrow band gap (2.3−2.9 eV) and is, among others, considered promising for oxygen evolution reactions from water splitting under visible light, either in a Z-scheme configuration or when sacrificial agents are used.[178−181] Indeed, $AgNO_3$ is often used as a sacrificial agent.[178−180] Zhang et al.[182] prepared Ag/$BiVO_4$ films through photodeposition, where the size of the Ag particles was 10−20 nm. The Ag particles enhanced the activity of $BiVO_4$ in the photocatalytic degradation of phenol under visible light. Kohtani et al.[92] studied the photocatalytic degradation of phenol species under visible light with Ag/$BiVO_4$ powders as well, but they prepared samples through both impregnation (1.3 wt % Ag) and photodeposition (2 wt % Ag). The authors found again that Ag enhanced the photocatalytic activity, but with impregnation this enhancement was larger than with photodeposition. They attributed this to the fact that, in the case of impregnation, Ag species were also present in an oxidized form (Ag_2O and/or AgO), as demonstrated by Auger electron spectra. The authors believed that these oxidized Ag species were formed on the surface of the metallic Ag particles. Ag_2O and AgO were not detected when photodeposition was used. The authors showed that the phenol species adsorb more easily on oxidized silver, hence explaining the higher activities when impregnation was used rather than photodeposition. It is noteworthy that, in the case of photodeposition, Ag particles could not be detected with scanning electron microscopy (SEM). For impregnation, Ag particles were visible with SEM in the size range of ≤10 nm. This means that photodeposition resulted in smaller and highly dispersed particles. In the studies of both Zhang et al.[182] and Kohtani et al.,[92] no sacrificial agents and gases were used in the photodeposition process.

A very relevant study on photodeposition, concerning structure-directed reductive and oxidative photodeposition of a metal (oxide) on $BiVO_4$, has been provided by Li et al.[90] The authors demonstrate that Ag, Au, and Pt can be loaded on monoclinic $BiVO_4$ with well-defined morphology through reductive photodeposition, while MnO_x and PbO_2 nanoparticles are formed through oxidative photodeposition. We will discuss the geometric distribution intensively in section 8, but for now we will focus on the oxidation state of the obtained metal nanoparticles. Photodeposition took place in an aqueous solution with $HAuCl_4$, H_2PtCl_6, or $AgNO_3$ without the use of a sacrificial agent or gas purge. The authors found through XPS that, besides metallic Pt, also a small amount of PtO was formed, whereas for Ag and Au only metallic particles were identified. It should be noted that the binding energies of metallic Ag were found at 374.2 and 368.2 eV. In contrast to the many studies of

DOI: 10.1021/acs.chemrev.6b00327
Chem. Rev. 2016, 116, 14587−14619

Ag/ZnO discussed earlier in this review, the XPS data are fully explicable by the formation of metallic Ag, and ionic Ag species are thus not formed on $BiVO_4$. The as-deposited particle sizes were found to be dependent on the metal, with Ag particles being the largest, followed by Au, and last Pt.

Photodeposition of Pt on $BiVO_4$ has been performed by other authors as well. Murakami et al.[183] have demonstrated that Pt photodeposition enhances the activity of $BiVO_4$/silica composites for acetaldehyde decomposition, with 1 wt % Pt being the optimal loading. The authors used $H_2PtCl_6{\cdot}6H_2O$ as a precursor, ethanol as a sacrificial agent, and a purge of nitrogen. Bard and coworkers have also studied the photodeposition of Pt on films of W-doped $BiVO_4$ (BiVW-O)[184] and on bare $BiVO_4$ and reduced graphene oxide (RG-O)/$BiVO_4$ composites.[185] The authors performed the photodeposition with H_2PtCl_6 as a precursor, methanol as a sacrificial agent, and no gas purge. Increased water oxidation photocurrents were observed for BiVW-O and RG-O/$BiVO_4$ films when loaded with Pt. Interestingly, XPS studies revealed that Pt on BiVW-O was mainly present as PtO_2, but some metallic Pt was observed as well. The latter became oxidized after use in the oxygen evolution reaction (OER). The authors discussed that they likely observed a PtO_2 surface layer on metallic Pt.

5.3. Tantalum Oxide (Ta_2O_5)

Similar to gallium oxide, tantalum oxide (Ta_2O_5) has a wide band gap (4.0 eV).[95,186,187] Interestingly, Zhou et al.[95] demonstrate that photocatalytic activities under visible-light illumination can be achieved by performing photodeposition of plasmonic Au on mesoporous Ta_2O_5. The precursor was $HAuCl_4$, methanol was used as sacrificial reagent, N_2 purging was applied, and the temperature was kept constant at room temperature by use of a water bath. They found an optimum loading of 1.0 wt % Au for photocatalytic reforming of methanol yielding hydrogen. The authors demonstrate that the particle size of Au can be controlled by changing the irradiation time (10, 15, and 20 nm after 10 min, 1 h, and 3 h respectively). An increase in photocatalytic hydrogen production from methanol (λ > 400 nm) was observed with increasing particle size, which the authors attribute to a stronger SPR effect. However, the authors did not measure the Au loading as a function of irradiation time by using, for example, inductively coupled plasma (ICP) methods. Therefore, it cannot be assumed that the loading was identical for all three samples, especially when different photodeposition times were employed. The difference in photocatalytic activity could therefore also (partly) be the result of different loading. Still, we agree with Zhou et al.[95] that the size of the metallic nanoparticles is a crucial aspect to induce surface plasmon resonance, thus playing an important role in the final activity of Au-loaded mesoporous Ta_2O_5.

5.4. Strontium Titanate ($SrTiO_3$)

Aside from TiO_2, one of the more frequently studied photocatalysts is strontium titanate ($SrTiO_3$). The band gap of $SrTiO_3$ is relatively large (3.2 eV),[9] but many researchers overcome this problem by introducing one or multiple dopants in the crystal lattice. Examples of dopants include but are not limited to rhodium,[96,181,188] chromium,[189,190] and niobium.[191,192] Often (doped) $SrTiO_3$ is used as a hydrogen-generating photocatalyst, either with the use of a sacrificial agent or in Z-scheme applications for overall water splitting.[96,138,181,193,194] Many authors make use of photodeposition to load a catalyst on (doped) $SrTiO_3$. Often Pt has been used.[138,139,181,189,194−201] However, in a study by Sasaki et al.,[96] it was demonstrated that Ru might be more effective than Pt. When a Z-scheme configuration of M/$SrTiO_3$:Rh-$BiVO_4$ (M = 0.7 wt % Ru or 0.1 wt % Pt) was tested for overall water splitting under visible-light illumination, the activity of the two systems was initially similar, with the Pt/$SrTiO_3$:Rh-$BiVO_4$ system being slightly more active than Ru/$SrTiO_3$:Rh-$BiVO_4$. However, the hydrogen and oxygen evolution rates observed for the Pt/$SrTiO_3$:Rh-$BiVO_4$ system decreased over the course of time, whereas the H_2 and O_2 generation rate of the Ru/$SrTiO_3$:Rh-$BiVO_4$ system remained stable. The authors attributed this to suppression of the back-reaction of hydrogen and oxygen on the Ru cocatalyst compared to the Pt cocatalyst. This might have been related to the oxidation state of as-deposited particles: Sasaki et al.[96] discuss that the surface of Pt was metallic, whereas the surface of Ru was oxidized after the photodeposition procedure. Aside from photodeposition of Pt and Ru, Sasaki et al.[96] also performed photodeposition of Ni, Rh, and Ag, as well as impregnation of Au, Fe_2O_3, NiO_x, and RuO_2. When investigated for activity in Z-scheme water splitting with WO_3 under visible light, none of these materials was as active as Pt or Ru. More recently, additional studies have appeared where photodeposition was used to obtain Ru-loaded $SrTiO_3$:Rh[202−206] and was claimed to yield more effective catalysts than Pt-deposited samples.

Although photodeposition is a popular technique to load a cocatalyst on (doped) $SrTiO_3$, it is remarkable that the photodeposition procedure is hardly addressed in detail. XPS studies are necessary to compare performance of Pt- or Ru-loaded (doped) $SrTiO_3$. Some detail is provided by Sasaki et al.[96] They observed metallic Pt on $SrTiO_3$:Rh after photodeposition in the presence of a sacrificial agent and purging with Ar, whereas Lee et al.[200] observed platinum oxide after photodeposition on $SrTiO_3$:Rh in the absence of a sacrificial agent and without an inert gas purge. Finally, Yu et al.[181] also performed photodeposition in the absence of a sacrificial agent and without an inert gas purge, but they found both platinum oxide and metallic platinum on $SrTiO_3$:Rh. These authors attribute platinum oxide formation to air oxidation of Pt during storage. This discrepancy in results should be further investigated.

Aside from the photodeposition of Pt and Ru, photodeposition of Ag on (doped) $SrTiO_3$ has also been performed.[207−214] In contrast to Pt and Ru, the photodeposition of Ag has often been studied on a more fundamental level. For instance, Sun et al.[210] studied two different photodeposition methods to obtain Ag-loaded $SrTiO_3$ nanotube arrays. One method involved a "classical" photodeposition method for 3 h in $AgNO_3$ solution without a sacrificial agent. The other method involved immersion of $SrTiO_3$ nanotube arrays in $AgNO_3$ solution at 60 °C for 24 h. Afterward, as-prepared samples were irradiated for 1 h in methanol. In the first case, hardly any Ag particles were deposited on the $SrTiO_3$ nanotubes, whereas Ag particles were obviously present when the second photodeposition method was used. XPS results confirmed the formation of metallic Ag. The photocatalytic activity of $SrTiO_3$ nanotube arrays in methyl orange degradation increased when they were loaded with Ag. In a different article,[207] the authors demonstrated that photodeposition of Ag on $SrTiO_3$ nanotube arrays also results in increased activity in photocatalytic hydrogen production with methanol as a sacrificial agent.

Interestingly, Tanaka et al.[212] demonstrated that when photodeposition of Ag is performed on Nb:$SrTiO_3$ with $AgNO_3$ as a precursor, $Ag_7O_8NO_3$ formation rather than Ag formation can take place as well. The authors found that $Ag_7O_8NO_3$ was formed on the crystal surface through photo-

DOI: 10.1021/acs.chemrev.6b00327
Chem. Rev. 2016, 116, 14587−14619

catalytic oxidation, whereas metallic Ag was found along the edges through photoreduction. This implies that structure-directed deposition is taking place at the Nb:$SrTiO_3$ crystal. Passivation of the edges resulted in metallic Ag being deposited on the crystal surface. For undoped $SrTiO_3$, $Ag_7O_8NO_3$ formation was considerably more difficult, although not impossible, as it did occur at high concentrations of $AgNO_3$.

Photodeposition of Ni/NiO,[215] MnO_x,[191] PbO_2,[201,214] and $Rh_{2-y}Cr_yO_3$[93] has also been performed on (doped) $SrTiO_3$. It is interesting to point out that Yoshida et al.[191] demonstrated that the light intensity used in the photodeposition procedure of MnO_x on Nb:$SrTiO_3$ has consequences for the morphology of MnO_x. In one case, MnO_x particles with sizes of 50−100 nm were deposited, whereas in another case MnO_x thin films were deposited on the Nb:$SrTiO_3$ substrate. Using in situ Mn K-edge XAFS spectroscopy, the authors demonstrated that MnO_x species act as oxygen evolution cocatalysts most effectively when present as a thin film, under UV illumination, and at a bias of 1.0 V. Mn^{3+} species changed to Mn^{4+} species during the water oxidation reaction.

6. PHOTODEPOSITION OF NANOPARTICLES ON CDS

6.1. Introduction

CdS has a narrow band gap of only ∼2.4 eV, while the conduction band minimum at −0.9 V versus NHE allows unbiased proton reduction upon visible-light illumination (H^+/H_2 reduction potential is 0 V vs NHE).[9,99] However, a major disadvantage of CdS is its instability, assigned to photocorrosion (oxidation and dissolution of Cd^{2+}):

$$CdS + 2h^+ \rightarrow Cd^{2+} + S \quad (12)$$

Therefore, a sacrificial agent for hole scavenging needs to be present during the photodeposition process, preventing reaction 12 from happening. For example, sulfide (in the form of Na_2S) can be introduced in the reaction mixture, which is converted by the following reaction:[216]

$$S^{2-} + 2h^+ \rightarrow S \quad (13)$$

Besides sulfide, many other sacrificial agents (electron donors) can be applied to prevent reaction 12, including various alcohols or acids.

6.2. Comparison of Cocatalysts Inducing Hydrogen Evolution Activity

Photodeposition has been applied to functionalize CdS with a variety of metal nanoparticles. Cocatalysts other than platinum include gold,[217−221] rhodium,[216,222,223] cadmium,[224] nickel (oxides),[26,225] ruthenium,[226] and palladium.[227] In various papers, Rufus et al. discuss the photodeposition of Rh,[222,223] Ru,[226] Pt and Ir,[25] and Pd.[228] In one part of their studies, including Rh[223] and Ru,[226] they performed photodeposition on sintered pellets of CdS with metal chlorides as precursors, acetic acid as a sacrificial agent, and a 1000 W tungsten−halogen lamp as a light source. Unfortunately, it is not clear if degassing conditions were similar in all experiments (for instance, in ref 223, it is clearly stated that N_2 was used, whereas in ref 228, purging is not specifically mentioned). The authors studied the oxidation state of the metals in detail by XPS. They found that Rh was deposited as Rh_2O_3, Ru was present in different oxidation states (Ru or RuO_x, where $x = 0.5$, 1, 2, or <1), and Pd was in an oxidized state. When argon ion sputtering was applied, XPS peaks corresponding to metals in a zero oxidation state gained in intensity, suggesting an oxide shell was formed on a metal nanoparticle core. For all materials, the authors demonstrate (through photoelectrochemical studies and/or XPS) that an ohmic contact was formed between photodeposited metal and CdS. The authors thus conclude that metals are initially produced in a zero oxidation state but are likely prone to surface oxidation when exposed to air. Unfortunately, the time between sample preparation and XPS analysis was not mentioned. For Rh/CdS and Ru/CdS, an increase in photocatalytic H_2 evolution (with hole scavenger Na_2S) compared to bare CdS was observed.

In other studies, Rufus et al.[222] studied the in situ photodeposition of Rh on CdS during photocatalytic decomposition of aqueous sulfide (Na_2S). The authors demonstrate that a much higher photocatalytic activity in H_2 evolution is obtained with a CdS + $RhCl_3$ solution rather than with CdS, Rh/CdS, or Rh_2S_3/CdS in solution. They attribute this to two species being deposited on CdS: Rh and Rh_2S_3. Rh_2S_3 acts as a sulfide oxidation cocatalyst and Rh as a reduction cocatalyst, which explains the higher activities. Through photoelectrochemical characterization, it was demonstrated that CdS is less prone to photocorrosion when loaded with either Rh and Ru.[226]

In situ photodeposition of metals on CdS in solutions containing sulfide has been studied in detail,[25] revealing that the optimal order of metals to use in photocatalytic H_2 evolution is Rh > Pt > Pd > Ru ≈ Ir > Co ≈ Ni ≈ Fe. Also for Pt, in situ photodeposition resulted in higher photocatalytic activities than use of ex situ obtained Pt/CdS (Figure 16). Similar to the explanation for Rh-based catalysis, the higher activities of Pt/CdS obtained through in situ photodeposition was attributed to the simultaneous formation of metallic Pt particles and Pt sulfides. As with Rh and Rh_2S_3, the metallic Pt particles act as reduction cocatalysts, whereas the platinum sulfides act as oxidation cocatalysts (for reaction 13).

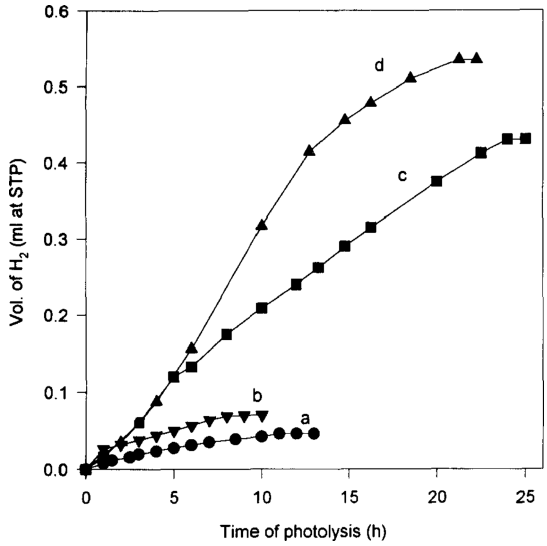

Figure 16. H_2 evolution rates measured in situ for (a) CdS, (b) CdS with 1.37 wt % Ir^{3+}, (c) 1.37 wt % Pt/CdS, and (d) CdS with 1.37 wt % Pt^{4+} (in the form of H_2PtCl_6), with Na_2S as sacrificial agent. In cases b and d, in situ photodeposition took place. Reprinted with permission from ref 25. Copyright 1995 Elsevier.

Li and co-workers[229,230] have investigated the role of several cocatalysts on CdS as well. They found through monitoring of H_2 generation during photodeposition, with lactic acid as a sacrificial agent, that the order of most active to least active cocatalyst was Pt > Ru > Rh > Pd > Au at 0.2 wt %[229] and Pt > Ru > Rh > Au at 1

DOI: 10.1021/acs.chemrev.6b00327
Chem. Rev. 2016, 116, 14587−14619

wt %.[230] This is a different order than that found by Rufus et al.,[25] likely induced by use of a different sacrificial agent (sulfide vs lactic acid). It should be noted that Li and co-workers demonstrate in their work that impregnated metal sulfides act as excellent cocatalysts as well, with MoS_2 outperforming even the noble metal cocatalysts.

Chen et al.[26,225] have studied the in situ photodeposition of nickel (NiO_x) species on CdS. Nickel acetate and methanol were used as precursor and sacrificial agent, respectively. Illumination took place with a 300 W Xe lamp and a >400 nm filter. The amount of H_2 formed was monitored during photodeposition. The authors demonstrate that higher H_2 production rates could be obtained when CdS was loaded with NiO_x (more specifically Ni_2O_3), than when 1.5 wt % Pt was loaded in situ. The authors also demonstrate that the form and amount of NiO_x deposited on CdS is dependent on the pH of the solution. Under acidic conditions almost no Ni was deposited, under neutral conditions most of the Ni was photo-oxidized in the form of Ni_2O_3, and under alkaline conditions only little more than half of the Ni was deposited as NiO. The latter formation was ascribed to Ni^{2+} depositing as $Ni(OH)_2$ on CdS. This allows the photoreduction of Ni^{2+} to Ni^0. However, Ni^0 is not stable and oxidizes to NiO. Both NiO/CdS and Ni_2O_3/CdS demonstrate enhanced activity in in situ H_2 production compared to bare CdS, where the NiO/CdS outperforms the Ni_2O_3/CdS clearly. In alkaline conditions, an optimum Ni/Cd mol ratio of 0.01 was determined. Surprisingly, formation of nickel sulfides was not extensively discussed, which appears likely under the applied process conditions.

6.3. Photodeposition of Pt on CdS

6.3.1. Overview of Reaction Conditions. The effect of reaction conditions on Pt morphology on CdS has been investigated extensively. Sacrificial agents used include methanol,[231] ethanol,[232] 2-propanol,[233] acetic acid,[99,231,234−237] triethanol amine,[238] formaldehyde,[239] a mixture of Na_2S and Na_2SO_3,[99,240,241] and ammonium sulfite $[(NH_4)_2SO_3]$.[231] In some cases, photodeposition was not performed in an aqueous solution but rather in an organic solution, such as methanol[242] or toluene.[101] An additional sacrificial agent was then added, such as triethylamine[101,242] or diisopropylethylamine.[101] Bamwenda et al.[243] used formaldehyde in methanol/water (40 vol % MeOH) solution, whereas Park et al.[244] used an aqueous solution containing Na_2S/Na_2SO_3 mixture and methanol. Some authors do not report usage of a sacrificial agent.[97,98,100,245−247]

Most of the time (hydrated) H_2PtCl_6 is used as a precursor. Other precursors are K_2PtCl_6 (for MO/CdS, MO = RuO_2 or Rh_2O_3),[248] (1,5-cyclooctadiene)dimethylplatinum(II) $[(CH_3)_2PtCOD]$,[101] and $PtCl_2$[241] (although in the supporting information for this work H_2PtCl_6 is mentioned). Fox and Pettit[100] studied the influence of precursor on the photodeposition of Pt on CdS-loaded zeolites using the precursors $Pt(NH_3)_6$ and H_2PtCl_6. Remarkably, they observed Pt on the zeolite when $Pt(NH_3)_6$ was used but none when H_2PtCl_6 was used. This was tentatively explained by $[PtCl_6]^{2-}$ ions not being able to penetrate the negatively charged zeolite pores.

As we have seen for other semiconductors, there is not much consistency in the literature on the light source used, and the applied photodeposition time. For instance, Bao et al.[245] used illumination for a period of 30 min, with a 450 W high-pressure Hg lamp, while Xin et al.[249] used illumination for 2 h with a 300 W Xe lamp. Even 24 h of illumination with a 300 W Quartzline lamp at 90 V has been reported by Harbour et al.[242] It should be noted that some authors make use of optical filters to block (part of) the UV spectrum[235,240,241,250,251] or (part of) the IR spectrum.[98,231,252,253] Bühler et al.[234] performed photodeposition of Pt on CdS (pretreated with acetic acid to remove CdO) using a water-cooled Hg immersion lamp both with and without a UV filter (λ > 300 nm). Although the weight percent Pt is similar in both cases, considerably more photoetching of CdS took place when no filter was used. This was attributed to photolysis of the sacrificial agent carboxylic acid at λ < 300 nm, resulting in strongly oxidizing radicals. The authors found that the amount of photoetching was dependent on the amount of Pt photodeposited, therefore linking the photoetching to the reduction of Pt. A higher photocatalytic activity in H_2 production was observed when no light filter was used in the photodeposition process.

A surprisingly large amount of research has been performed on the formation of H_2 during in situ photodeposition of Pt on CdS.[25,99,249−253] In these cases, photodeposition took place while H_2 production was monitored. The sacrificial agents (Na_2S,[25] Na_2S/Na_2SO_3,[99,249,250] lactic acid,[249,251] formic acid,[252,253] or methanol[249]) were thus used for both Pt and proton photoreduction. Several researchers have tried to find an optimum loading of Pt on CdS for hydrogen evolution from water.[99,233,234,243,245,251−253] Sacrificial agents used include formic acid,[243] alcohols,[246,254] sodium sulfite (Na_2SO_3),[234,237,238] sodium sulfide (Na_2S),[25,234,237] or a combination of Na_2S and Na_2SO_3.[99,233,234,237] Remarkably, different optimal Pt loadings were reported. For instance, the highest optimal Pt loading in H_2 production was found by Bao et al.[245] to be 13 wt %, whereas the lowest optimal loading was found by Li et al.[252] to be 0.025 wt %, although in an earlier study by Li et al.,[253] a somewhat higher optimal loading of 0.050 wt % was mentioned. The extreme difference in conclusions by Bao et al.[245] and Li et al.[252,253] could be explained by multiple factors. For instance, the preparation methods of CdS were different (resulting in different material properties). Also, Li et al. measured H_2 production during in situ photodeposition of Pt whereas Bao et al. measured H_2 production with ex situ obtained Pt/CdS. Furthermore, Bao et al. did not use a sacrificial agent in the photodeposition process, as opposed to Li et al., who used formic acid. Bao et al. used a combination of Na_2SO_3 and Na_2S as sacrificial agents in the H_2 evolution itself. As rightfully pointed out by Li et al., a low optimum of Pt loading would be preferable when the high cost of Pt is considered.

6.3.2. Controlling Morphology of Pt. An exemplary study where multiple photodeposition parameters were varied has been provided by Dukovic et al.[101] An Ar-ion laser (458 nm, 100 mW, 50% of beam area taken up by sample) was used to deposit Pt particles on CdS nanorods. The precursor was $(CH_3)PtCOD$, and photodeposition was performed under argon in toluene with the tertiary amines triethylamine (TEA) or diisopropylethylamine (DIPEA) as hole scavengers. The influences of illumination time, laser power, and CdS and $(CH_3)PtCOD$ concentrations were studied. Over 240 min, the amount of Pt deposited on the nanorods scaled linearly with photodeposition time. Up to 60 min, the number of Pt particles per nanorod increased, but it remained constant afterward. Subsequently, the diameter of Pt nanoparticles increased as a function of time (reaching 2.44 nm after 90 min). Not surprisingly, the authors found that increasing the laser power to 25 mW resulted in an increased rate of photodeposition. For even higher laser powers, this increase became less prominent, likely due to saturation of the number of effective charge carriers (electron−hole pairs).

DOI: 10.1021/acs.chemrev.6b00327
Chem. Rev. 2016, 116, 14587−14619

Replacing the sacrificial agents with a primary or secondary amine led to no or very little photodeposition activity, respectively. The authors explain this on the basis of inhibition of the sites, the latter in the absence of the amines being available for adsorption of the Pt precursor. The presence of the primary amine octylamine even led to complete blocking of CdS sites, inhibiting photodeposition.

Berr et al.[238] also investigated the influence of photodeposition time (λ = 366 nm) on the morphology of Pt on CdS nanorods and correlated morphology to activity in H_2 production. Photodeposition was performed with triethanolamine as hole scavenger and in the presence of the mild reducing agent ascorbic acid. In agreement with the observations of Dukovic et al.,[101] 20 min of photodeposition yields a highly uniform distribution of very small Pt particles, most of them unobservable by TEM. However, after 120 min, 90% of the nanorods were decorated with exactly one, relatively large Pt particle per nanorod (mean size 4.8 nm, see Figure 17). The authors attribute this phenomenon to a catalytic effect of subnanometer Pt particles, stimulating ascorbic acid-assisted additional growth of Pt, as illustrated in Figure 18. Surprisingly, the catalytic performance in H_2 production of the samples was relatively similar (hole scavenger Na_2SO_3), as shown in Figure 18a. The authors conclude that the photocatalytic activity is determined by the subnanometer-sized Pt particles rather than the large particles. Additional ICP and XPS studies are recommended to obtain more information on the loading and oxidation state, respectively, of subnanometer-sized and large Pt particles.

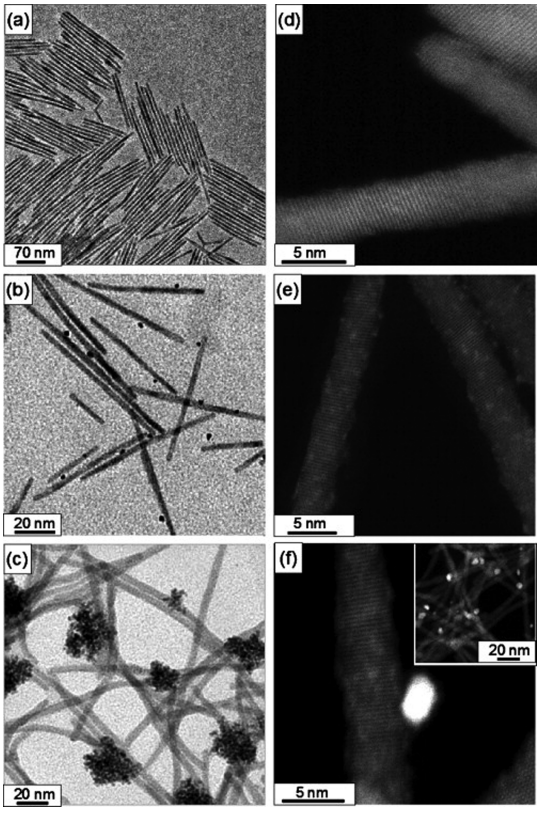

Figure 17. (a–c) TEM images of (Pt/)CdS prepared by Berr et al.[238] (a) Undecorated CdS nanorods, (b) Pt/CdS with one large Pt particle per nanorod after 120 min of photodeposition, and (c) Pt/CdS with agglomerates of Pt nanoparticles. The sample depicted in panel c was prepared by a chemical deposition method, with single Pt nanoparticles acting as reaction seeds (not discussed in this review). (d–f) High-angle annular dark-field scanning transmission electron microscopic (HAADF-STEM) images of (d) CdS nanorods, (e) Pt/CdS prepared after 20 min, and (f) Pt/CdS prepared after 120 min of photodeposition (the inset is an overview image). The lighter spots in panels e and f indicate Pt on CdS. Reprinted with permission from ref 238. Copyright 2010 AIP Publishing.

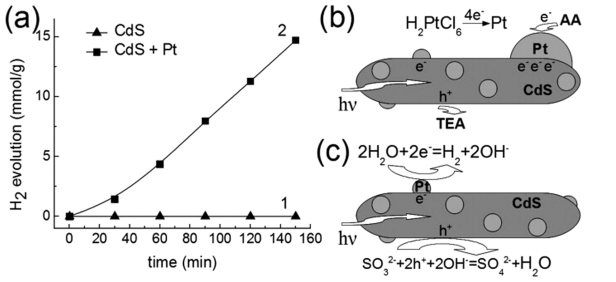

Figure 18. (a) Photocatalytic hydrogen production under UV–visible light (360–440 nm) over (Pt/)CdS as a function of time with Na_2SO_3 as hole scavenger, as measured by Berr et al.[238] The Pt/CdS graph is representative for Pt/CdS obtained after either 20 or 120 min of photodeposition. (b) Schematic overview of photodeposition procedure occurring in this study. Pt is reduced, while triethanolamine (TEA) acts as electron scavenger. At the site where larger Pt particle is growing, the weak reducing agent ascorbic acid (AA) assists in Pt reduction and particle growth. (c) Schematic overview of hydrogen production chemistry occurring, explaining data of panel a, with Pt acting as reduction sites. Reprinted with permission from ref 238. Copyright 2010 AIP Publishing.

Despite different loadings, photodeposition conditions, and CdS synthetic procedures, the size of the Pt particles is generally smaller than 10 nm.[97,99,101,235,238,242,245,246,255] Jin and co-workers[97,246] even show histograms of the Pt particle size in their studies. In some studies, due to detection limits of, for example, applied TEM, the Pt particle size could not always be determined.[238,250] With the rapid development of TEM systems nowadays, even allowing detection of particles on atomic scales, it is interesting to perform TEM measurements once more on such samples, including that by Berr et al.,[238] to obtain in-depth insight into the structure of the initially formed particles.

6.3.3. Chemical Reactions and Mechanism of Pt Deposition. A relative large amount of research has been done to understand photodeposition of Pt on CdS. For instance, Jin and co-workers[97,98,246,254] have spent much effort in studying the mechanism of Pt photodeposition on commercial CdS. Through XPS and differential thermal analysis (DTA), they demonstrate that when Pt is photodeposited upon CdS in an acidic environment (with $H_2PtCl_6{\cdot}xH_2O$ as precursor and deaeration through N_2 bubbling prior to illumination), PtS is the dominant species formed on CdS. They propose that this originates from mild dissolution of CdS in water:

$$CdS + H_2O \rightarrow Cd(OH)^+ + SH^- \quad (14)$$

Then the following photodeposition reactions occur:

$$[PtCl_6]^{2-} + 2e^- \rightarrow [PtCl_4]^{2-} + 2Cl^- \quad (15)$$

$$[PtCl_4]^{2-} + SH^- \rightarrow PtS\downarrow + H^+ + 4Cl^- \quad (16)$$

The authors demonstrate that both CdS and PtS/CdS are very poor in catalyzing alcohol dehydrogenation. When calcination of CdS and PtS/CdS takes place in air, much higher activities are obtained, especially for Pt-loaded CdS. The authors claim that a

DOI: 10.1021/acs.chemrev.6b00327
Chem. Rev. 2016, 116, 14587–14619

$Cd(OH)_2$-CdO-CdS layer is formed on the surface of the CdS, whereas PtS is converted to Pt^0 through the following reaction:

$$PtS + O_2 \rightarrow Pt^0 + SO_2 \quad (17)$$

Metallic Pt acts as a cocatalyst, enhancing the photocatalytic activity of CdS in hydrogen evolution.

When photodeposition is performed under basic conditions rather than acidic conditions, Jin and co-workers[97] demonstrate that Pt is mostly deposited in an oxidized form. In 1992, they proposed that $Pt(OH)_2$ is formed through the following reactions:

$$[PtCl_6]^{2-} + 2e^- \rightarrow [PtCl_4]^{2-} + 2Cl^- \quad (18)$$

$$[PtCl_4]^{2-} + 2OH^- \rightarrow Pt(OH)_2\downarrow + 4Cl^- \quad (19)$$

Interestingly, when photodeposition of Pt takes place after heat treatment of CdS, in both alkaline and acidic medium, $Pt(OH)_2$ is formed. It is likely that a $Cd(OH)_2$-CdO-CdS layer is formed due to heat treatment of CdS, which prevents dissolution of CdS in water and thus PtS formation. In a different study from 1994, Jin et al.[98] studied photodeposition of Pt on heat-treated Pt/CdS. Metallic Pt was obtained at pH = 2.2, whereas PtO_2 and $Pt(OH)_2$ were observed at high pH. In the latter case, at low Pt precursor concentrations, mainly $Pt(OH)_2$ was formed rather than PtO_2. The authors attribute the formation of $Pt(OH)_2$ to a reduction reaction and the formation of PtO_2 to an oxidation reaction:

$$[Pt(OH)_2Cl_4]^{2-} + 2e^- \rightarrow Pt(OH)_2 + 4Cl^- \quad (20)$$

$$[Pt(OH)_2Cl_4]^{2-} + 4h^+ \rightarrow PtO_2 + 2H^+ + 4Cl^- \quad (21)$$

$[Pt(OH)_2Cl_4]^{2-}$ is formed due to hydrolysis of $[PtCl_6]^{2-}$ at high pH:

$$[Pt(OH)_nCl_{6-n}]^{2-} + OH^- \leftrightarrow [Pt(OH)_{n+1}Cl_{5-n}]^{2-} + Cl^- \quad (22)$$

where $n = 0-5$. It is noteworthy that the reaction mechanism proposed in this paper is slightly different from the reaction mechanism proposed by the same authors in an earlier paper. We think that the latter reaction pathway is more likely, as it takes the phenomenon of hydrolysis into account. Furthermore, when the authors performed photodeposition of Pt on unloaded, heat-treated CdS under basic conditions, PtO_2 formation was observed as well, in addition to $Pt(OH)_2$, which was not reported in the 1992 study of Jin and co-workers.[97] This is likely the result of (small) differences in the experimental procedure.

6.3.4. In Situ Photodeposition. Another important contribution to understand photodeposition of Pt on CdS has been provided by Wang et al.[99] These authors studied the influence of solution environment on the photodeposition process (performed under vacuum). Experiments were performed in neutral pH conditions, alkaline conditions (obtained with various concentrations of NaOH), acidic conditions (obtained with acetic acid) and in an aqueous solution with a sulfide/sulfite mixture. As-obtained Pt/CdS was tested for its photocatalytic activity in H_2 evolution, with Na_2S/Na_2SO_3 as sacrificial agent. Also, in situ photodeposition of Pt on CdS was performed, where H_2 production was monitored with Na_2S/Na_2SO_3 as sacrificial agent. When photodeposition was performed under alkaline conditions, by far the highest H_2 evolution rate was obtained (more than 20-fold increase when a neutral pH or in situ photodeposition was used, and more than a 50-fold increase compared to the other solutions). Similar trends (but different activities) were also observed when the morphology (and potentially crystal structure) of the CdS changes. Through XPS studies, Wang et al.[99] reveal that, under alkaline conditions, predominantly metallic Pt was observed, with some Pt^{2+} corresponding to $Pt(OH)_2$. This is a very different result compared to that of Jin and co-workers.[97,98] At lower pH values, no metallic Pt was formed and Pt was present in an oxidic state. According to Wang et al.,[99] metallic Pt can be formed at high pH due to hydrolysis of $[PtCl_6]^{2-}$ (see eq 22). At low pH, $[PtCl_6]^{2-}$ will first be reduced to $[PtCl_4]^{2-}$. However, Cl^- must dissociate from $[PtCl_4]^{2-}$ before further reduction can take place, which Wang et al. propose is a slow process. If the Cl^- groups are replaced by OH^- groups, the Cl^- dissociation step is avoided and full Pt reduction can take place efficiently. TEM demonstrated that Pt particles of 2−3 nm are formed under alkaline conditions, whereas no Pt particles were observed when one of the other solutions was used. We think it is likely these particles were too small to detect.

6.3.5. Comparing Sacrificial Agents. In a study by Xin et al.,[249] the role of sacrificial agent was studied during in situ photodeposition of 0.1 wt % Pt on a mixture of cubic and hexagonal CdS. As sacrificial agents, 10 vol % lactic acid, 0.1 M Na_2S/Na_2SO_3, and 10 vol % methanol were used. Illumination took place for 2 h with a 300 W Xe lamp. The authors demonstrated that the amount of Pt deposited changed drastically when the sacrificial agent was changed: 0.0894 wt % was deposited when methanol was used, whereas only 0.0248 and 0.0124 wt % were deposited, respectively, when lactic acid and Na_2S/Na_2SO_3 were used. However, the latter two samples did show considerably higher photocatalytic H_2 production rates than Pt/CdS obtained with methanol, with Pt/CdS obtained with lactic acid showing the highest activity. The authors speculate that this is due to a difference in form of Pt, although they do not provide evidence. Yao et al.[231] have performed photodeposition of Pt (0.5 wt %) on CdS with the sacrificial agents ammonium sulfite $[(NH_4)_2SO_3]$, glacial acetic acid, and methanol. Vacuum degassing took place before irradiation. Photodeposition was performed for 5 h with a Xe lamp plus filters to eliminate UV and IR radiation. Photocatalytic H_2 production was measured for as-obtained Pt/CdS, with $(NH_4)_2SO_3$ as sacrificial agent. No noteworthy activity was measured when methanol or $(NH_4)_2SO_3$ was used, but with glacial acetic acid activity was observed. The authors speculate that this is due to glacial acetic acid preventing formation of CdO on the surface of CdS, which is, according to the authors, detrimental for the photocatalytic activity.

Yao et al.[231] investigate in detail the effect of photoetching on Pt/CdS obtained with $(NH_4)_2SO_3$. This photoetching results in a drastic enhancement of photocatalytic activity, outperforming the H_2 production rate of Pt/CdS obtained with glacial acetic acid. Apart from a change in surface area of CdS, the authors demonstrate with TEM that the particle size of Pt increases (not detectable before photoetching, 3−6 nm particle size after photoetching), although no explanation is provided. Despite the focus of the study being on use of $(NH_4)_2SO_3$ as a sacrificial agent for H_2 production, it might have been interesting to see if similar effects were present for Pt/CdS obtained with methanol or glacial acetic acid. Earlier work on photoetching of Pt/CdS obtained through photodeposition was performed by Li et al.[235] For the photodeposition process, acetic acid was used as a sacrificial agent. Photocatalytic H_2 evolution was monitored with a different sacrificial agent, namely, formic acid. Photodeposition

DOI: 10.1021/acs.chemrev.6b00327
Chem. Rev. 2016, 116, 14587−14619

of Pt (1.5 wt %) did result in considerably higher activity. Again, photoetching contributed to even higher activity.

6.3.6. Comparison with Other Methods. Some studies have focused on comparing photodeposition of Pt on CdS with other deposition methods. For instance, the study of Xin et al.[249] mentioned earlier compared samples of Pt on a mixture of cubic and hexagonal CdS, prepared not only by in situ photodeposition but also by coprecipitation and impregnation. The authors concluded that these two methods (especially the former) resulted in higher H_2 productions than when photodeposition was used. However, this comparison is not completely fair. The authors demonstrated that the amount of Pt deposited was considerably less for photodeposition than when one of the other methods was used. Also, no metallic Pt was observed in XPS spectra for photodeposited Pt, whereas some metallic Pt was observed when coprecipitation and impregnation were used. The authors did not provide clear information how the morphology and size of the Pt obtained through photodeposition compared with those from the other deposition methods. It can be concluded that the obtained Pt/CdS was very different when photodeposition was used rather than one of the other two methods. Previously mentioned PtS formation during photodeposition might be at the origin of the lower activity of this sample.

Bühler et al.[234] showed that Pt-loaded CdS (where CdO was removed through acetic acid treatment) obtained through photodeposition was more active in H_2 production with Na_2SO_3 and/or Na_2S or $Na_2S/H_3PO_2/NaOH$ than when thermal reduction was applied. Even when Pt/CdS was photoetched, activities were generally lower than when photodeposition was used (with the exception of usage of Na_2SO_3 as a sacrificial agent). A difference in the amount of Pt loading was reported between the two methods, and the oxidation state was not determined by XPS. Matsumara et al.[256] compared photodeposition with a shaking method, and Sakamoto et al.[241] compared in situ photodeposition with impregnation. In both cases, the latter worked better in H_2 production. Important characterization (such as XPS) is missing in both studies to explain the as-observed differences, although Sakamoto et al.[241] discuss the possibility of Pt blocking active sites of CdS in the photocatalytic process. In Scheme 4, the applied process conditions discussed in this section are summarized:

Scheme 4. Overview of Process Parameters Used in Studies Concerning Photodeposition of Pt on CdS

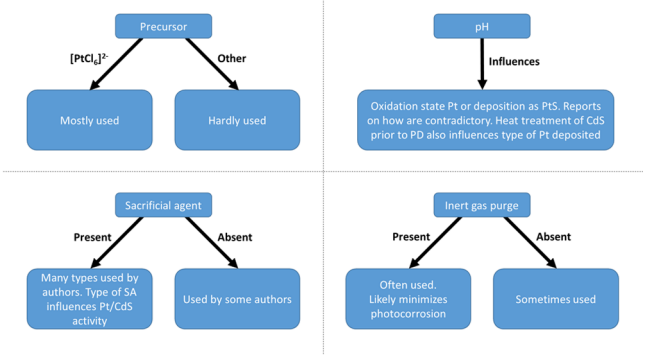

7. PHOTODEPOSITION OF COMPLEX PARTICLES ON GAN:ZNO

Domen and co-workers[257−260] have extensively discussed photodeposition of Rh/Cr_2O_3 core/shell particles on a solid solution of GaN and ZnO $(Ga_{1-x}Zn_x)(N_{1-x}O_x)$, referred to as GaN:ZnO from this point on. The usage of GaN:ZnO is considered promising for storage of solar energy in the form of hydrogen, as it is capable of full water splitting under visible-light illumination. However, cocatalytic nanoparticles are needed to obtain the production of H_2 and O_2. At first sight, a suitable cocatalyst could be Rh. Domen and co-workers[258] discussed that Rh serves as an electron trap, capable of producing H_2. However, when O_2 is present, O_2 and H_2 react immediately with each other on the Rh surface, thus producing water. To prevent this back-reaction from happening, a Cr_2O_3 shell can be engineered on the Rh nanoparticles. A schematic of the role of Rh/Cr_2O_3 core/shell particles in photocatalytic H_2 production during water splitting is depicted in Figure 19. When Rh/Cr_2O_3 core/shell particles are

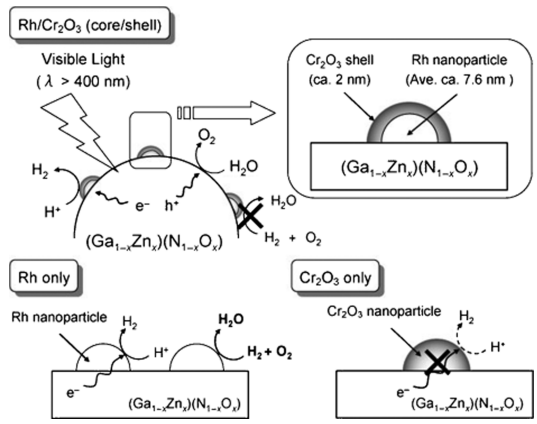

Figure 19. Working principle of Rh/Cr_2O_3 core/shell particles on GaN:ZnO during water splitting as proposed by Domen and co-workers. Rh nanoparticles act as a cocatalyst, whereas Cr_2O_3 shells prevent reaction of O_2 and H_2 on the Rh nanoparticles. Reprinted with permission from ref 257. Copyright 2006 Wiley.

engineered upon the surface of GaN:ZnO, Rh is photodeposited first, followed by photodeposition of Cr_2O_3. The latter takes place through reduction of chromate:

$$4[CrO_4]^{2-} + 8H^+ \rightarrow 4H_2O + 2Cr_2O_3 + 3O_2 \quad (23)$$

Interestingly, there is a maximum amount of Cr_2O_3 that can be loaded, corresponding with a shell thickness of 2 nm.[258] Further addition of the precursor K_2CrO_4 does not result in additional Cr_2O_3 being deposited. It should be noted that Rh does not have to be deposited by photodeposition per se. In fact, Domen and co-workers[260,261] showed that higher photocatalytic activities in water splitting were achieved when a liquid-phase reduction method was used to load Rh rather than conventional photodeposition. This was attributed to better dispersion of Rh particles, even though the Rh was in a lower valence state than when photodeposition was used. It is also worth mentioning that in the case of liquid-phase reduction some irregularly shaped shell structures were observed as well as the majority of core/shell nanoparticles. The authors did not observe this irregularly shaped shell structure formation when Rh/Cr_2O_3 was obtained through photodeposition. Both methods were more suited than impregnation, though, where dominantly featureless particles

DOI: 10.1021/acs.chemrev.6b00327
Chem. Rev. 2016, 116, 14587−14619

rather than core/shell particles were formed, and the Rh was detected to be in the lowest (metallic) state.

The addition of a Cr_2O_3 shell is not limited to the cocatalyst Rh. Domen and co-workers[257,260,261] have also performed photodeposition of such a shell on NiO_x, RuO_2, Rh_2O_3, Pd, Pt, and Ir. Nevertheless, on GaN:ZnO, none of the as-obtained cocatalytic particles showed the same promise in photocatalytic water splitting as the Rh/Cr_2O_3 core/shell nanoparticles. Interestingly, a core/shell structure was not evident when NiO_x and Rh_2O_3 were used, as determination of the interface between the NiO_x or Rh_2O_3 and the Cr_2O_3 turned out to be difficult. In the case of RuO_2, core/shell structures were observed, but some of the RuO_2 particles remained uncoated despite a significant amount of K_2CrO_4 being available in the photodeposition procedure. The authors attributed this to uncoated RuO_2 particles acting as oxidation cocatalysts, whereas coated RuO_2 particles should function as reduction cocatalysts.

Aside from photodeposition of noble metal/Cr_2O_3 core/shell nanoparticles, Domen and co-workers[93] also tried to photodeposit rhodium and chromium simultaneously on GaN:ZnO as well as on $SrTiO_3$. Remarkably, impregnation yielded higher photocatalytic activities in water splitting for $Rh_{2-y}Cr_yO_3/(Ga_{1-x}Zn_x)(N_{1-x}O_x)$ (x = 0.12) in comparison with photodeposition, whereas photodeposition was more beneficial for the activity of $Rh_{2-y}Cr_yO_3/SrTiO_3$. Although the authors mentioned that they did not optimize their deposition method, they discussed that the effectiveness of their photodeposition method seemed to be dependent on the photocatalyst used. In a more recent study, the authors studied simultaneous photodeposition of Rh and Cr on $(Ga_{1-x}Zn_x)(N_{1-x}O_x)$ under visible light as a function of the K_2CrO_4 concentration used in the procedure.[262] A saturation limit was detected in the amount of Cr deposited: ca. 0.25 wt %. With a constant Rh loading of 0.75 ± 0.15 wt %, optimal results in visible-light water splitting were achieved when 0.175 wt % Cr was added. With increasing amounts of Cr added, the photocatalytic activity actually decreased until a steady state was reached at 0.5 wt % Cr addition and higher. The authors discussed that the highest activity obtained at 0.175 wt % is due to the formation of $Rh/Rh_{2-y}Cr_yO_3$ core−shell particles, whereas at higher Cr loadings $Rh_{2-y}Cr_yO_3$ particles are exclusively formed. From their results, the authors concluded that metallic Rh is a better electron sink than $Rh_{2-y}Cr_yO_3$. The authors also showed that usage of Rh/Cr_2O_3 core/shell cocatalytic nanoparticles yielded considerably higher activities in visible-light water splitting than when $Rh_{2-y}Cr_yO_3$ was used (about 6-fold higher when 0.75 ± 0.15 wt % Rh and 0.24 ± 0.03 wt % Cr were used).

Cavalca et al.[8] studied photodeposition of Pt on GaN:ZnO in situ by TEM. To do so, H_2PtCl_6 solution was deposited on a GaN:ZnO surface, followed by evaporation and deposition on a gold TEM grid covered with an amorphous carbon film. Before illumination, TEM images were recorded for reference. Then a small amount of water vapor was introduced into the specimen chamber, and illumination took place at 405 nm for 4 h with an intensity of 6 $W \cdot cm^{-2}$ over the entire grid. Afterward, the specimen chamber was evacuated and TEM images were recorded again. Prior to deposition, a thin homogeneous and amorphous layer of salt was observed on the GaN:ZnO surface. After illumination, a homogeneous distribution of particles with diameter of ∼1 nm was observed, whereas the amorphous layer was almost completely gone. Following this procedure, TEM is very well suited to determine the transients in particle morphology as a function of illumination time. If this method is extended to other semiconductors, this will no doubt contribute to the fundamental understanding of photodeposition, in particular when complementary atomic force microscopic (AFM) analyses are performed.

8. STRUCTURE-DIRECTED PHOTODEPOSITION

In recent years, interest in crystal facet engineering has grown significantly in the community studying photocatalysis.[263−266] In crystal facet engineering, the aim is to synthesize semiconductors in such a way that certain facets are preferentially exposed, thereby improving photocatalytic performance. For instance, for well-defined TiO_2 anatase, there has been extensive discussion of which facet is the most active for inducing photocatalytic activity: many researchers claim the presence of high concentrations of {001} facets, rather than {101} facets is beneficial,[264,267−270] although some researchers conclude otherwise.[271,272]

A popular technique to perform crystal facet engineering is the employment of (microwave-assisted) hydrothermal synthetic techniques using surfactants, also known as capping agents. Normally, when capping agents are absent, crystals tend to grow in directions that are thermodynamically favorable. However, when capping agents are introduced during growth, they will adsorb on specific facets, changing the surface energy of those facets. This results in inhibition of growth in the thermodynamically most favorable direction, yielding crystals with thermodynamically less favorable facets exposed. For more detailed information on crystal facet engineering, we recommend some of the excellent reviews written in recent years: see refs 264, 266, 273, and 274.

Structure-directed photodeposition has been applied to study the redox activity of facet-engineered crystals. The concept is that spatially preferred formation of reduced metal nanoparticles reveals the presence of preferentially reductive facets, whereas spatially preferred formation of oxidized metal nanoparticles identifies facets that preferentially induce oxidative reactions. For instance, this concept can be used for photocatalytic systems consisting of a combination of semiconductor and metal (oxide) particles, revealing on which semiconductor/metal reduction or oxidation takes place.[215,275,276] Alternatively, photodeposition can also be used to demonstrate reductive and oxidative sites in a heterojunction of two photocatalysts. For instance, Latorre-Sánchez et al.[277] performed reductive and oxidative photodeposition of Pt and MnO_2, respectively, on a heterojunction consisting of nitrogen-doped graphene (n-type semiconductor) and boron-doped graphene (p-type semiconductor). The authors observed that Pt and MnO_2 were deposited at N-doped and B-doped graphene, respectively, under a bias of 0.5 V (with N-doped graphene being the negative electrode), whereas no Pt and MnO_2 were deposited on B-doped and N-doped graphene, respectively, under a bias of −0.5 V. The authors concluded that electrons were preferentially migrating from B-doped to N-doped graphene, while holes were preferentially located in B-doped graphene. There is also evidence that favored reductive and oxidative sites exist in a single semiconductor particle, as probed by structure-directed photodeposition.

Although the field of structure-directed deposition is relatively new, research on reductive facets had already been performed in the 1990s.[278−280] In 1998, Morris Hotsenpiller and co-workers[278,279] tried to relate the photoreduction rate of Ag^+ to the surface orientation of rutile. Initially, they demonstrated that rutile films with (101), (111), and (001) orientations are more active in Ag photoreduction than films with (100) and (110) orientations.[278] Not much later, they revealed the same kind of behavior for rutile polycrystals, where they concluded that the

DOI: 10.1021/acs.chemrev.6b00327
Chem. Rev. 2016, 116, 14587−14619

most reactive surfaces were near the {101} plane.[279] Although the authors did not draw real conclusions yet, they did speculate that differences between the surfaces in adsorption/desorption mechanisms, as well as differences in efficient charge separation, could be possible explanations for the differences in reduction rates. In 1999, Farneth et al.[280] demonstrated structure-directed photodeposition of Ag as well on rutile. They hypothesize that this must have taken place on the {110} faces. Ohno et al.[53] demonstrated in 2002 through Pt photoreduction that the favored reduction site of rutile is again the {110} face. Clearly, the results of Farneth and Ohno and their co-workers are quite different from the results of Morris Hotsenpiller and co-workers. Ohno et al. also noticed this and hypothesized that the differences observed are due to the size of the faces: Morris Hotsenpiller and co-workers looked at films or very large crystallites, whereas Farneth and Ohno and their co-workers looked at considerably smaller individual particles. Therefore, Ohno et al. suggest that Morris Hotsenpiller and co-workers must have looked at single crystal faces, making a synergistic effect between faces improbable.

Structure-directed photodeposition has sparked a lot of interest since Ohno et al.[53] demonstrated that Pt is selectively deposited on the {110} facet of rutile or the {011} facet of anatase through photoreduction. In their studies, they also showed that PbO_2 is selectively deposited on the {011} facet of rutile and the {001} facet of anatase through photo-oxidation. As-found particles are depicted in Figure 20. One should keep in

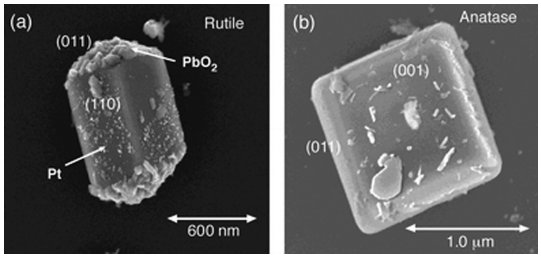

Figure 20. SEM images of (a) rutile and (b) anatase particles after photodeposition with first Pt and then PbO_2. Reprinted with permission from ref 53. Copyright 2002 Royal Society of Chemistry.

mind, however, that the latter photodeposition was done when the TiO_2 was already loaded with Pt; increased charge separation will take place on the latter due to Pt acting as an electron sink.[27,36] Nevertheless, the article has formed an important basis for subsequent studies in structure-directed photodeposition. Photocatalysts studied include TiO_2,[53,281−284] TiO_x,[285] $SrTiO_3$,[201,286] ZnO,[287,288] Cu_2O,[289−291] $BiVO_4$,[90,91,292,293] WO_3,[151] $PbTiO_3$,[294] (La-doped) $NaTaO_3$,[295] $BaLa_4Ti_4O_{15}$,[30,296] $[H_{1-x}Ca_2Nb_3O_{10}]^{x-}$,[297] $[TBA,H]$-$Ca_2Nb_3O_{10}$,[298] CdS,[253] Cu_2WS_4,[104] BiOCl,[299] and AgI.[300] A selection of important papers where both photoreduction and photo-oxidation were used to probe the reactive facets is provided in Table 2. Typically, a noble metal such as Pt, Ag, or Au is deposited in the photoreduction reactions, revealing the reductive site of a photocatalyst, whereas a metal oxide such as PbO_2, Co_3O_4, or MnO_x is deposited by an oxidation reaction, revealing the oxidative site. However, structure-directed photodeposition does not always have to occur. Sabio et al.[298] tried to perform both reductive and oxidative photodeposition with multiple cocatalysts on $[TBA,H]$-$Ca_2Nb_3O_{10}$ nanosheets. However, the authors observed cocatalysts on both edges and the nanosheet surface. Aside from the photocatalysts mentioned, structure-directed photodeposition has also been attempted to obtain metal-tipped ZnO nanorods/nanowires[83,301] or pyramids.[302,303] In these cases, structure-directed photodeposition does not occur on a specific facet but rather on a single location.

In general, an accepted explanation of why structure-directed photodeposition occurs is related to light-induced charge separation.[53,90] In such a case, the band structures of different facets will be slightly different, resulting in slight shifts in energy of conduction bands and valence bands. Electrons and holes will migrate to the facet that is energetically the most favorable for each, resulting in favored reduction and oxidation sites. Despite this theory, some authors (including ourselves) discussed that other phenomena may contribute to structure-directed photodeposition as well.[151,253,264,287] Although charge migration in several cases may be the dominant driving force, it should not be ruled out that adsorption phenomena could play an important role as well.[151,253] We have demonstrated that wet impregnation will result in structure-directed deposition as well.[151] Furthermore, we have shown by additional AFM studies that different faces of crystals in contact with water intrinsically show differences in surface charges in the absence of illumination. Liu et al.[264] have advocated that competitive adsorption of ionic compounds similar in charge to the metal precursor can adsorb as well on specific facets (such as Cl^- in H_2PtCl_6), blocking these for (structure-directed) photodeposition. They based this conclusion on a study performed by Read et al.,[287] where photodeposition of Au on the {0001} facet of ZnO hexagonal rods was observed only in the absence of Cl^- (Figure 21). The authors concluded that Cl^- must have absorbed on this particular facet, blocking possible Au formation.

When structure-directed photodeposition is indeed the result of spatial charge-carrier separation, possibilities for a drastic increase in the activity of a photocatalyst open up. In such a case, reduction and oxidation (co)catalysts can be loaded on facets where electrons and holes accumulate, respectively. A good example of a very complete study in this field has been provided by Li et al.,[90] where structure-directed photodeposition was ultimately used to obtain a $BiVO_4$ system with very high photocatalytic activity. Initially, the authors demonstrated that Au, Pt, and Ag were deposited on the {010} facet of $BiVO_4$ through photoreduction from both anionic ($[AuCl_4]^-$, $[PtCl_6]^{2-}$) and cationic (Ag^+) precursors. In a similar way, they showed that MnO_x and PbO_2 were selectively formed on the {110} facets through photo-oxidation of Mn^{2+} and Pb^{2+}. These phenomena happened not only when oxidative/reductive photodeposition was performed separately but also when this took place simultaneously (Figure 22). Also, several precursors were used for MnO_x deposition [$MnCl_2$, $Mn(NO_3)_2$ and $MnSO_4$], all resulting in similar structure-directed photodeposition. Furthermore, when impregnation was performed, a uniform distribution of metals/metal oxides was observed. Interestingly, photocatalytic activity in water oxidation (with IO_3^- as electron acceptor) of $BiVO_4$ loaded with Pt and MnO_x through photodeposition was significantly higher than when impregnation was used. In a later study, Li et al.[91] demonstrated the same phenomenon for $Pt/Co_3O_4/BiVO_4$ (in dye degradation). Comparisons between structure-directed photodeposition and impregnation have been made by other authors as well.[30,294] Zhen et al.[294] showed that higher photocatalytic activities in hydrogen production were achieved with Pt-loaded ferroelectric $PbTiO_3$ when Pt was selectively photodeposited on the positively charged {001} facet than when the Pt was randomly distributed by impregnation. Structure-directed photodeposition does not

DOI: 10.1021/acs.chemrev.6b00327
Chem. Rev. 2016, 116, 14587−14619

Table 2. Selection of Articles in Which Structure-Directed Photodeposition on Semiconductors Has Been Studied to Distinguish Sites for Reduction and Oxidation[a,b]

semiconductor	reduction reaction	oxidation reaction	PC activity after deposition	additional notes	ref
TiO_2 (rutile)	Pt, {110} facet	PbO_2, {011} facet	NA	PO performed after PR	53
TiO_2 (anatase)	Pt, {011} facet	PbO_2, {001} facet	NA	PO performed after PR	53
TiO_2 (decahedral anatase)	Pt, {101} facet	PbO_2, {001} facet	NA		281
TiO_x (nanosheets)	Ag, Cu, Cu_2O, edges	MnO_2, all over surface	NA		285
$SrTiO_3$ (faceted)	Ag, {100} surfaces	PbO_2, {100} surfaces	NA	{100} surface is nonpolar	286
$SrTiO_3$ (cube and tetrahexahedron)	Pt, {001} facet	PbO_2, {023} facet	NA		201
$BaLa_4Ti_4O_{15}$ (platelike)	Pt, all over surface; Au, edges; Ni, basal plane	PbO_2, basal plane	Ni oxidized to NiO_x[c]	[d]	296
$BiVO_4$	Au, Pt, Ag, {010} facet	PbO_2, MnO_x, {110} facet	increased activity in PC water oxidation and PEC performance	impregnation studies disproved a role of preferred adsorption	90
$BiVO_4$	Pt, {010} facet	Co_3O_4, MnO_x, {110} facet	increased activity in water oxidation and RhB and MO degradation	impregnation studies disproved a role of preferred adsorption	91
Cu_2O (multifaceted)	Pt, apices with high index	PbO_2 {100} facet	NA		289
Cu_2O (p-type, with 26 anisotropic facets)	Au, Ag, Pt, {001} facet	Co_3O_4, MnO_x {111} facet	increased activity in MO degradation	Cu_2O with eight isotropic facets did not yield SD photodeposition	290
$PbTiO_3$ (ferroelectric nanoplates)	Pt, Au, Ag, (+) {001} facet[e]	MnO_x, (−) {001} facet[e]	increased activity in H_2 generation for $Pt/PbTiO_3$	impregnation studies disproved a role of preferred adsorption	294
AgI (microplates with polar 0001 facets)	Ag (0001) facet	MnO_x, $(000\bar{1})$ facet	increased activity in MO degradation		300
Cu_2WS_4	Pt, Ru, {001} facet	MnS, PbS, evenly dispersed	increased activity in H_2 generation for Pt/Cu_2WS_4	SD etching through PO observed	104
BiOCl	Au, {001} facet	MnO_x[f]	increased activity in water splitting; also PEC studies performed		299

[a]In the second column, both the reduced metal and the preferred location of the semiconductor where it has been deposited are given. Similarly, the oxidized metal oxide/sulfide and corresponding location are depicted in the third column. [b]NA, not available; PO, photooxidation; PR, photoreduction; PC, photocatalytic; PEC, photoelectrochemical, SD, structure-directed. [c]Activity lower than when NiO_x is prepared by impregnation. [d]Two Pt precursors were used. $[Pt(NH_3)_4]^{2+}$ yielded larger particles at the edge than on the basal plane. Structure-directed deposition was not observed for $CaLa_4Ti_4O_{15}$. [e](+), positively charged; (−), negatively charged. [f]{110} facet in simultaneous deposition; all over surface in single deposition.

always have to result in the highest activity of a photocatalytic material, though. Jiang et al.[282] showed that higher photocatalytic activities under visible light were achieved in rhodamine B degradation when an in situ photodeposition method was used, rather than a classical photodeposition method, to load anatase with Ag. When classical photodeposition was performed, photodeposition of Ag took place simply by illuminating a solution containing anatase and $AgNO_3$. In the case of in situ photodeposition, $NaIO_3$ was also added to the solution. It should be noted that the term "in situ" is infelicitous, as no real in situ measurements take place during this photodeposition procedure. The authors hypothesized that $AgIO_3$ was formed during stirring in the dark, which could uniformly coat all facets of the anatase particles. As a result, structure-directed photodeposition was observed only when classical photodeposition was used. The authors elaborated that the size of the Ag particles themselves played a large role in photocatalytic activity, affecting the surface plasmon resonance: the in situ method yielded small Ag particles (1−6 nm), compared to 20 nm Ag particles when classical structure-directed photodeposition was used. Iizuka et al.[30] also demonstrated that liquid-phase chemical reduction of Ag on $BaLa_4Ti_4O_{15}$ plates yielded higher photocatalytic activity in CO_2 reduction than when either in situ photodeposition or impregnation was used. In this case Ag was at first randomly distributed on the $BaLa_4Ti_4O_{15}$ plates, but after 1 h of photocatalytic reaction, the authors found that Ag particles were disappearing from the basal plane and reappearing at the edges. The authors attributed this to photo-oxidation of Ag particles on the basal plane, which were subsequently selectively photodeposited on the edges. The size of the rephotodeposited Ag particles was smaller than the size of the classical in situ photodeposited Ag particles (<10 nm vs 30−40 nm), explaining the higher activity in CO_2 reduction.

9. POINTS FOR IMPROVEMENT IN PHOTODEPOSITION STUDIES

9.1. Terminology: Loading versus Doping

Several researchers confuse *loading* of metal (oxide) nanoparticles on semiconductor surfaces with *doping*. To understand the difference between loading and doping, we emphasize the description of the two concepts and the goals researchers want to achieve.

- *Loading* is the concept of depositing nanoparticles **on** the surface of semiconductor substrates. This is a means to enhance photocatalytic activity, with the nanoparticles acting as a **cocatalyst**.
- *Doping* of a material is the introduction of ionic species **in** the crystal lattice of a semiconductor. This is done to

DOI: 10.1021/acs.chemrev.6b00327
Chem. Rev. 2016, 116, 14587−14619

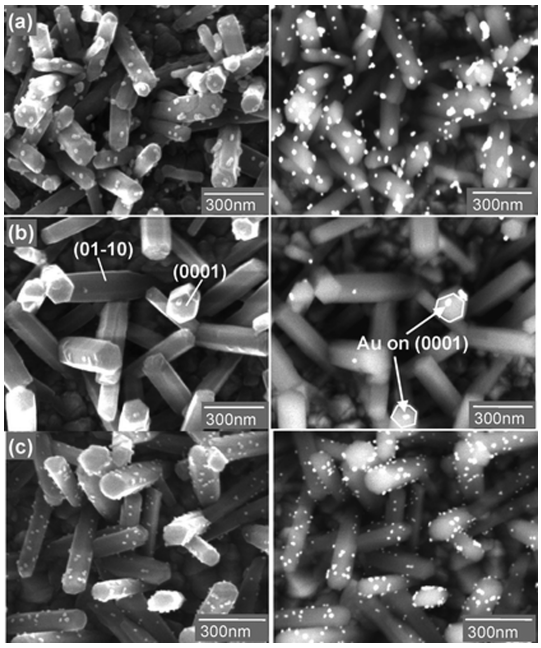

Figure 21. Left side: Au/ZnO nanorods prepared through photodeposition with (a) 0.1 mM $Au(CH_3COO)_3$, (b) 0.05 mM $Au(CH_3COO)_3$, and (c) 0.05 mM $AuCl_3$ ethanol solution. Right side: corresponding backscattered electron images. Reprinted with permission from ref 287. Copyright 2009 American Chemical Society.

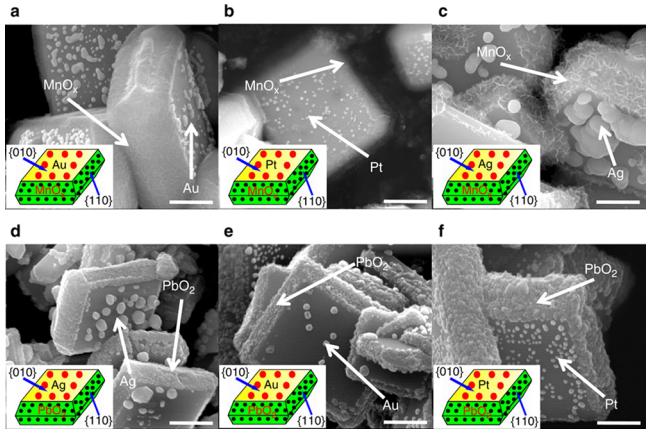

Figure 22. M/MO/$BiVO_4$ samples (M = Au, Pt, Ag; MO = MnO_x, PbO_2), where M and MO were simultaneously deposited through, respectively, photoreduction and photo-oxidation over $BiVO_4$. Metals/metal oxides (5 wt %) were loaded, and the scale bar corresponds to 500 nm. Reprinted with permission from ref 90. Copyright 2013 Macmillan Publishers Limited.

introduce a new intraband energy level in the band gap, yielding visible-light sensitivity of the semiconductor.

9.2. Band-Gap Changes

Quite often authors compare the band gap of their photocatalysts, determined by UV−vis diffuse reflectance spectroscopy, before and after nanoparticulate deposition. In several cases, a change in absorption spectrum of the semiconductor is observed after deposition of nanoparticles, which is then tentively assigned to a change in band gap (likely based on the confusion that deposition leads to "doping"). We consider this to be very unlikely, as only surface properties of a semiconductor crystal are changed when nanoparticles are deposited by photodeposition. At the interface of the metal particle and the semiconductor, a physical phenomenon does occur, known as band-bending. However, this typically does not change the intrinsic band-gap values. It is more likely that changes in diffuse reflectance absorption spectra after nanoparticle deposition are due to (plasmonic) absorption characteristics of these metal (oxide) nanoparticles, superimposed on the (original) spectrum of the semiconductor. This should be considered when (minor) shifts in apparent band-gap absorption are deduced from Tauc plots.

9.3. Measurement of Photon Flux

Although the type and wattage of lamps used is usually mentioned in experimental procedures of photodeposition, the photon flux (in milliwatts per square centimeter) arriving at the slurry of the semiconductor particles is not. This should be measured and provided, since the photon flux will largely affect the rate of deposition and the resulting size of the deposited nanoparticles. Reporting of the photon flux is also essential to allow comparison of studies aimed at determining the effects of process parameters on photodeposition rates.

9.4. High-Temperature Treatment

Some authors perform high-temperature treatment after photodeposition, to remove remaining organics (sacrificial electron donors, such as ethanol). It should be mentioned that an elevated temperature is often insufficient to completely remove hydrocarbon contaminants, and prolonged UV treatment in aqueous conditions is more effective. Furthermore, properties of as-deposited particles will change at elevated temperatures. This should be taken into consideration when nanoparticle engineering is proposed through optimizing photodeposition conditions. Finally, from a cost and green chemistry perspective, high-temperature treatment will, to some extent, forfeit the favorable energy requirements for photodeposition.

9.5. Verification of Weight Loading

After photodeposition, it is important to verify the obtained weight loading of the metal (oxide) on the photocatalyst, for example, by XRF or ICP analysis. Knowledge of the amount of deposited metal (oxide) quantity is essential to explain differences in photocatalytic performance after variation in photodeposition procedures. If ICP is used, measuring the remaining metal ion content in solution after a certain illumination time is preferred over dissolving synthesized powder, for example, in aqua regia. Dissolution of metal oxides is not straightforward, even if present in nanoparticulate morphology, and might be incomplete.

9.6. Verification of Valence State of As-Deposited Particles

Although some authors study the oxidation state of the metal after deposition, usually by XPS, quite often such analysis is not provided. Before any conclusions can be drawn from the behavior of cocatalytic nanoparticles in stimulating photocatalytic performance of a semiconductor, knowledge of the valence state is indispensable. Although we have provided indications on how the oxidation state can be controlled by the process conditions applied during photodeposition (nature of the sacrificial agent and pH), verification of the oxidation state after preparation is recommended. This has been emphasized as well by Lee and Choi[36] and Murcia et al.[42]

9.7. Preferential Deposition on Facet-Engineered Crystals

As discussed earlier, structure-directed photodeposition is an upcoming field to determine the presence of reductive or oxidative facets on a semiconductor particle upon illumination.

DOI: 10.1021/acs.chemrev.6b00327
Chem. Rev. 2016, 116, 14587−14619

However, sorption phenomena in the absence of illumination might also play an important role in selective deposition of metal (oxide) particles on a specific semiconductor facet. Therefore, researchers working in the field of structure-directed photodeposition should always verify by experiment whether a geometrical distribution of metal (oxide) particles is the result of site-selective reductive or oxidative deposition or (dark) sorption phenomena. The latter can be verified by applying impregnation and is related to differences in intrinsic surface charges when semiconductor crystals are in contact with solutions used in photodeposition. Atomic force microscopy studies, capable of distinguishing the two phenomena, are highly recommended.

10. SUMMARY AND FUTURE PERSPECTIVES OF PHOTODEPOSITION

In this review, we discussed the concept of photodeposition and the promise it might hold for efficient preparation of cocatalytic nanoparticles on semiconductors. We showed that photodeposition, in particular deposition of Pt on TiO_2, Ag on ZnO, and Pt on CdS, yields very attractive materials for photocatalytic applications. However, optimization of the method of photodeposition to obtain catalyst materials with maximized activity is still largely empirical, since fundamental understanding of the physical chemistry of photodeposition is limited. We recommend performing additional studies to understand the mechanism of photodeposition and to provide rational guidelines for synthesis of nanoparticles with specific sizes and oxidation states on semiconductor substrates. Recent developments in the research domain of photodeposition are aimed at investigation of structure-directed photodeposition: photodeposition is then used to create nanoparticles on facets of engineered crystals with favorable reductive and oxidative properties. With these facet-engineered crystals of semiconductors, and the right set of conditions for optimized photodeposition, it should be possible to prepare materials with unprecedented photocatalytic activities.

AUTHOR INFORMATION

Corresponding Author

*E-mail g.mul@utwente.nl.

Notes

The authors declare no competing financial interest.

Biographies

Kasper Wenderich (1987, born in Hengelo, The Netherlands) obtained his M.Sc. in applied physics at the University of Twente, Enschede, The Netherlands, in 2011. Afterwards, he obtained a Ph.D. in photocatalysis in 2016 at the same university, in the Photocatalytic Synthesis (PCS) group, led by Professor Dr. Guido Mul. At the moment, he is a guest researcher in the PCS group. He is interested in photocatalysis, especially in understanding photocatalysis on a fundamental level. Other research interests include semiconductor science and spectroscopic techniques.

Guido Mul obtained his masters degree in chemistry with specialization in heterogeneous catalysis (Professor Geus) from Utrecht University in 1992. He received his Ph.D. in 1997 from the Delft University of Technology on the in situ DRIFT analysis of catalytic oxidation of (diesel) soot, research conducted under the supervision of Professor Jacob Moulijn. After a postdoc position at SRI International, USA (1997−1999), investigating propane oxidation and conversion of sulfur containing compounds, he was awarded a fellowship of the KNAW (Royal Netherlands Academy of Arts and Sciences). This allowed him to determine the mechanism of oxidation reactions in detail, using an integrated approach based on IR and Raman spectroscopies and transient kinetics, again at the Delft University of Technology (TUD). He was appointed associate professor at TU Delft in 2007, where his research continued with developing/evaluating spectroscopies (attenuated total reflection and Raman) for analyses of liquid-phase (photo)catalytic processes. He was appointed full professor to conduct research in the field of photocatalytic synthesis at the University of Twente in 2010, with research activities in photocatalysis for water splitting and CO_2 to fuel conversion, as well as in photocatalytic oxidation reactions (gas and liquid phase). Furthermore, development and evaluation of electrocatalytic processes, including electrocatalytic CO_2 reduction, are part of his current research activities.

ACKNOWLEDGMENTS

We express our gratitude to Joana Sobral Romão for valuable discussions. Furthermore, we thank the Dutch National Research School Combination Catalysis Controlled by Chemical Design (NRSC-C) for financial support.

REFERENCES

(1) Clark, W. C.; Vondjidis, A. G. An infrared study of the photocatalytic reaction between titanium dioxide and silver nitrate. *J. Catal.* **1965**, *4* (6), 691−696.
(2) Kraeutler, B.; Bard, A. J. Heterogeneous photocatalytic preparation of supported catalysts. Photodeposition of platinum on titanium dioxide powder and other substrates. *J. Am. Chem. Soc.* **1978**, *100* (13), 4317−4318.
(3) Grätzel, M. Photoelectrochemical cells. *Nature* **2001**, *414* (6861), 338−344.
(4) Lide, D. R. *CRC Handbook of Chemistry and Physics*, 87th ed.; CRC Press/Taylor and Francis Group: Boca Raton, FL, 2006.
(5) Kydd, R.; Scott, J.; Teoh, W. Y.; Chiang, K.; Amal, R. Understanding photocatalytic metallization of preadsorbed ionic gold on titania, ceria, and zirconia. *Langmuir* **2010**, *26* (3), 2099−2106.
(6) Liu, Y.; Wei, S.; Gao, W. Ag/ZnO heterostructures and their photocatalytic activity under visible light: Effect of reducing medium. *J. Hazard. Mater.* **2015**, *287*, 59−68.
(7) Sun, S.; Wang, W.; Zeng, S.; Shang, M.; Zhang, L. Preparation of ordered mesoporous Ag/WO_3 and its highly efficient degradation of acetaldehyde under visible-light irradiation. *J. Hazard. Mater.* **2010**, *178* (1−3), 427−433.
(8) Cavalca, F.; Laursen, A. B.; Kardynal, B. E.; Dunin-Borkowski, R. E.; Dahl, S.; Wagner, J. B.; Hansen, T. W. In situ transmission electron microscopy of light-induced photocatalytic reactions. *Nanotechnology* **2012**, *23* (7), No. 075705.
(9) Kudo, A.; Miseki, Y. Heterogeneous photocatalyst materials for water splitting. *Chem. Soc. Rev.* **2009**, *38* (1), 253−278.
(10) Maeda, K. Photocatalytic water splitting using semiconductor particles: history and recent developments. *J. Photochem. Photobiol., C* **2011**, *12* (4), 237−268.
(11) Roy, S. C.; Varghese, O. K.; Paulose, M.; Grimes, C. A. Toward solar fuels: photocatalytic conversion of carbon dioxide to hydrocarbons. *ACS Nano* **2010**, *4* (3), 1259−1278.
(12) Chong, M. N.; Jin, B.; Chow, C. W. K.; Saint, C. Recent developments in photocatalytic water treatment technology: a review. *Water Res.* **2010**, *44* (10), 2997−3027.
(13) Ahmed, S.; Rasul, M. G.; Martens, W. N.; Brown, R.; Hashib, M. A. Heterogeneous photocatalytic degradation of phenols in wastewater: a review on current status and developments. *Desalination* **2010**, *261* (1−2), 3−18.
(14) Zhao, J.; Yang, X. Photocatalytic oxidation for indoor air purification: a literature review. *Build. Environ.* **2003**, *38* (5), 645−654.

DOI: 10.1021/acs.chemrev.6b00327
Chem. Rev. 2016, 116, 14587−14619

(15) Di Paola, A.; García-López, E.; Marcì, G.; Palmisano, L. A survey of photocatalytic materials for environmental remediation. *J. Hazard. Mater.* **2012**, *211−212*, 3−29.
(16) Ran, J.; Zhang, J.; Yu, J.; Jaroniec, M.; Qiao, S. Z. Earth-abundant cocatalysts for semiconductor-based photocatalytic water splitting. *Chem. Soc. Rev.* **2014**, *43* (22), 7787−7812.
(17) Zhou, N.; López-Puente, V.; Wang, Q.; Polavarapu, L.; Pastoriza-Santos, I.; Xu, Q. H. Plasmon-enhanced light harvesting: Applications in enhanced photocatalysis, photodynamic therapy and photovoltaics. *RSC Adv.* **2015**, *5* (37), 29076−29097.
(18) Maeda, K.; Abe, R.; Domen, K. Role and function of ruthenium species as promoters with TaON-based photocatalysts for oxygen evolution in two-step water splitting under visible light. *J. Phys. Chem. C* **2011**, *115* (7), 3057−3064.
(19) Kang, J. G.; Sohn, Y. Interfacial nature of Ag nanoparticles supported on TiO_2 photocatalysts. *J. Mater. Sci.* **2012**, *47* (2), 824−832.
(20) Ma, L. L.; Cui, Z. D.; Li, Z. Y.; Zhu, S. L.; Liang, Y. Q.; Yin, Q. W.; Yang, X. J. The fabrication of SnSe/Ag nanoparticles on TiO_2 nanotubes. *Mater. Sci. Eng., B* **2013**, *178* (1), 77−82.
(21) Dasgupta, N. P.; Liu, C.; Andrews, S.; Prinz, F. B.; Yang, P. Atomic layer deposition of platinum catalysts on nanowire surfaces for photoelectrochemical water reduction. *J. Am. Chem. Soc.* **2013**, *135* (35), 12932−12935.
(22) Murata, A.; Oka, N.; Nakamura, S.; Shigesato, Y. Visible-light active photocatalytic WO_3 films loaded with Pt nanoparticles deposited by sputtering. *J. Nanosci. Nanotechnol.* **2012**, *12* (6), 5082−5086.
(23) Bamwenda, G. R.; Tsubota, S.; Nakamura, T.; Haruta, M. Photoassisted hydrogen production from a water-ethanol solution: a comparison of activities of Au-TiO_2 and Pt-TiO_2. *J. Photochem. Photobiol., A* **1995**, *89* (2), 177−189.
(24) Busser, G. W.; Mei, B.; Muhler, M. Optimizing the deposition of hydrogen evolution sites on suspended semiconductor particles using on-line photocatalytic reforming of aqueous methanol solutions. *ChemSusChem* **2012**, *5* (11), 2200−2206.
(25) Rufus, I. B.; Viswanathan, B.; Ramakrishnan, V.; Kuriacose, J. C. Cadmium sulfide with iridium sulfide and platinum sulfide deposits as a photocatalyst for the decomposition of aqueous sulfide. *J. Photochem. Photobiol., A* **1995**, *91* (1), 63−66.
(26) Chen, X.; Chen, W.; Gao, H.; Yang, Y.; Shangguan, W. In situ photodeposition of NiO_X on CdS for hydrogen production under visible light: Enhanced activity by controlling solution environment. *Appl. Catal., B* **2014**, *152−153*, 68−72.
(27) Jiang, X.; Fu, X.; Zhang, L.; Meng, S.; Chen, S. Photocatalytic reforming of glycerol for H_2 evolution on Pt/TiO_2: fundamental understanding the effect of co-catalyst Pt and the Pt deposition route. *J. Mater. Chem. A* **2015**, *3* (5), 2271−2282.
(28) Kozlova, E. A.; Vorontsov, A. V. Influence of mesoporous and platinum-modified titanium dioxide preparation methods on photocatalytic activity in liquid and gas phase. *Appl. Catal., B* **2007**, *77* (1−2), 35−45.
(29) Li, J.; Xu, J.; Dai, W. L.; Fan, K. Dependence of Ag deposition methods on the photocatalytic activity and surface state of TiO_2 with twistlike helix structure. *J. Phys. Chem. C* **2009**, *113* (19), 8343−8349.
(30) Iizuka, K.; Wato, T.; Miseki, Y.; Saito, K.; Kudo, A. Photocatalytic reduction of carbon dioxide over Ag cocatalyst-loaded $ALa_4Ti_4O_{15}$ (A = Ca, Sr, and Ba) using water as a reducing reagent. *J. Am. Chem. Soc.* **2011**, *133* (51), 20863−20868.
(31) Abe, R.; Higashi, M.; Domen, K. Overall water splitting under visible light through a two-step photoexcitation between TaON and WO_3 in the presence of an iodate-iodide shuttle redox mediator. *ChemSusChem* **2011**, *4* (2), 228−237.
(32) Gunji, T.; Tsuda, T.; Jeevagan, A. J.; Hashimoto, M.; Tanabe, T.; Kaneko, S.; Miyauchi, M.; Saravanan, G.; Abe, H.; Matsumoto, F. Visible light induced decomposition of organic compounds on WO_3 loaded PtPb co-catalysts. *Catal. Commun.* **2014**, *56*, 96−100.
(33) Oros-Ruiz, S.; Pedraza-Avella, J. A.; Guzmán, C.; Quintana, M.; Moctezuma, E.; Del Angel, G.; Gómez, R.; Pérez, E. Effect of gold particle size and deposition method on the photodegradation of 4-chlorophenol by Au/TiO_2. *Top. Catal.* **2011**, *54* (8−9), 519−526.
(34) Sungbom, C.; Kawai, M.; Tanaka, K. XPS studies of the platinum species photodeposited on titania from aqueous chloroplatinic acid. *Bull. Chem. Soc. Jpn.* **1984**, *57* (3), 871−872.
(35) Nakamatsu, H.; Kawai, T.; Koreeda, A.; Kawai, S. Electron-microscopic observation of photodeposited Pt on TiO_2 particles in relation to photocatalytic activity. *J. Chem. Soc., Faraday Trans. 1* **1986**, *82* (2), 527−531.
(36) Lee, J.; Choi, W. Photocatalytic reactivity of surface platinized TiO_2: substrate specificity and the effect of Pt oxidation state. *J. Phys. Chem. B* **2005**, *109* (15), 7399−7406.
(37) Xi, C.; Chen, Z.; Li, Q.; Jin, Z. Effects of H^+, Cl^- and CH_3COOH on the photocatalytic conversion of $PtCl_6^{2-}$ in aqueous TiO_2 dispersion. *J. Photochem. Photobiol., A* **1995**, *87* (3), 249−255.
(38) Zhang, F.; Chen, J.; Zhang, X.; Gao, W.; Jin, R.; Guan, N.; Li, Y. Synthesis of titania-supported platinum catalyst: the effect of pH on morphology control and valence state during photodeposition. *Langmuir* **2004**, *20* (21), 9329−9334.
(39) Qamar, M.; Ganguli, A. K. Self-assembling behaviour of Pt nanoparticles onto surface of TiO_2 and their resulting photocatalytic activity. *Bull. Mater. Sci.* **2013**, *36* (6), 945−951.
(40) Mahlamvana, F.; Kriek, R. J. Photocatalytic reduction of platinum(II and IV) from their chloro complexes in a titanium dioxide suspension in the absence of an organic sacrificial reducing agent. *Appl. Catal., B* **2014**, *148−149*, 387−393.
(41) Herrmann, J. M.; Disdier, J.; Pichat, P. Photoassisted platinum deposition on TiO_2 powder using various platinum complexes. *J. Phys. Chem.* **1986**, *90* (22), 6028−6034.
(42) Murcia, J. J.; Navío, J. A.; Hidalgo, M. C. Insights towards the influence of Pt features on the photocatalytic activity improvement of TiO_2 by platinisation. *Appl. Catal., B* **2012**, *126*, 76−85.
(43) Yang, J. C.; Kim, Y. C.; Shul, Y. G.; Shin, C. H.; Lee, T. K. Characterization of photoreduced Pt/TiO_2 and decomposition of dichloroacetic acid over photoreduced Pt/TiO_2 catalysts. *Appl. Surf. Sci.* **1997**, *121−122*, 525−529.
(44) Chowdhury, P.; Malekshoar, G.; Ray, M. B.; Zhu, J.; Ray, A. K. Sacrificial hydrogen generation from formaldehyde with Pt/TiO_2 photocatalyst in solar radiation. *Ind. Eng. Chem. Res.* **2013**, *52* (14), 5023−5029.
(45) Li, Y.; Lu, G.; Li, S. Photocatalytic hydrogen generation and decomposition of oxalic acid over platinized TiO_2. *Appl. Catal., A* **2001**, *214* (2), 179−185.
(46) Zhao, W.; Chen, C.; Li, X.; Zhao, J.; Hidaka, H.; Serpone, N. Photodegradation of sulforhodamine-B dye in platinized titania dispersions under visible light irradiation: influence of platinum as a functional co-catalyst. *J. Phys. Chem. B* **2002**, *106* (19), 5022−5028.
(47) Sclafani, A.; Mozzanega, M. N.; Pichat, P. Effect of silver deposits on the photocatalytic activity of titanium dioxide samples for the dehydrogenation or oxidation of 2-propanol. *J. Photochem. Photobiol., A* **1991**, *59* (2), 181−189.
(48) Piwoński, I.; Kadzioła, K.; Kisielewska, A.; Soliwoda, K.; Wolszczak, M.; Lisowska, K.; Wrońska, N.; Felczak, A. The effect of the deposition parameters on size, distribution and antimicrobial properties of photoinduced silver nanoparticles on titania coatings. *Appl. Surf. Sci.* **2011**, *257* (16), 7076−7082.
(49) Iliev, V.; Tomova, D.; Bilyarska, L.; Tyuliev, G. Influence of the size of gold nanoparticles deposited on TiO_2 upon the photocatalytic destruction of oxalic acid. *J. Mol. Catal. A: Chem.* **2007**, *263* (1−2), 32−38.
(50) Fernandez, A.; Caballero, A.; Gonzalez-Elipe, A. R.; Herrmann, J. M.; Dexpert, H.; Villain, F. In situ EXAFS study of the photocatalytic reduction and deposition of gold on colloidal titania. *J. Phys. Chem.* **1995**, *99* (10), 3303−3309.
(51) Kriek, R. J.; Mahlamvana, F. Dependency on chloride concentration and 'in-sphere' oxidation of H_2O for the effective TiO_2-photocatalysed electron transfer from H_2O to $[PdCl_n(H_2O)_{4-n}]^{2-n}$ (n = 0−4) in the absence of an added sacrificial reducing agent. *Appl. Catal., A* **2012**, *423−424*, 28−33.
(52) Borgarello, E.; Serpone, N.; Emo, G.; Harris, R.; Pelizzetti, E.; Minero, C. Light-induced reduction of rhodium(III) and palladium(II)

DOI: 10.1021/acs.chemrev.6b00327
Chem. Rev. 2016, 116, 14587−14619

on titanium dioxide dispersions and the selective photochemical separation and recovery of gold(III), platinum(IV), and rhodium(III) in chloride media. *Inorg. Chem.* **1986**, *25* (25), 4499−4503.
(53) Ohno, T.; Sarukawa, K.; Matsumura, M. Crystal faces of rutile and anatase TiO_2 particles and their roles in photocatalytic reactions. *New J. Chem.* **2002**, *26* (9), 1167−1170.
(54) Li, C.; Zhang, S.; Zhang, B.; Su, D.; He, S.; Zhao, Y.; Liu, J.; Wang, F.; Wei, M.; Evans, D. G.; et al. Photohole-oxidation-assisted anchoring of ultra-small Ru clusters onto TiO_2 with excellent catalytic activity and stability. *J. Mater. Chem. A* **2013**, *1* (7), 2461−2467.
(55) Khnayzer, R. S.; Mara, M. W.; Huang, J.; Shelby, M. L.; Chen, L. X.; Castellano, F. N. Structure and activity of photochemically deposited ″CoPi″ oxygen evolving catalyst on titania. *ACS Catal.* **2012**, *2* (10), 2150−2160.
(56) Fujii, M.; Nagasuna, K.; Fujishima, M.; Akita, T.; Tada, H. Photodeposition of CdS quantum dots on TiO_2: preparation, characterization, and reaction mechanism. *J. Phys. Chem. C* **2009**, *113* (38), 16711−16716.
(57) Qin, N.; Liu, Y.; Wu, W.; Shen, L.; Chen, X.; Li, Z.; Wu, L. One-dimensional CdS/TiO_2 nanofiber composites as efficient visible-light-driven photocatalysts for selective organic transformation: synthesis, characterization, and performance. *Langmuir* **2015**, *31* (3), 1203−1209.
(58) Zhu, H.; Yang, B.; Xu, J.; Fu, Z.; Wen, M.; Guo, T.; Fu, S.; Zuo, J.; Zhang, S. Construction of Z-scheme type CdS-Au-TiO_2 hollow nanorod arrays with enhanced photocatalytic activity. *Appl. Catal., B* **2009**, *90* (3−4), 463−469.
(59) Kim, M.; Kim, Y. K.; Lim, S. K.; Kim, S.; In, S. I. Efficient visible light-induced H_2 production by $Au@CdS/TiO_2$ nanofibers: synergistic effect of core-shell structured Au@CdS and densely packed TiO_2 nanoparticles. *Appl. Catal., B* **2015**, *166−167*, 423−431.
(60) Zhou, H.; Pan, J.; Ding, L.; Tang, Y.; Ding, J.; Guo, Q.; Fan, T.; Zhang, D. Biomass-derived hierarchical porous $CdS/M/TiO_2$ (M = Au, Ag, Pt, Pd) ternary heterojunctions for photocatalytic hydrogen evolution. *Int. J. Hydrogen Energy* **2014**, *39* (29), 16293−16301.
(61) Tanaka, A.; Fuku, K.; Nishi, T.; Hashimoto, K.; Kominami, H. Functionalization of Au/TiO_2 plasmonic photocatalysts with Pd by formation of a core-shell structure for effective dechlorination of chlorobenzene under irradiation of visible light. *J. Phys. Chem. C* **2013**, *117* (33), 16983−16989.
(62) Herrmann, J. M.; Disdier, J.; Pichat, P.; Fernández, A.; González-Elipe, A.; Munuera, G.; Leclercq, C. Titania-supported bimetallic catalyst synthesis by photocatalytic codeposition at ambient temperature: preparation and characterization of Pt-Rh, Ag-Rh, and Pt-Pd couples. *J. Catal.* **1991**, *132* (2), 490−497.
(63) Qiao, P.; Zou, S.; Xu, S.; Liu, J.; Li, Y.; Ma, G.; Xiao, L.; Lou, H.; Fan, J. A general synthesis strategy of multi-metallic nanoparticles within mesoporous titania *via in situ* photo-deposition. *J. Mater. Chem. A* **2014**, *2* (41), 17321−17328.
(64) Chaudhary, R.; Singh, C. Removal of metal ions by means of solar oxidation processes based on pH, TiO_2 and oxidants. *Desalin. Water Treat.* **2014**, *52* (7−9), 1263−1271.
(65) Kabra, K.; Chaudhary, R.; Sawhney, R. L. Solar photocatalytic removal of Cu(II), Ni(II), Zn(II) and Pb(II): speciation modeling of metal-citric acid complexes. *J. Hazard. Mater.* **2008**, *155* (3), 424−432.
(66) Teramura, K.; Okuoka, S. I.; Yamazoe, S.; Kato, K.; Shishido, T.; Tanaka, T. In situ time-resolved energy-dispersive XAFS study on photodeposition of Rh particles on a TiO_2 photocatalyst. *J. Phys. Chem. C* **2008**, *112* (23), 8495−8498.
(67) Ohyama, J.; Teramura, K.; Okuoka, S. I.; Yamazoe, S.; Kato, K.; Shishido, T.; Tanaka, T. Investigation of the formation process of photodeposited Rh nanoparticles on TiO_2 by in situ time-resolved energy-dispersive XAFS analysis. *Langmuir* **2010**, *26* (17), 13907−13912.
(68) Huang, Q.; Liu, S.; Wei, W.; Yan, Q.; Wu, C. Selective synthesis of different ZnO/Ag nanocomposites as surface enhanced Raman scattering substrates and highly efficient photocatalytic catalysts. *RSC Adv.* **2015**, *5* (34), 27075−27081.
(69) Wang, J.; Fan, X. M.; Tian, K.; Zhou, Z. W.; Wang, Y. Largely improved photocatalytic properties of Ag/tetrapod-like ZnO nanocompounds prepared with different PEG contents. *Appl. Surf. Sci.* **2011**, *257* (17), 7763−7770.
(70) Kawano, K.; Komatsu, M.; Yajima, Y.; Haneda, H.; Maki, H.; Yamamoto, T. Photoreduction of Ag ion on ZnO single crystal. *Appl. Surf. Sci.* **2002**, *189* (3−4), 265−270.
(71) Behnajady, M. A.; Modirshahla, N.; Shokri, M.; Zeininezhad, A.; Zamani, H. A. Enhancement photocatalytic activity of ZnO nanoparticles by silver doping with optimization of photodeposition method parameters. *J. Environ. Sci. Health, Part A: Toxic/Hazard. Subst. Environ. Eng.* **2009**, *44* (7), 666−672.
(72) Lin, C. Y.; Lai, Y. H.; Balamurugan, A.; Vittal, R.; Lin, C. W.; Ho, K. C. Electrode modified with a composite film of ZnO nanorods and Ag nanoparticles as a sensor for hydrogen peroxide. *Talanta* **2010**, *82* (1), 340−347.
(73) Li, R.; Han, C.; Chen, Q. W. A facile synthesis of multifunctional ZnO/Ag sea urchin-like hybrids as highly sensitive substrates for surface-enhanced Raman detection. *RSC Adv.* **2013**, *3* (29), 11715−11722.
(74) Chen, S.; Nickel, U. Synthesis of hybrid metal-semiconductor ultrafine particles. Photochemical deposition of silver on a ZnO colloid surface. *J. Chem. Soc., Faraday Trans.* **1996**, *92* (9), 1555−1562.
(75) Peng, F.; Zhu, H.; Wang, H.; Yu, H. Preparation of Ag-sensitized ZnO and its photocatalytic performance under simulated solar light. *Korean J. Chem. Eng.* **2007**, *24* (6), 1022−1026.
(76) Xie, W.; Li, Y.; Sun, W.; Huang, J.; Xie, H.; Zhao, X. Surface modification of ZnO with Ag improves its photocatalytic efficiency and photostability. *J. Photochem. Photobiol., A* **2010**, *216* (2−3), 149−155.
(77) Deng, Q.; Duan, X.; Ng, D. H. L.; Tang, H.; Yang, Y.; Kong, M.; Wu, Z.; Cai, W.; Wang, G. Ag nanoparticle decorated nanoporous ZnO microrods and their enhanced photocatalytic activities. *ACS Appl. Mater. Interfaces* **2012**, *4* (11), 6030−6037.
(78) Kislov, N.; Lahiri, J.; Verma, H.; Goswami, D. Y.; Stefanakos, E.; Batzill, M. Photocatalytic degradation of methyl orange over single crystalline ZnO: Orientation dependence of photoactivity and photostability of ZnO. *Langmuir* **2009**, *25* (5), 3310−3315.
(79) Alammar, T.; Mudring, A. V. Facile preparation of Ag/ZnO nanoparticles via photoreduction. *J. Mater. Sci.* **2009**, *44* (12), 3218−3222.
(80) Habibi, M. H.; Sheibani, R. Nanostructure silver-doped zinc oxide films coating on glass prepared by sol-gel and photochemical deposition process: Application for removal of mercaptan. *J. Ind. Eng. Chem.* **2013**, *19* (1), 161−165.
(81) Liang, Y.; Guo, N.; Li, L.; Li, R.; Ji, G.; Gan, S. Fabrication of porous 3D flower-like Ag/ZnO heterostructure composites with enhanced photocatalytic performance. *Appl. Surf. Sci.* **2015**, *332*, 32−39.
(82) Ren, C.; Yang, B.; Wu, M.; Xu, J.; Fu, Z.; lv, Y.; Guo, T.; Zhao, Y.; Zhu, C. Synthesis of Ag/ZnO nanorods array with enhanced photocatalytic performance. *J. Hazard. Mater.* **2010**, *182* (1−3), 123−129.
(83) Wang, T.; Jiao, Z.; Chen, T.; Li, Y.; Ren, W.; Lin, S.; Lu, G.; Ye, J.; Bi, Y. Vertically aligned ZnO nanowire arrays tip-grafted with silver nanoparticles for photoelectrochemical applications. *Nanoscale* **2013**, *5* (16), 7552−7557.
(84) Zhang, Y.; Guo, S.; Ma, J.; Ge, H. Preparation, characterization, catalytic performance and antibacterial activity of Ag photodeposited on monodisperse ZnO submicron spheres. *J. Sol-Gel Sci. Technol.* **2014**, *72* (1), 171−178.
(85) Chen, C.; Zheng, Y.; Zhan, Y.; Lin, X.; Zheng, Q.; Wei, K. Enhanced Raman scattering and photocatalytic activity of Ag/ZnO heterojunction nanocrystals. *Dalton Trans.* **2011**, *40* (37), 9566−9570.
(86) Wu, J. J.; Tseng, C. H. Photocatalytic properties of nc-Au/ZnO nanorod composites. *Appl. Catal., B* **2006**, *66* (1−2), 51−57.
(87) Lu, L.; Hu, S.; Lee, H. I.; Wöll, C.; Fischer, R. A. Photoinduced growth of Cu nanoparticles on ZnO from $CuCl_2$ in methanol. *J. Nanopart. Res.* **2007**, *9* (3), 491−496.
(88) Gomathisankar, P.; Hachisuka, K.; Katsumata, H.; Suzuki, T.; Funasaka, K.; Kaneco, S. Enhanced photocatalytic hydrogen production from aqueous methanol solution using ZnO with simultaneous

DOI: 10.1021/acs.chemrev.6b00327
Chem. Rev. 2016, 116, 14587−14619

photodeposition of Cu. *Int. J. Hydrogen Energy* **2013**, *38* (27), 11840−11846.
(89) Stroyuk, A. L.; Shvalagin, V. V.; Kuchmii, S. Y. Photochemical synthesis and optical properties of binary and ternary metal-semiconductor composites based on zinc oxide nanoparticles. *J. Photochem. Photobiol., A* **2005**, *173* (2), 185−194.
(90) Li, R.; Zhang, F.; Wang, D.; Yang, J.; Li, M.; Zhu, J.; Zhou, X.; Han, H.; Li, C. Spatial separation of photogenerated electrons and holes among {010} and {110} crystal facets of $BiVO_4$. *Nat. Commun.* **2013**, *4*, No. 1432.
(91) Li, R.; Han, H.; Zhang, F.; Wang, D.; Li, C. Highly efficient photocatalysts constructed by rational assembly of dual-cocatalysts separately on different facets of $BiVO_4$. *Energy Environ. Sci.* **2014**, *7* (4), 1369−1376.
(92) Kohtani, S.; Hiro, J.; Yamamoto, N.; Kudo, A.; Tokumura, K.; Nakagaki, R. Adsorptive and photocatalytic properties of Ag-loaded $BiVO_4$ on the degradation of 4-n-alkylphenols under visible light irradiation. *Catal. Commun.* **2005**, *6* (3), 185−189.
(93) Maeda, K.; Lu, D.; Teramura, K.; Domen, K. Direct deposition of nanoparticulate rhodium-chromium mixed-oxides on a semiconductor powder by band-gap irradiation. *J. Mater. Chem.* **2008**, *18* (30), 3539−3542.
(94) Busser, G. W.; Mei, B.; Pougin, A.; Strunk, J.; Gutkowski, R.; Schuhmann, W.; Willinger, M. G.; Schlögl, R.; Muhler, M. Photodeposition of copper and chromia on gallium oxide: The role of co-catalysts in photocatalytic water splitting. *ChemSusChem* **2014**, *7* (4), 1030−1034.
(95) Zhou, C.; Shang, L.; Yu, H.; Bian, T.; Wu, L. Z.; Tung, C. H.; Zhang, T. Mesoporous plasmonic Au-loaded Ta_2O_5 nanocomposites for efficient visible light photocatalysis. *Catal. Today* **2014**, *225*, 158−163.
(96) Sasaki, Y.; Iwase, A.; Kato, H.; Kudo, A. The effect of co-catalyst for Z-scheme photocatalysis systems with an Fe^{3+}/Fe^{2+} electron mediator on overall water splitting under visible light irradiation. *J. Catal.* **2008**, *259* (1), 133−137.
(97) Li, Q.; Chen, Z.; Zheng, X.; Jin, Z. Study of photoreduction of $PtCl_6^{2-}$ on CdS. *J. Phys. Chem.* **1992**, *96* (14), 5959−5962.
(98) Jin, Z.; Chen, Z.; Li, Q.; Xi, C.; Zheng, X. On the conditions and mechanism of PtO_2 formation in the photoinduced conversion of H_2PtCl_6. *J. Photochem. Photobiol., A* **1994**, *81* (3), 177−182.
(99) Wang, Y.; Wang, Y.; Xu, R. Photochemical deposition of Pt on CdS for H_2 evolution from water: Markedly enhanced activity by controlling Pt reduction environment. *J. Phys. Chem. C* **2013**, *117* (2), 783−790.
(100) Fox, M. A.; Pettit, T. L. Photoactivity of zeolite-supported cadmium sulfide: Hydrogen evolution in the presence of sacrificial donors. *Langmuir* **1989**, *5* (4), 1056−1061.
(101) Dukovic, G.; Merkle, M. G.; Nelson, J. H.; Hughes, S. M.; Alivisatos, A. P. Photodeposition of Pt on colloidal CdS and CdSe/CdS semiconductor nanostructures. *Adv. Mater.* **2008**, *20* (22), 4306−4311.
(102) Ma, G.; Yan, H.; Shi, J.; Zong, X.; Lei, Z.; Li, C. Direct splitting of H_2S into H_2 and S on CdS-based photocatalyst under visible light irradiation. *J. Catal.* **2008**, *260* (1), 134−140.
(103) Li, T. L.; Cai, C. D.; Yeh, T. F.; Teng, H. Capped $CuInS_2$ quantum dots for H_2 evolution from water under visible light illumination. *J. Alloys Compd.* **2013**, *550*, 326−330.
(104) Li, N.; Liu, M.; Zhou, Z.; Zhou, J.; Sun, Y.; Guo, L. Charge separation in facet-engineered chalcogenide photocatalyst: a selective photocorrosion approach. *Nanoscale* **2014**, *6* (16), 9695−9702.
(105) Hara, M.; Nunoshige, J.; Takata, T.; Kondo, J. N.; Domen, K. Unusual enhancement of H_2 evolution by Ru on TaON photocatalyst under visible light irradiation. *Chem. Commun.* **2003**, *9* (24), 3000−3001.
(106) Liu, Y.; Zhou, Y.; Chen, G.; Guo, T.; Wang, L.; Huang, X.; Zeng, W. Loading cobalt phosphate on TaON surface as efficient noble-metal-free co-catalyst for enhanced photocatalytic water oxidation performance. *Mater. Lett.* **2015**, *148*, 155−158.
(107) Moudler, J. F.; Stickle, W. F.; Sobol, P. E.; Bomben, K. D. *Handbook of X-ray photoelectron spectroscopy: a reference book of standard spectra for identification and interpretation of XPS data*; Physical Electronics Division, Perkin-Elmer Corporation: 1992.
(108) Ferraria, A. M.; Carapeto, A. P.; Botelho Do Rego, A. M. X-ray photoelectron spectroscopy: Silver salts revisited. *Vacuum* **2012**, *86* (12), 1988−1991.
(109) Kaushik, V. K. XPS core level spectra and Auger parameters for some silver compounds. *J. Electron Spectrosc. Relat. Phenom.* **1991**, *56* (3), 273−277.
(110) Carabineiro, S. A. C.; MacHado, B. F.; Bacsa, R. R.; Serp, P.; Drazić, G.; Faria, J. L.; Figueiredo, J. L. Catalytic performance of Au/ZnO nanocatalysts for CO oxidation. *J. Catal.* **2010**, *273* (2), 191−198.
(111) Dulnee, S.; Luengnaruemitchai, A.; Wanchanthuek, R. Activity of Au/ZnO catalysts prepared by photo-deposition for the preferential CO oxidation in a H_2-rich gas. *Int. J. Hydrogen Energy* **2014**, *39* (12), 6443−6453.
(112) Naknam, P.; Luengnaruemitchai, A.; Wongkasemjit, S. Preferential CO oxidation over Au/ZnO and Au/ZnO-Fe_2O_3 catalysts prepared by photodeposition. *Int. J. Hydrogen Energy* **2009**, *34* (24), 9838−9846.
(113) Wu, M.; Chen, W. J.; Shen, Y. H.; Huang, F. Z.; Li, C. H.; Li, S. K. In situ growth of matchlike ZnO/Au plasmonic heterostructure for enhanced photoelectrochemical water splitting. *ACS Appl. Mater. Interfaces* **2014**, *6* (17), 15052−15060.
(114) He, W.; Kim, H. K.; Wamer, W. G.; Melka, D.; Callahan, J. H.; Yin, J. J. Photogenerated charge carriers and reactive oxygen species in ZnO/Au hybrid nanostructures with enhanced photocatalytic and antibacterial activity. *J. Am. Chem. Soc.* **2014**, *136* (2), 750−757.
(115) Chang, C. M.; Hon, M. H.; Leu, I. C. Outstanding H_2 sensing performance of Pd nanoparticle-decorated ZnO nanorod arrays and the temperature-dependent sensing mechanisms. *ACS Appl. Mater. Interfaces* **2013**, *5* (1), 135−143.
(116) Chang, C. M.; Hon, M. H.; Leu, I. C. Improvement in CO sensing characteristics by decorating ZnO nanorod arrays with Pd nanoparticles and the related mechanisms. *RSC Adv.* **2012**, *2* (6), 2469−2475.
(117) Jin, Y.; Xi, J.; Zhang, Z.; Xiao, J.; Xiao, F.; Qian, L.; Wang, S. An ultra-low Pd loading nanocatalyst with efficient catalytic activity. *Nanoscale* **2015**, *7* (12), 5510−5515.
(118) Liqiang, J.; Baiqi, W.; Baifu, X.; Shudan, L.; Keying, S.; Weimin, C.; Honggang, F. Investigations on the surface modification of ZnO nanoparticle photocatalyst by depositing Pd. *J. Solid State Chem.* **2004**, *177* (11), 4221−4227.
(119) Kozytskiy, A. V.; Stroyuk, A. L.; Kuchmy, S. Y.; Streltsov, E. A.; Skorik, N. A.; Moskalyuk, V. O. Effect of the method of preparation of ZnO/CdS and TiO_2/CdS film nanoheterostructures on their photoelectrochemical properties. *Theor. Exp. Chem.* **2013**, *49* (3), 165−171.
(120) Shvalagin, V. V.; Stroyuk, A. L.; Kotenko, I. E.; Kuchmii, S. Y. Photocatalytic formation of porous CdS/ZnO nanospheres and CdS nanotubes. *Theor. Exp. Chem.* **2007**, *43* (4), 229−234.
(121) Lu, L.; Wohlfart, A.; Parala, H.; Birkner, A.; Fischer, R. A. A novel preparation of nano-Cu/ZnO by photo-reduction of $Cu(OCH(Me)CH_2NMe_2)_2$ on ZnO at room temperature. *Chem. Commun.* **2003**, *9* (1), 40−41.
(122) Arsana, P.; Bubpa, C.; Sang-aroon, W. Photocatalytic activity under solar irradiation of silver and copper doped zincoxide: Photodeposition versus liquid impregnation methods. *J. Appl. Sci.* **2012**, *12* (17), 1809−1816.
(123) Boccuzzi, F.; Chiorino, A.; Guglielminotti, E. Effects of structural defects and alloying on the FTIR spectra of CO adsorbed on Pt/ZnO. *Surf. Sci.* **1996**, *368* (1−3), 264−269.
(124) Carabineiro, S. A. C.; Machado, B. F.; Dražić, G.; Bacsa, R. R.; Serp, P.; Figueiredo, J. L.; Faria, J. L. Photodeposition of Au and Pt on ZnO and TiO_2. In *Scientific Bases for the Preparation of Heterogeneous Catalysts*; Proceedings of the 10th International Symposium, Louvain-la-Neuve, Belgium, July 11−15, 2010; Studies in Surface Science and Catalysis, Vol. *175*; Elsevier: Amsterdam, 2010; pp 629−633.
(125) Siboni, M. S.; Samadi, M. T.; Yang, J. K.; Lee, S. M. Photocatalytic reduction of Cr(VI) and Ni(II) in aqueous solution by

DOI: 10.1021/acs.chemrev.6b00327
Chem. Rev. 2016, 116, 14587−14619

synthesized nanoparticle ZnO under ultraviolet light irradiation: A kinetic study. *Environ. Technol.* **2011**, *32* (14), 1573−1579.
(126) Doménech, J.; Andrés, M.; Munùz, J. Photoinduced oxygen uptake in aqueous suspensions of ZnO. *Electrochim. Acta* **1987**, *32* (5), 773−775.
(127) Park, S.; Kim, H. S.; Lee, J. H.; Kim, Y. C.; Lee, J. C.; Chung, Y. J. Photoreaction of gold ions from potassium gold cyanide wastewater using solution-combusted ZnO nanopowders. *J. Eur. Ceram. Soc.* **2010**, *30* (2), 177−180.
(128) Kozytskiy, A. V.; Stroyuk, A. L.; Kuchmy, S. Y.; Skorik, N. A.; Moskalyuk, V. O. Morphology, photochemical and photocatalytic properties of nanocrystalline zinc oxide films. *Theor. Exp. Chem.* **2012**, *48* (5), 331−337.
(129) Su, L.; Qin, N. A facile method for fabricating Au-nanoparticles-decorated ZnO nanorods with greatly enhanced near-band-edge emission. *Ceram. Int.* **2015**, *41* (2), 2673−2679.
(130) Zheng, H.; Ou, J. Z.; Strano, M. S.; Kaner, R. B.; Mitchell, A.; Kalantar-Zadeh, K. Nanostructured tungsten oxide - properties, synthesis, and applications. *Adv. Funct. Mater.* **2011**, *21* (12), 2175−2196.
(131) Kumar, S. G.; Rao, K. S. R. K. Tungsten-based nanomaterials (WO_3 & Bi_2WO_6): modifications related to charge carrier transfer mechanisms and photocatalytic applications. *Appl. Surf. Sci.* **2015**, *355*, 939−958.
(132) Huang, Z. F.; Song, J.; Pan, L.; Zhang, X.; Wang, L.; Zou, J. J. Tungsten oxides for photocatalysis, electrochemistry, and phototherapy. *Adv. Mater.* **2015**, *27* (36), 5309−5327.
(133) Kim, J.; Lee, C. W.; Choi, W. Platinized WO_3 as an environmental photocatalyst that generates OH radicals under visible light. *Environ. Sci. Technol.* **2010**, *44* (17), 6849−6854.
(134) Arai, T.; Yanagida, M.; Konishi, Y.; Ikura, A.; Iwasaki, Y.; Sugihara, H.; Sayama, K. The enhancement of WO_3-catalyzed photodegradation of organic substances utilizing the redox cycle of copper ions. *Appl. Catal., B* **2008**, *84* (1−2), 42−47.
(135) Joshi, U. A.; Darwent, J. R.; Yiu, H. H. P.; Rosseinsky, M. J. The effect of platinum on the performance of WO_3 nanocrystal photocatalysts for the oxidation of Methyl Orange and iso-propanol. *J. Chem. Technol. Biotechnol.* **2011**, *86* (8), 1018−1023.
(136) Wicaksana, Y.; Liu, S.; Scott, J.; Amal, R. Tungsten trioxide as a visible light photocatalyst for volatile organic carbon removal. *Molecules* **2014**, *19* (11), 17747−17762.
(137) Arai, T.; Horiguchi, M.; Yanagida, M.; Gunji, T.; Sugihara, H.; Sayama, K. Complete oxidation of acetaldehyde and toluene over a Pd/WO_3 photocatalyst under fluorescent- or visible-light irradiation. *Chem. Commun.* **2008**, No. 43, 5565−5567.
(138) Sayama, K.; Mukasa, K.; Abe, R.; Abe, Y.; Arakawa, H. Stoichiometric water splitting into H_2 and O_2 using a mixture of two different photocatalysts and an IO_3^-/I^- shuttle redox mediator under visible light irradiation. *Chem. Commun.* **2001**, *23*, 2416−2417.
(139) Sayama, K.; Mukasa, K.; Abe, R.; Abe, Y.; Arakawa, H. A new photocatalytic water splitting system under visible light irradiation mimicking a Z-scheme mechanism in photosynthesis. *J. Photochem. Photobiol., A* **2002**, *148* (1−3), 71−77.
(140) Abe, R.; Takami, H.; Murakami, N.; Ohtani, B. Pristine simple oxides as visible light driven photocatalysts: Highly efficient decomposition of organic compounds over platinum-loaded tungsten oxide. *J. Am. Chem. Soc.* **2008**, *130* (25), 7780−7781.
(141) Tomita, O.; Ohtani, B.; Abe, R. Highly selective phenol production from benzene on a platinum-loaded tungsten oxide photocatalyst with water and molecular oxygen: selective oxidation of water by holes for generating hydroxyl radical as the predominant source of the hydroxyl group. *Catal. Sci. Technol.* **2014**, *4* (11), 3850−3860.
(142) Gunji, T.; Jeevagan, A. J.; Hashimoto, M.; Nozawa, T.; Tanabe, T.; Kaneko, S.; Miyauchi, M.; Matsumoto, F. Photocatalytic decomposition of various organic compounds over WO_3-supported ordered intermetallic PtPb co-catalysts. *Appl. Catal., B* **2016**, *181*, 475−480.
(143) Shiraishi, Y.; Sugano, Y.; Ichikawa, S.; Hirai, T. Visible light-induced partial oxidation of cyclohexane on WO_3 loaded with Pt nanoparticles. *Catal. Sci. Technol.* **2012**, *2* (2), 400−405.
(144) Tomita, O.; Abe, R.; Ohtani, B. Direct synthesis of phenol from benzene over platinum-loaded tungsten(VI) oxide photocatalysts with water and molecular oxygen. *Chem. Lett.* **2011**, *40* (12), 1405−1407.
(145) Sclafani, A.; Palmisano, L.; Marcí, G.; Venezia, A. M. Influence of platinum on catalytic activity of polycrystalline WO_3 employed for phenol photodegradation in aqueous suspension. *Sol. Energy Mater. Sol. Cells* **1998**, *51* (2), 203−219.
(146) Wang, S.; Wang, T.; Liu, Y.; Gao, Y.; Ding, Y.; Xu, X.; Zhang, X.; Chen, W. Visible light-driven photodecomposition system: Preparation and application of highly dispersed Pt-loaded WO_3 microparticles. *Micro Nano Lett.* **2011**, *6* (4), 229−232.
(147) Xu, Z.; Tabata, I.; Hirogaki, K.; Hisada, K.; Wang, T.; Wang, S.; Hori, T. Preparation of platinum-loaded cubic tungsten oxide: A highly efficient visible light-driven photocatalyst. *Mater. Lett.* **2011**, *65* (9), 1252−1256.
(148) Qamar, M.; Gondal, M. A.; Yamani, Z. H. Removal of Rhodamine 6G induced by laser and catalyzed by Pt/WO_3 nanocomposite. *Catal. Commun.* **2010**, *11* (8), 768−772.
(149) Purwanto, A.; Widiyandari, H.; Ogi, T.; Okuyama, K. Role of particle size for platinum-loaded tungsten oxide nanoparticles during dye photodegradation under solar-simulated irradiation. *Catal. Commun.* **2011**, *12* (6), 525−529.
(150) Zhang, G.; Guan, W.; Shen, H.; Zhang, X.; Fan, W.; Lu, C.; Bai, H.; Xiao, L.; Gu, W.; Shi, W. Organic additives-free hydrothermal synthesis and visible-light-driven photodegradation of tetracycline of WO_3 nanosheets. *Ind. Eng. Chem. Res.* **2014**, *53* (13), 5443−5450.
(151) Wenderich, K.; Klaassen, A.; Siretanu, I.; Mugele, F.; Mul, G. Sorption-determined deposition of platinum on well-defined platelike WO_3. *Angew. Chem., Int. Ed.* **2014**, *53* (46), 12476−12479.
(152) Sadakane, M.; Sasaki, K.; Kunioku, H.; Ohtani, B.; Ueda, W.; Abe, R. Preparation of nano-structured crystalline tungsten(VI) oxide and enhanced photocatalytic activity for decomposition of organic compounds under visible light irradiation. *Chem. Commun.* **2008**, No. 48, 6552−6554.
(153) Aminian, M. K.; Ye, J. Morphology influence on photocatalytic activity of tungsten oxide loaded by platinum nanoparticles. *J. Mater. Res.* **2010**, *25* (1), 141−148.
(154) Qamar, M.; Yamani, Z. H.; Gondal, M. A.; Alhooshani, K. Synthesis and comparative photocatalytic activity of Pt/WO_3 and Au/WO_3 nanocomposites under sunlight-type excitation. *Solid State Sci.* **2011**, *13* (9), 1748−1754.
(155) Shibuya, M.; Miyauchi, M. Site-selective deposition of metal nanoparticles on aligned WO_3 nanotrees for super-hydrophilic thin films. *Adv. Mater.* **2009**, *21* (13), 1373−1376.
(156) Sakai, Y.; Shimanaka, A.; Shioi, M.; Kato, S.; Satokawa, S.; Kojima, T.; Yamasaki, A. Fabrication of high-sensitivity palladium loaded tungsten trioxide photocatalyst by photodeposite method. *Catal. Today* **2015**, *241* (PA), 2−7.
(157) Katsumata, H.; Oda, Y.; Kaneco, S.; Suzuki, T. Photocatalytic activity of Ag/CuO/WO_3 under visible-light irradiation. *RSC Adv.* **2013**, *3* (15), 5028−5035.
(158) Chen, X.; Li, P.; Tong, H.; Kako, T.; Ye, J. Nanoarchitectonics of a Au nanoprism array on WO_3 film for synergistic optoelectronic response. *Sci. Technol. Adv. Mater.* **2011**, *12* (4), No. 044604.
(159) Iliev, V.; Tomova, D.; Rakovsky, S.; Eliyas, A.; Puma, G. L. Enhancement of photocatalytic oxidation of oxalic acid by gold modified WO_3/TiO_2 photocatalysts under UV and visible light irradiation. *J. Mol. Catal. A: Chem.* **2010**, *327* (1−2), 51−57.
(160) Karácsonyi, É.; Baia, L.; Dombi, A.; Danciu, V.; Mogyorósi, K.; Pop, L. C.; Kovács, G.; Coşoveanu, V.; Vulpoi, A.; Simon, S.; et al. The photocatalytic activity of TiO_2/WO_3/noble metal (Au or Pt) nanoarchitectures obtained by selective photodeposition. *Catal. Today* **2013**, *208*, 19−27.
(161) Reiche, H.; Dunn, W. W.; Bard, A. J. Heterogeneous photocatalytic and photosynthetic deposition of copper on TiO_2 and WO_3 powders. *J. Phys. Chem.* **1979**, *83* (17), 2248−2251.

DOI: 10.1021/acs.chemrev.6b00327
Chem. Rev. 2016, 116, 14587−14619

(162) Litter, M. I. Heterogeneous photocatalysis: Transition metal ions in photocatalytic systems. *Appl. Catal., B* **1999**, *23* (2−3), 89−114.
(163) Erbs, W.; Desilvestro, J.; Borgarello, E.; Grätzel, M. Visible-light-induced O_2 generation from aqueous dispersions of WO_3. *J. Phys. Chem.* **1984**, *88* (18), 4001−4006.
(164) Amano, F.; Ishinaga, E.; Yamakata, A. Effect of particle size on the photocatalytic activity of WO_3 particles for water oxidation. *J. Phys. Chem. C* **2013**, *117* (44), 22584−22590.
(165) Xie, Y. P.; Liu, G.; Yin, L.; Cheng, H. M. Crystal facet-dependent photocatalytic oxidation and reduction reactivity of monoclinic WO_3 for solar energy conversion. *J. Mater. Chem.* **2012**, *22* (14), 6746−6751.
(166) Hong, S. J.; Jun, H.; Borse, P. H.; Lee, J. S. Size effects of WO_3 nanocrystals for photooxidation of water in particulate suspension and photoelectrochemical film systems. *Int. J. Hydrogen Energy* **2009**, *34* (8), 3234−3242.
(167) http://coinapps.com/, Accessed August 22, 2016.
(168) Huang, K.; Zhang, Q.; Yang, F.; He, D. Ultraviolet photoconductance of a single hexagonal WO_3 nanowire. *Nano Res.* **2010**, *3* (4), 281−287.
(169) Pang, H. F.; Xiang, X.; Li, Z. J.; Fu, Y. Q.; Zu, X. T. Hydrothermal synthesis and optical properties of hexagonal tungsten oxide nanocrystals assisted by ammonium tartrate. *Phys. Status Solidi A* **2012**, *209* (3), 537−544.
(170) Sun, S.; Chang, X.; Dong, L.; Zhang, Y.; Li, Z.; Qiu, Y. $W_{18}O_{49}$ nanorods decorated with Ag/AgCl nanoparticles as highly-sensitive gas-sensing material and visible-light-driven photocatalyst. *J. Solid State Chem.* **2011**, *184* (8), 2190−2195.
(171) Chen, D.; Li, T.; Chen, Q.; Gao, J.; Fan, B.; Li, J.; Li, X.; Zhang, R.; Sun, J.; Gao, L. Hierarchically plasmonic photocatalysts of Ag/AgCl nanocrystals coupled with single-crystalline WO_3 nanoplates. *Nanoscale* **2012**, *4* (17), 5431−5439.
(172) Wang, P.; Huang, B.; Qin, X.; Zhang, X.; Dai, Y.; Whangbo, M. H. Ag/AgBr/$WO_3{\cdot}H_2O$: visible-light photocatalyst for bacteria destruction. *Inorg. Chem.* **2009**, *48* (22), 10697−10702.
(173) Kovács, G.; Baia, L.; Vulpoi, A.; Radu, T.; Karácsonyi, T.; Dombi, A.; Hernádi, K.; Danciu, V.; Simon, S.; Pap, Z. TiO_2/WO_3/Au nanoarchitectures' photocatalytic activity, "from degradation intermediates to catalysts' structural peculiarities", Part I: Aeroxide P25 based composites. *Appl. Catal., B* **2014**, *147*, 508−517.
(174) Baia, L.; Vulpoi, A.; Radu, T.; Karácsonyi, T.; Dombi, A.; Hernádi, K.; Danciu, V.; Simon, S.; Norén, K.; Canton, S. E.; et al. TiO_2/WO_3/Au nanoarchitectures' photocatalytic activity "from degradation intermediates to catalysts' structural peculiarities" Part II: Aerogel based composites - fine details by spectroscopic means. *Appl. Catal., B* **2014**, *148−149*, 589−600.
(175) Ohno, T.; Murakami, N.; Koyanagi, T.; Yang, Y. Photocatalytic reduction of CO_2 over a hybrid photocatalyst composed of WO_3 and graphitic carbon nitride (g-C_3N_4) under visible light. *J. CO2 Util.* **2014**, *6*, 17−25.
(176) Liu, Z.; Zhao, Z. G.; Miyauchi, M. Efficient visible light active $CaFe_2O_4$/WO_3 based composite photocatalysts: effect of interfacial modification. *J. Phys. Chem. C* **2009**, *113* (39), 17132−17137.
(177) Yaipimai, W.; Subjalearndee, N.; Tumcharern, G.; Intasanta, V. Multifunctional metal and metal oxide hybrid nanomaterials for solar light photocatalyst and antibacterial applications. *J. Mater. Sci.* **2015**, *50* (23), 7681−7697.
(178) Kudo, A.; Omori, K.; Kato, H. A novel aqueous process for preparation of crystal form-controlled and highly crystalline $BiVO_4$ powder from layered vanadates at room temperature and its photocatalytic and photophysical properties. *J. Am. Chem. Soc.* **1999**, *121* (49), 11459−11467.
(179) Kudo, A.; Ueda, K.; Kato, H.; Mikami, I. Photocatalytic O_2 evolution under visible light irradiation on $BiVO_4$ in aqueous $AgNO_3$ solution. *Catal. Lett.* **1998**, *53* (3−4), 229−230.
(180) Tokunaga, S.; Kato, H.; Kudo, A. Selective preparation of monoclinic and tetragonal $BiVO_4$ with scheelite structure and their photocatalytic properties. *Chem. Mater.* **2001**, *13* (12), 4624−4628.
(181) Yu, S. C.; Huang, C. W.; Liao, C. H.; Wu, J. C. S.; Chang, S. T.; Chen, K. H. A novel membrane reactor for separating hydrogen and oxygen in photocatalytic water splitting. *J. Membr. Sci.* **2011**, *382* (1−2), 291−299.
(182) Zhang, X.; Zhang, Y.; Quan, X.; Chen, S. Preparation of Ag doped $BiVO_4$ film and its enhanced photoelectrocatalytic (PEC) ability of phenol degradation under visible light. *J. Hazard. Mater.* **2009**, *167* (1−3), 911−914.
(183) Murakami, N.; Takebe, N.; Tsubota, T.; Ohno, T. Improvement of visible light photocatalytic acetaldehyde decomposition of bismuth vanadate/silica nanocomposites by cocatalyst loading. *J. Hazard. Mater.* **2012**, *211−212*, 83−87.
(184) Ye, H.; Park, H. S.; Bard, A. J. Screening of electrocatalysts for photoelectrochemical water oxidation on W-doped $BiVO_4$ photocatalysts by scanning electrochemical microscopy. *J. Phys. Chem. C* **2011**, *115* (25), 12464−12470.
(185) Park, H. S.; Ha, H. W.; Ruoff, R. S.; Bard, A. J. On the improvement of photoelectrochemical performance and finite element analysis of reduced graphene oxide-$BiVO_4$ composite electrodes. *J. Electroanal. Chem.* **2014**, *716*, 8−15.
(186) Takahara, Y.; Kondo, J. N.; Takata, T.; Lu, D.; Domen, K. Mesoporous tantalum oxide. 1. Characterization and photocatalytic activity for the overall water decomposition. *Chem. Mater.* **2001**, *13* (4), 1194−1199.
(187) Sayama, K.; Arakawa, H. Effect of Na_2CO_3 addition on photocatalytic decomposition of liquid water over various semiconductor catalysis. *J. Photochem. Photobiol., A* **1994**, *77* (2−3), 243−247.
(188) Kang, H. W.; Lim, S. N.; Song, D.; Park, S. B. Organic-inorganic composite of g-C_3N_4-$SrTiO_3$:Rh photocatalyst for improved H_2 evolution under visible light irradiation. *Int. J. Hydrogen Energy* **2012**, *37* (16), 11602−11610.
(189) Ishii, T.; Kato, H.; Kudo, A. H_2 evolution from an aqueous methanol solution on $SrTiO_3$ photocatalysts codoped with chromium and tantalum ions under visible light irradiation. *J. Photochem. Photobiol., A* **2004**, *163* (1−2), 181−186.
(190) Sulaeman, U.; Yin, S.; Sato, T. Solvothermal synthesis and photocatalytic properties of chromium-doped $SrTiO_3$ nanoparticles. *Appl. Catal., B* **2011**, *105* (1−2), 206−210.
(191) Yoshida, M.; Yomogida, T.; Mineo, T.; Nitta, K.; Kato, K.; Masuda, T.; Nitani, H.; Abe, H.; Takakusagi, S.; Uruga, T.; et al. *In situ* observation of carrier transfer in the Mn-oxide/Nb:$SrTiO_3$ photoelectrode by X-ray absorption spectroscopy. *Chem. Commun.* **2013**, *49* (71), 7848−7850.
(192) Tanaka, R.; Takata, S.; Takahashi, R.; Grepstad, J. K.; Tybell, T.; Matsumoto, Y. Photo-electrochemical synthesis of silver-oxide clathrate $Ag_7O_8NO_3$ on $SrTiO_3$. *Electrochem. Solid-State Lett.* **2012**, *15* (4), E19−E22.
(193) Domen, K.; Naito, S.; Onishi, T.; Tamaru, K.; Soma, M. Study of the photocatalytic decomposition of water vapor over a NiO-$SrTiO_3$ catalyst. *J. Phys. Chem.* **1982**, *86* (18), 3657−3661.
(194) Abe, R.; Sayama, K.; Sugihara, H. Development of new photocatalytic water splitting into H_2 and O_2 using two different semiconductor photocatalysts and a shuttle redox mediator IO_3^-/I^-. *J. Phys. Chem. B* **2005**, *109* (33), 16052−16061.
(195) Konta, R.; Ishii, T.; Kato, H.; Kudo, A. Photocatalytic activities of noble metal ion doped $SrTiO_3$ under visible light irradiation. *J. Phys. Chem. B* **2004**, *108* (26), 8992−8995.
(196) Kudo, A.; Tanaka, A.; Domen, K.; Onishi, T. The effects of the calcination temperature of $SrTiO_3$ powder on photocatalytic activities. *J. Catal.* **1988**, *111* (2), 296−301.
(197) Mills, A.; Porter, G. Photosensitised dissociation of water using dispersed suspensions of n-type semiconductors. *J. Chem. Soc., Faraday Trans. 1* **1982**, *78* (12), 3659−3669.
(198) Niishiro, R.; Kato, H.; Kudo, A. Nickel and either tantalum or niobium-codoped TiO_2 and $SrTiO_3$ photocatalysts with visible-light response for H_2 or O_2 evolution from aqueous solutions. *Phys. Chem. Chem. Phys.* **2005**, *7* (10), 2241−2245.
(199) Bae, S. W.; Ji, S. M.; Hong, S. J.; Jang, J. W.; Lee, J. S. Photocatalytic overall water splitting with dual-bed system under visible light irradiation. *Int. J. Hydrogen Energy* **2009**, *34* (8), 3243−3249.

DOI: 10.1021/acs.chemrev.6b00327
Chem. Rev. 2016, 116, 14587−14619

(200) Lee, W. H.; Liao, C. H.; Tsai, M. F.; Huang, C. W.; Wu, J. C. S. A novel twin reactor for CO_2 photoreduction to mimic artificial photosynthesis. *Appl. Catal., B* **2013**, *132*−*133*, 445−451.
(201) Wang, B.; Shen, S.; Guo, L. $SrTiO_3$ single crystals enclosed with high-indexed {023} facets and {001} facets for photocatalytic hydrogen and oxygen evolution. *Appl. Catal., B* **2015**, *166*−*167*, 320−326.
(202) Iwase, A.; Ng, Y. H.; Ishiguro, Y.; Kudo, A.; Amal, R. Reduced graphene oxide as a solid-state electron mediator in Z-scheme photocatalytic water splitting under visible light. *J. Am. Chem. Soc.* **2011**, *133* (29), 11054−11057.
(203) Suzuki, H.; Tomita, O.; Higashi, M.; Abe, R. Z-scheme water splitting into H_2 and O_2 using tungstic acid as an oxygen-evolving photocatalyst under visible light irradiation. *Chem. Lett.* **2015**, *44* (8), 1134−1136.
(204) Suzuki, T. M.; Iwase, A.; Tanaka, H.; Sato, S.; Kudo, A.; Morikawa, T. Z-scheme water splitting under visible light irradiation over powdered metal-complex/semiconductor hybrid photocatalysts mediated by reduced graphene oxide. *J. Mater. Chem. A* **2015**, *3* (25), 13283−13290.
(205) Sasaki, Y.; Kato, H.; Kudo, A. $[Co(bpy)_3]^{3+/2+}$ and $[Co(phen)_3]^{3+/2+}$ electron mediators for overall water splitting under sunlight irradiation using Z-scheme photocatalyst system. *J. Am. Chem. Soc.* **2013**, *135* (14), 5441−5449.
(206) Sasaki, Y.; Nemoto, H.; Saito, K.; Kudo, A. Solar water splitting using powdered photocatalysts driven by Z-schematic interparticle electron transfer without an electron mediator. *J. Phys. Chem. C* **2009**, *113* (40), 17536−17542.
(207) Liu, J.; Sun, Y.; Li, Z.; Li, S.; Zhao, J. Photocatalytic hydrogen production from water/methanol solutions over highly ordered Ag-$SrTiO_3$ nanotube arrays. *Int. J. Hydrogen Energy* **2011**, *36* (10), 5811−5816.
(208) Matsumoto, Y.; Ohsawa, T.; Nakajima, K.; Koinuma, H. Atomic force microscope analysis of photodecomposition of pentacene film on the epitaxial thin film photocatalyst library. *Meas. Sci. Technol.* **2005**, *16* (1), 199−202.
(209) Ohsawa, T.; Nakajima, K.; Matsumoto, Y.; Koinuma, H. Combinatorial discovery of anomalous substrate effect on the photochemical properties of transition metal-doped epitaxial $SrTiO_3$ heterostructures. *Appl. Surf. Sci.* **2006**, *252* (7), 2603−2607.
(210) Sun, Y.; Liu, J.; Li, Z. Design of highly ordered Ag-$SrTiO_3$ nanotube arrays for photocatalytic degradation of methyl orange. *J. Solid State Chem.* **2011**, *184* (8), 1924−1930.
(211) Yan, X.; Sun, S.; Hu, B.; Wang, X.; Lu, W.; Shi, W. Enhanced photocatalytic activity induced by surface plasmon resonance on Ag-loaded strontium titanate nanoparticles. *Micro Nano Lett.* **2013**, *8* (9), 504−507.
(212) Tanaka, R.; Takata, S.; Katayama, M.; Takahashi, R.; Grepstad, J. K.; Tybell, T.; Matsumoto, Y. Photocatalytic synthesis of silver-oxide clathrate $Ag_7O_8NO_3$. *J. Electrochem. Soc.* **2010**, *157* (12), E181−E183.
(213) Xian, T.; Yang, H.; Di, L. J.; Dai, J. F. Enhanced photocatalytic activity of $SrTiO_3$ particles by surface decoration with Ag nanoparticles for dye degradation. *Phys. Scr.* **2015**, *90* (5), No. 055801.
(214) Giocondi, J. L.; Rohrer, G. S. Structure sensitivity of photochemical oxidation and reduction reactions on $SrTiO_3$ surfaces. *J. Am. Ceram. Soc.* **2003**, *86* (7), 1182−1189.
(215) Townsend, T. K.; Browning, N. D.; Osterloh, F. E. Overall photocatalytic water splitting with NiO_x-$SrTiO_3$ - a revised mechanism. *Energy Environ. Sci.* **2012**, *5* (11), 9543−9550.
(216) Borgarello, E.; Serpone, N.; Pelizzetti, E.; Barbeni, M. Efficient photochemical conversion of aqueous sulphides and sulphites to hydrogen using a rhodium-loaded CdS photocatalyst. *J. Photochem.* **1986**, *33* (1), 35−48.
(217) Carbone, L.; Jakab, A.; Khalavka, Y.; Sönnichsen, C. Light-controlled one-sided growth of large plasmonic gold domains on quantum rods observed on the single particle level. *Nano Lett.* **2009**, *9* (11), 3710−3714.
(218) Menagen, G.; Macdonald, J. E.; Shemesh, Y.; Popov, I.; Banin, U. Au growth on semiconductor nanorods: Photoinduced versus thermal growth mechanisms. *J. Am. Chem. Soc.* **2009**, *131* (47), 17406−17411.
(219) Singh, R.; Pal, B. Influence of Au photodeposition and doping in CdS nanorods: Optical and photocatalytic study. *Part. Sci. Technol.* **2015**, *33* (1), 53−58.
(220) Singh, R.; Pal, B. Study of excited charge carrier's lifetime for the observed photoluminescence and photocatalytic activity of CdS nanostructures of different shapes. *J. Mol. Catal. A: Chem.* **2013**, *371*, 77−85.
(221) Gupta, N.; Pal, B. Selective photo-reduction of p-nitrophenol to p-aminophenol by au deposited CdS nanostructures of different shapes having large surface area. *J. Nanosci. Nanotechnol.* **2013**, *13* (7), 4917−4924.
(222) Rufus, I. B.; Ramakrishnan, V.; Viswanathan, B.; Kuriacose, J. C. Rhodium and rhodium sulfide coated cadmium sulfide as a photocatalyst for photochemical decomposition of aqueous sulfide. *Langmuir* **1990**, *6* (3), 565−567.
(223) Rufus, I. B.; Ramakrishnan, V.; Viswanathan, B.; Kuriacose, J. C. Surface analysis of Rh/CdS. *J. Mater. Sci. Lett.* **1995**, *14* (1), 15−18.
(224) Weiss, V.; Friesem, A. A.; Peled, A. Photodeposition of thin cadmium films from CdS colloid solutions. *Thin Solid Films* **1992**, *218* (1−2), 193−200.
(225) Chen, X.; Chen, W.; Lin, P.; Yang, Y.; Gao, H.; Yuan, J.; Shangguan, W. In situ photodeposition of nickel oxides on CdS for highly efficient hydrogen production via visible-light-driven photocatalysis. *Catal. Commun.* **2013**, *36*, 104−108.
(226) Rufus, I. B.; Ramakrishnan, V.; Viswanathan, B.; Kuriacose, J. C. Interface and surface analysis of Ru/CdS. *J. Mater. Sci. Lett.* **1996**, *15* (21), 1921−1923.
(227) Alemseghed, M. G.; Ruberu, T. P. A.; Vela, J. Controlled fabrication of colloidal semiconductor-metal hybrid heterostructures: Site selective metal photo deposition. *Chem. Mater.* **2011**, *23* (15), 3571−3579.
(228) Rufus, I. B.; Ramakrishnan, V.; Viswanathan, B.; Kuriacose, J. C. X-ray photoelectron spectroscopic studies on Pd/CdS. *J. Mater. Sci. Lett.* **1993**, *12* (19), 1536−1538.
(229) Zong, X.; Yan, H.; Wu, G.; Ma, G.; Wen, F.; Wang, L.; Li, C. Enhancement of photocatalytic H_2 evolution on CdS by loading MoS_2 as cocatalyst under visible light irradiation. *J. Am. Chem. Soc.* **2008**, *130* (23), 7176−7177.
(230) Zong, X.; Han, J.; Ma, G.; Yan, H.; Wu, G.; Li, C. Photocatalytic H_2 evolution on CdS loaded with WS_2 as cocatalyst under visible light irradiation. *J. Phys. Chem. C* **2011**, *115* (24), 12202−12208.
(231) Yao, W.; Song, X.; Huang, C.; Xu, Q.; Wu, Q. Enhancing solar hydrogen production via modified photochemical treatment of Pt/CdS photocatalyst. *Catal. Today* **2013**, *199* (1), 42−47.
(232) Li, C.; Yuan, J.; Han, B.; Jiang, L.; Shangguan, W. TiO_2 nanotubes incorporated with CdS for photocatalytic hydrogen production from splitting water under visible light irradiation. *Int. J. Hydrogen Energy* **2010**, *35* (13), 7073−7079.
(233) Muruganandham, M.; Kusumoto, Y.; Okamoto, C.; Muruganandham, A.; Abdulla-Al-Mamun, M.; Ahmmad, B. Mineralizer-assisted shape-controlled synthesis, characterization, and photocatalytic evaluation of CdS microcrystals. *J. Phys. Chem. C* **2009**, *113* (45), 19506−19517.
(234) Bühler, N.; Meier, K.; Reber, J. F. Photochemical hydrogen production with cadmium sulfide suspensions. *J. Phys. Chem.* **1984**, *88* (15), 3261−3268.
(235) Li, Y.; Du, J.; Peng, S.; Xie, D.; Lu, G.; Li, S. Enhancement of photocatalytic activity of cadmium sulfide for hydrogen evolution by photoetching. *Int. J. Hydrogen Energy* **2008**, *33* (8), 2007−2013.
(236) Peng, S.; Xie, D.; Li, Y.; Lu, G.; Li, S. Preparation of SiO_2-Pt-CdS composite photocatalyst and its photocatalytic activity for hydrogen evolution under visible light. *React. Kinet. Catal. Lett.* **2008**, *95* (1), 185−192.
(237) Reber, J. F.; Rusek, M. Photochemical hydrogen production with platinized suspensions of cadmium sulfide and cadmium zinc sulfide modified by silver sulfide. *J. Phys. Chem.* **1986**, *90* (5), 824−834.
(238) Berr, M.; Vaneski, A.; Susha, A. S.; Rodríguez-Fernández, J.; Döblinger, M.; Jäckel, F.; Rogach, A. L.; Feldmann, J. Colloidal CdS nanorods decorated with subnanometer sized Pt clusters for photo-

DOI: 10.1021/acs.chemrev.6b00327
Chem. Rev. 2016, 116, 14587−14619

catalytic hydrogen generation. *Appl. Phys. Lett.* **2010**, *97* (9), No. 093108.
(239) Dung, D.; Ramsden, J.; Grätzel, M. Dynamics of interfacial electron-transfer processes in colloidal semiconductor systems. *J. Am. Chem. Soc.* **1982**, *104* (11), 2977−2985.
(240) He, K.; Wang, M.; Guo, L. Novel-CdS-nanorod with stacking fault structures: Preparation and properties of visible-light-driven photocatalytic hydrogen production from water. *Chem. Eng. J.* **2015**, *279*, 747−756.
(241) Sakamoto, M.; Xiong, A.; Kanakubo, R.; Ikeda, T.; Yoshinaga, T.; Maeda, K.; Domen, K.; Teranishi, T. Highly dispersive deposition of Pt nanoparticles on CdS nanostructures for photocatalytic hydrogen evolution. *Chem. Lett.* **2012**, *41* (10), 1325−1327.
(242) Harbour, J. R.; Wolkow, R.; Hair, M. L. Effect of platinization on the photoproperties of CdS pigments in dispersion. Determination by H_2 evolution, O_2 uptake, and electron spin resonance spectroscopy. *J. Phys. Chem.* **1981**, *85* (26), 4026−4029.
(243) Bamwenda, G.; Mika, A. M.; Winnicki, T. Z. Photochemical H_2 production from aqueous solution of formic acid on sintered luminophore-grade CdS pellets. *Electrochim. Acta* **1991**, *36* (1), 153−154.
(244) Park, H.; Choi, W.; Hoffmann, M. R. Effects of the preparation method of the ternary CdS/TiO_2/Pt hybrid photocatalysts on visible light-induced hydrogen production. *J. Mater. Chem.* **2008**, *18* (20), 2379−2385.
(245) Bao, N.; Shen, L.; Takata, T.; Domen, K. Self-templated synthesis of nanoporous CdS nanostructures for highly efficient photocatalytic hydrogen production under visible light. *Chem. Mater.* **2008**, *20* (1), 110−117.
(246) Zhensheng, Jin; Qinglin, Li; Liangbo, Feng; Zhengshi, Chen; Xinhua, Zheng; Chanjuan, Xi Investigation of the functions of CdS surface composite layer and Pt on treated Pt/CdS for photocatalytic dehydrogenation of aqueous alcohol solutions. *J. Mol. Catal.* **1989**, *50* (3), 315−332.
(247) Jang, J. S.; Ham, D. J.; Lakshminarasimhan, N.; Choi, W. y.; Lee, J. S. Role of platinum-like tungsten carbide as cocatalyst of CdS photocatalyst for hydrogen production under visible light irradiation. *Appl. Catal., A* **2008**, *346* (1−2), 149−154.
(248) Dimitrijevic, N. M.; Li, S.; Graetzel, M. Visible light induced oxygen evolution in aqueous CdS suspensions. *J. Am. Chem. Soc.* **1984**, *106* (22), 6565−6569.
(249) Xin, G.; Yu, B.; Xia, Y.; Hu, T.; Liu, L.; Li, C. Highly efficient deposition method of platinum over CdS for H_2 evolution under visible light. *J. Phys. Chem. C* **2014**, *118* (38), 21928−21934.
(250) Jing, D.; Guo, L. A novel method for the preparation of a highly stable and active CdS photocatalyst with a special surface nanostructure. *J. Phys. Chem. B* **2006**, *110* (23), 11139−11145.
(251) Yu, J.; Yu, Y.; Cheng, B. Enhanced visible-light photocatalytic H_2-production performance of multi-armed CdS nanorods. *RSC Adv.* **2012**, *2* (31), 11829−11835.
(252) Li, Y.; Tang, L.; Peng, S.; Li, Z.; Lu, G. Phosphate-assisted hydrothermal synthesis of hexagonal CdS for efficient photocatalytic hydrogen evolution. *CrystEngComm* **2012**, *14* (20), 6974−6982.
(253) Li, Y.; Hu, Y.; Peng, S.; Lu, G.; Li, S. Synthesis of CdS nanorods by an ethylenediamine assisted hydrothermal method for photocatalytic hydrogen evolution. *J. Phys. Chem. C* **2009**, *113* (21), 9352−9358.
(254) Jin, Z.; Li, Q.; Zheng, X.; Xi, C.; Wang, C.; Zhang, H.; Feng, L.; Wang, H.; Chen, Z.; Jiang, Z. Surface properties of Pt-CdS and mechanism of photocatalytic dehydrogenation of aqueous alcohol. *J. Photochem. Photobiol., A* **1993**, *71* (1), 85−96.
(255) Zong, X.; Wu, G.; Yan, H.; Ma, G.; Shi, J.; Wen, F.; Wang, L.; Li, C. Photocatalytic H_2 evolution on MoS_2/CdS catalysts under visible light irradiation. *J. Phys. Chem. C* **2010**, *114* (4), 1963−1968.
(256) Matsumura, M.; Furukawa, S.; Saho, Y.; Tsubomura, H. Cadmium sulfide photocatalyzed hydrogen production from aqueous solutions of sulfite: effect of crystal structure and preparation method of the catalyst. *J. Phys. Chem.* **1985**, *89* (8), 1327−1329.
(257) Maeda, K.; Teramura, K.; Lu, D.; Saito, N.; Inoue, Y.; Domen, K. Noble-metal/Cr_2O_3 core/shell nanoparticles as a cocatalyst for photocatalytic overall water splitting. *Angew. Chem., Int. Ed.* **2006**, *45* (46), 7806−7809.
(258) Maeda, K.; Teramura, K.; Lu, D.; Saito, N.; Inoue, Y.; Domen, K. Roles of Rh/Cr_2O_3 (core/shell) nanoparticles photodeposited on visible-light-responsive ($Ga_{1-x}Zn_x$)($N_{1-x}O_x$) solid solutions in photocatalytic overall water splitting. *J. Phys. Chem. C* **2007**, *111* (20), 7554−7560.
(259) Maeda, K.; Xiong, A.; Yoshinaga, T.; Ikeda, T.; Sakamoto, N.; Hisatomi, T.; Takashima, M.; Lu, D.; Kanehara, M.; Setoyama, T.; Teranishi, T.; Domen, K. Photocatalytic overall water splitting promoted by two different cocatalysts for hydrogen and oxygen evolution under visible light. *Angew. Chem., Int. Ed.* **2010**, *49* (24), 4096−4099.
(260) Maeda, K.; Sakamoto, N.; Ikeda, T.; Ohtsuka, H.; Xiong, A.; Lu, D.; Kanehara, M.; Teranishi, T.; Domen, K. Preparation of core-shell-structured nanoparticles (with a noble-metal or metal oxide core and a chromia shell) and their application in water splitting by means of visible light. *Chem. - Eur. J.* **2010**, *16* (26), 7750−7759.
(261) Sakamoto, N.; Ohtsuka, H.; Ikeda, T.; Maeda, K.; Lu, D.; Kanehara, M.; Teramura, K.; Teranishi, T.; Domen, K. Highly dispersed noble-metal/chromia (core/shell) nanoparticles as efficient hydrogen evolution promoters for photocatalytic overall water splitting under visible light. *Nanoscale* **2009**, *1* (1), 106−109.
(262) Maeda, K.; Lu, D.; Teramura, K.; Domen, K. Simultaneous photodeposition of rhodium-chromium nanoparticles on a semiconductor powder: Structural characterization and application to photocatalytic overall water splitting. *Energy Environ. Sci.* **2010**, *3* (4), 471−478.
(263) Fresno, F.; Portela, R.; Suárez, S.; Coronado, J. M. Photocatalytic materials: Recent achievements and near future trends. *J. Mater. Chem. A* **2014**, *2* (9), 2863−2884.
(264) Liu, G.; Yu, J. C.; Lu, G. Q.; Cheng, H. M. Crystal facet engineering of semiconductor photocatalysts: motivations, advances and unique properties. *Chem. Commun.* **2011**, *47* (24), 6763−6783.
(265) Tong, H.; Ouyang, S.; Bi, Y.; Umezawa, N.; Oshikiri, M.; Ye, J. Nano-photocatalytic materials: Possibilities and challenges. *Adv. Mater.* **2012**, *24* (2), 229−251.
(266) Zheng, J. Y.; Haider, Z.; Van, T. K.; Pawar, A. U.; Kang, M. J.; Kim, C. W.; Kang, Y. S. Tuning of the crystal engineering and photoelectrochemical properties of crystalline tungsten oxide for optoelectronic device applications. *CrystEngComm* **2015**, *17* (32), 6070−6093.
(267) Chen, W.; Kuang, Q.; Wang, Q.; Xie, Z. Engineering a high energy surface of anatase TiO_2 crystals towards enhanced performance for energy conversion and environmental applications. *RSC Adv.* **2015**, *5* (26), 20396−20409.
(268) Dozzi, M. V.; Selli, E. Specific facets-dominated anatase TiO_2: Fluorine-mediated synthesis and photoactivity. *Catalysts* **2013**, *3* (2), 455−485.
(269) Yang, H. G.; Sun, C. H.; Qiao, S. Z.; Zou, J.; Liu, G.; Smith, S. C.; Cheng, H. M.; Lu, G. Q. Anatase TiO_2 single crystals with a large percentage of reactive facets. *Nature* **2008**, *453* (7195), 638−641.
(270) Xu, H.; Ouyang, S.; Liu, L.; Reunchan, P.; Umezawa, N.; Ye, J. Recent advances in TiO_2-based photocatalysis. *J. Mater. Chem. A* **2014**, *2* (32), 12642−12661.
(271) Gordon, T. R.; Cargnello, M.; Paik, T.; Mangolini, F.; Weber, R. T.; Fornasiero, P.; Murray, C. B. Nonaqueous synthesis of TiO_2 nanocrystals using TiF_4 to engineer morphology, oxygen vacancy concentration, and photocatalytic activity. *J. Am. Chem. Soc.* **2012**, *134* (15), 6751−6761.
(272) Pan, J.; Liu, G.; Lu, G. Q.; Cheng, H. M. On the true photoreactivity order of {001}, {010}, and {101} facets of anatase TiO_2 crystals. *Angew. Chem., Int. Ed.* **2011**, *50* (9), 2133−2137.
(273) Huang, K.; Yuan, L.; Feng, S. Crystal facet tailoring arts in perovskite oxides. *Inorg. Chem. Front.* **2015**, *2* (11), 965−981.
(274) Huang, Z. F.; Pan, L.; Zou, J. J.; Zhang, X.; Wang, L. Nanostructured bismuth vanadate-based materials for solar-energy-driven water oxidation: A review on recent progress. *Nanoscale* **2014**, *6* (23), 14044−14063.

DOI: 10.1021/acs.chemrev.6b00327
Chem. Rev. 2016, 116, 14587−14619

(275) Chen, Y. C.; Pu, Y. C.; Hsu, Y. J. Interfacial charge carrier dynamics of the three-component In_2O_3-TiO_2-Pt heterojunction system. *J. Phys. Chem. C* **2012**, *116* (4), 2967−2975.
(276) Wei, Y.; Jiao, J.; Zhao, Z.; Zhong, W.; Li, J.; Liu, J.; Jiang, G.; Duan, A. 3D ordered macroporous TiO_2-supported Pt@CdS core-shell nanoparticles: design, synthesis and efficient photocatalytic conversion of CO_2 with water to methane. *J. Mater. Chem. A* **2015**, 3 (20), 11074−11085.
(277) Latorre-Sánchez, M.; Primo, A.; Atienzar, P.; Forneli, A.; García, H. p-n heterojunction of doped graphene films obtained by pyrolysis of biomass precursors. *Small* **2015**, *11* (8), 970−975.
(278) Morris Hotsenpiller, P. A.; Bolt, J. D.; Farneth, W. E.; Lowekamp, J. B.; Rohrer, G. S. Orientation dependence of photochemical reactions on TiO_2 surfaces. *J. Phys. Chem. B* **1998**, *102* (17), 3216−3226.
(279) Lowekamp, J. B.; Rohrer, G. S.; Morris Hotsenpiller, P. A.; Bolt, J. D.; Farneth, W. E. Anisotropic photochemical reactivity of bulk TiO_2 crystals. *J. Phys. Chem. B* **1998**, *102* (38), 7323−7327.
(280) Farneth, W. E.; McLean, R. S.; Bolt, J. D.; Dokou, E.; Barteau, M. A. Tapping mode atomic force microscopy studies of the photoreduction of Ag^+ on individual submicrometer TiO_2 particles. *Langmuir* **1999**, *15* (25), 8569−8573.
(281) Murakami, N.; Kurihara, Y.; Tsubota, T.; Ohno, T. Shape-controlled anatase titanium(IV) oxide particles prepared by hydrothermal treatment of peroxo titanic acid in the presence of polyvinyl alcohol. *J. Phys. Chem. C* **2009**, *113* (8), 3062−3069.
(282) Jiang, Z.; Ouyang, Q.; Peng, B.; Zhang, Y.; Zan, L. Ag size-dependent visible-light-responsive photoactivity of Ag-TiO_2 nanostructure based on surface plasmon resonance. *J. Mater. Chem. A* **2014**, *2* (46), 19861−19866.
(283) Sofianou, M. V.; Boukos, N.; Vaimakis, T.; Trapalis, C. Decoration of TiO_2 anatase nanoplates with silver nanoparticles on the {101} crystal facets and their photocatalytic behaviour. *Appl. Catal., B* **2014**, *158−159*, 91−95.
(284) Bian, Z.; Tachikawa, T.; Kim, W.; Choi, W.; Majima, T. Superior electron transport and photocatalytic abilities of metal-nanoparticle-loaded TiO_2 superstructures. *J. Phys. Chem. C* **2012**, *116* (48), 25444−25453.
(285) Matsumoto, Y.; Ida, S.; Inoue, T. Photodeposition of metal and metal oxide at the TiO_x nanosheet to observe the photocatalytic active site. *J. Phys. Chem. C* **2008**, *112* (31), 11614−11616.
(286) Giocondi, J. L.; Salvador, P. A.; Rohrer, G. S. The origin of photochemical anisotropy in $SrTiO_3$. *Top. Catal.* **2007**, *44* (4), 529−533.
(287) Read, C. G.; Steinmiller, E. M. P.; Choi, K. S. Atomic plane-selective deposition of gold nanoparticles on metal oxide crystals exploiting preferential adsorption of additives. *J. Am. Chem. Soc.* **2009**, *131* (34), 12040−12041.
(288) Yu, Z. B.; Xie, Y. P.; Liu, G.; Lu, G. Q.; Ma, X. L.; Cheng, H. M. Self-assembled CdS/Au/ZnO heterostructure induced by surface polar charges for efficient photocatalytic hydrogen evolution. *J. Mater. Chem. A* **2013**, *1* (8), 2773−2776.
(289) Zhang, L.; Shi, J.; Liu, M.; Jing, D.; Guo, L. Photocatalytic reforming of glucose under visible light over morphology controlled Cu_2O: efficient charge separation by crystal facet engineering. *Chem. Commun.* **2014**, *50* (2), 192−194.
(290) Li, R.; Tao, X.; Chen, R.; Fan, F.; Li, C. Synergetic effect of dual co-catalysts on the activity of *p*-type Cu_2O crystals with anisotropic facets. *Chem. - Eur. J.* **2015**, *21* (41), 14337−14341.
(291) Wang, L.; Ge, J.; Wang, A.; Deng, M.; Wang, X.; Bai, S.; Li, R.; Jiang, J.; Zhang, Q.; Luo, Y.; Xiong, Y. Designing p-type semiconductor-metal hybrid structures for improved photocatalysis. *Angew. Chem., Int. Ed.* **2014**, *53* (20), 5107−5111.
(292) Li, H.; Sun, Y.; Cai, B.; Gan, S.; Han, D.; Niu, L.; Wu, T. Hierarchically Z-scheme photocatalyst of Ag@AgCl decorated on $BiVO_4$ (040) with enhancing photoelectrochemical and photocatalytic performance. *Appl. Catal., B* **2015**, *170−171*, 206−214.
(293) Booshehri, A. Y.; Chun-Kiat Goh, S.; Hong, J.; Jiang, R.; Xu, R. Effect of depositing silver nanoparticles on $BiVO_4$ in enhancing visible light photocatalytic inactivation of bacteria in water. *J. Mater. Chem. A* **2014**, *2* (17), 6209−6217.
(294) Zhen, C.; Yu, J. C.; Liu, G.; Cheng, H. M. Selective deposition of redox co-catalyst(s) to improve the photocatalytic activity of single-domain ferroelectric $PbTiO_3$ nanoplates. *Chem. Commun.* **2014**, *50* (72), 10416−10419.
(295) Kato, H.; Asakura, K.; Kudo, A. Highly efficient water splitting into H_2 and O_2 over lanthanum-doped $NaTaO_3$ photocatalysts with high crystallinity and surface nanostructure. *J. Am. Chem. Soc.* **2003**, *125* (10), 3082−3089.
(296) Miseki, Y.; Kato, H.; Kudo, A. Water splitting into H_2 and O_2 over niobate and titanate photocatalysts with (111) plane-type layered perovskite structure. *Energy Environ. Sci.* **2009**, *2* (3), 306−314.
(297) Compton, O. C.; Carroll, E. C.; Kim, J. Y.; Larsen, D. S.; Osterloh, F. E. Calcium niobate semiconductor nanosheets as catalysts for photochemical hydrogen evolution from water. *J. Phys. Chem. C* **2007**, *111* (40), 14589−14592.
(298) Sabio, E. M.; Chi, M.; Browning, N. D.; Osterloh, F. E. Charge separation in a niobate nanosheet photocatalyst studied with photochemical labeling. *Langmuir* **2010**, *26* (10), 7254−7261.
(299) Zhang, L.; Wang, W.; Sun, S.; Jiang, D.; Gao, E. Selective transport of electron and hole among {001} and {110} facets of BiOCl for pure water splitting. *Appl. Catal., B* **2015**, *162*, 470−474.
(300) Kuang, Q.; Zheng, X.; Yang, S. AgI microplate monocrystals with polar {0001} facets: spontaneous photocarrier separation and enhanced photocatalytic activity. *Chem. - Eur. J.* **2014**, *20* (9), 2637−2645.
(301) Pacholski, C.; Kornowski, A.; Weller, H. Site-specific photodeposition of silver on ZnO nanorods. *Angew. Chem., Int. Ed.* **2004**, *43* (36), 4774−4777.
(302) Yao, K. X.; Liu, X.; Zhao, L.; Zeng, H. C.; Han, Y. Site-specific growth of Au particles on ZnO nanopyramids under ultraviolet illumination. *Nanoscale* **2011**, *3* (10), 4195−4200.
(303) Chanaewa, A.; Schmitt, J.; Meyns, M.; Volkmann, M.; Klinke, C.; Von Hauff, E. Charge redistribution and extraction in photocatalytically synthesized Au-ZnO nanohybrids. *J. Phys. Chem. C* **2015**, *119* (37), 21704−21710.

DOI: 10.1021/acs.chemrev.6b00327
Chem. Rev. 2016, 116, 14587−14619